SYNTHESIS AND MATERIAL PROPERTIES OF SUPRAMOLECULES CONTAINING FLUORINATED ORGANOMERCURIALS

A Dissertation

by

THOMAS JACKSON TAYLOR

Submitted to the Office of Graduate Studies of
Texas A&M University
in partial fulfillment of the requirements for the degree of

DOCTOR OF PHILOSOPHY

May 2007

Major Subject: Chemistry

SYNTHESIS AND MATERIAL PROPERTIES OF SUPRAMOLECULES CONTAINING FLUORINATED ORGANOMERCURIALS

A Dissertation

by

THOMAS JACKSON TAYLOR

Submitted to the Office of Graduate Studies of
Texas A&M University
in partial fulfillment of the requirements for the degree of

DOCTOR OF PHILOSOPHY

Approved by:

Chair of Committee,	François P. Gabbaï
Committee Members,	Donald Darensbourg
	Kim Dunbar
	Michael Bevan
Head of Department,	David Russell

May 2007

Major Subject: Chemistry

ABSTRACT

Synthesis and Material Properties of Supramolecules Containing Fluorinated Organomercurials. (May 2007)
Thomas Jackson Taylor, B.S., University of Chicago
Chair of Advisory Committee: Dr. François P. Gabbaï

This dissertation details the synthesis and analysis of novel supramolecular species that feature simple fluorinated organomercurials, such as trimeric perfluoro-*ortho*-phenylene mercury ($[o\text{-}C_6F_4Hg]_3$). These organomercurials can complex a variety of unsaturated substrates including arenes and alkynes. The major emphasis was on developing molecular architectures that are held together in part by secondary $Hg\text{-}C_{alkyne}$ interactions.

Diphenylpolyynes, hydrocarbons featuring extended regions of unsaturation, were found to complex with $[o\text{-}C_6F_4Hg]_3$ in a series of adducts. While the internal structures of the hydrocarbons themselves were found to be basically unaltered, within the crystals the polyynes were physically separated from one another by intervening molecules of $[o\text{-}C_6F_4Hg]_3$, preventing them from cross-linking. This leads to a substantial stabilizing effect, for example $[o\text{-}C_6F_4Hg]_3$ and $Ph(C{\equiv}C)_4Ph$ form a 2:1 adduct that is stable at temperatures up to 120 ºC above the pure hydrocarbon.

Adducts of $[o\text{-}C_6F_4Hg]_3$ and molecules containing a 1,3,5-triethynyl benzene core display a variety of novel properties. 1,3,5-tris(trimethylsilylethynyl) benzene forms binary supramolecular stacks with $[o\text{-}C_6F_4Hg]_3$. The structure also displays large cylindrical 1-dimensional cavities. These cavities are lined with non-polar groups, have an internal diameter of 6.2 Å, and remain stable in the absence of guests. The compound readily interacts with and reversibly adsorbs simple alkanes.

1,3,5-tris(phenylethynyl) benzene forms similar stacks with $[o\text{-}C_6F_4Hg]_3$, albeit without the cavities. Upon irradiation with visible and ultraviolet light, this adduct emits

a long-lived emission that was hitherto unreported. From computer calculations and lifetime measurements, it appears this radiation is the phosphorescence of the pure hydrocarbon.

Intensive structural studies have also been performed on adducts containing polyaromatic compounds, including phenanthrene, and the organomercurials [*o*-$C_6F_4Hg]_3$, pentafluorophenyl mercury chloride and bromide. These experiments were performed to determine if Lewis acid-π complexes could be made with monofunctional mercury compounds. Polyaromatic hydrocarbons, such as phenanthrene and diphenylacetylene, were used as the substrates for these investigations. While all the mercurials formed adducts with the substrates, the photophysical measurements were not uniform and indicate that [*o*-$C_6F_4Hg]_3$ has a stronger heavy-atom effect because of the cooperativity of the three mercury atoms.

ACKNOWLEDGMENTS

I would like thank Prof. François P. Gabbaï, my research advisor, for his support and encouragement during the last four and a half years. He was always available and had some great ideas for new wrinkles in the course of this chemistry. Additionally, he really helped with the completion of my Ph.D. by firmly putting his foot down and telling me that sometimes a project just can't be made to work, and it is time to move on. I would like to thank my committee, including Dr. Michael A. Bevan, Dr. Donald J. Darensbourg, Dr. Kim R. Dunbar, and Dr. John Fackler who served as a replacement member for my Preliminary examination. Other faculty members I want to mention are Dr. Raymond Schaak and Dr. Timothy Hughbanks. Staff members who gave me a great deal of advice and assistance include Dr. Nattamai Bhuvanesh, Dr. Joseph H. Reibenspies, Dr. Ahmed A. Mohamed, and Dr. Vladimir Bakhmoutov.

The Gabbaï research group has been incredibly important to me, and I want to mention Dr. Mason R. Haneline and Dr. Mitsukimi Tsunoda, who eased me into this supramolecular chemistry, Dr. Charlotte N. Burress, who was my compatriot for almost the duration of my time here, Dr. Mohand A. Melaimi, who is a good friend in addition to teaching me a great deal of synthetic tricks, as well as well as Ching-Wen Chiu, Christopher Dorsey, Todd Hudnall, Dr. Mieock Kim, Youngmin Kim, Dr. Min Hyung Lee, Dr. Alexandre Picot, Dr. Stephane Solé, and Dr. Huadong Wang. Laxman Pandey was a great help in analyzing monofunctional species during the summer he came here as a NSF-REU student in 2006.

I would like to thank Prof. William Wulff and Dr. Daniel Goldberg from a long time ago at the University of Chicago for giving me my first taste of synthetic chemistry.

I would like to acknowledge the NSF, the Welch Foundation, and the Texas Advanced Technology Program for research funding, and the Department of Chemistry and Office of Graduate Studies for travel grants.

Finally, I want to thank my family and my wife Sarah for their love and understanding, and good friends in Texas who helped make these last few years just fly by.

TABLE OF CONTENTS

CHAPTER Page

CHAPTER Page

LIST OF FIGURES

FIGURE Page

FIGURE Page

FIGURE Page

FIGURE Page

LIST OF TABLES

CHAPTER I

INTRODUCTION TO THE LEWIS ACIDIC BEHAVIOR OF FLUORINATED ORGANOMERCURIALS*

I.1. Introduction

Organomercurials, which have been known for over 150 years,[1-5] are common reagents in both organic and organometallic chemistry.[6] Despite its linear geometry and apparent unsaturation, the mercury atoms of such compounds exhibit little coordination ability.[7] Although several adducts involving organomercurials have been isolated, both structural and spectroscopic studies have served to confirm the absence of significant Lewis acidity. For example, in its adduct with 2,9-dimethyl-1,10-phenantroline, the mercury atom of diphenylmercury retains a linear C-Hg-C geometry indicating extremely weak Hg···N interactions.[8] Comparable results have been obtained in the chemistry of organomercury halide derivatives such as MeHgCl which only forms very labile anionic complexes in the presence of halide anions in solution.[9] This chemical trait may be traced back to the diffuseness and energy of the vacant mercury orbitals which preclude favorable interactions with the filled orbitals of the donor. Moreover, because mercury and carbon have comparable Pauling electronegativity ($\chi_{(Hg)}$ = 2.00, $\chi_{(C)}$ = 2.55), the mercury atoms of organomercurials do not accumulate a significant positive character and therefore fail to engage in strong electrostatic interactions with electron-rich substrates.

This situation can be altered upon fluorination of the organic substituents. Early

---

This dissertation follows the style and format of the *Journal of the American Chemical Society.*

* Reprinted in part with permission from, Taylor, T. J.; Burress, C. N., Gabbaï, F. P. "Lewis Acidic Behavior of Fluorinated Organomercurials" *Organometallics*, submitted, Copyright 2007 by the American Chemical Society.

evidence for the Lewis acidic behavior of fluorinated organomercurials was obtained by Emeleus and Lagowski who found that addition of alkali iodide to $(CF_3)_2Hg$ or CF_3HgI results in the precipitation of salts that contain the $[(CF_3)_2HgI_2]^{2-}$ and $[CF_3HgI_2]^-$ anions. Further evidence for the Lewis acidic behavior of such compounds came from conductometric titrations which, for example, showed the formation of 1:1 and 2:1 halide complexes involving $Hg(CF_3)_2$.[10, 11] This seminal work was followed by numerous reports which firmly established the affinity of fluorinated organomercurials not only for anionic[7, 12-16] but also neutral electron-rich substrates. Indeed oscillometric titrations indicate that mercurials such as $(CF_3)_2Hg$, $(CF_3CF_2)_2Hg$, $((CF_3)_2CF)_2Hg$, $(CF_3CH_2)_2Hg$ and $(CF_3CHF)_2Hg$ form both 1:1 and 2:1 complexes with neutral bases such as piperidine, dimethylsulfoxide (DMSO), and pyridine N-oxide in benzene solution.[17] Despite their documented lability, some of these complexes including $[(CF_3)_2Hg(ONC_5H_5)_2]$ and $[(CF_3CHF)_2Hg(OSC_4H_8)_2]$ could be obtained as pure species and characterized by IR and elemental analysis.[18]

These early investigations confirmed that fluorinated organomercurials are indeed Lewis acids. Unlike many Lewis acids, however, fluorinated organomercurials are air stable and are usually not neutralized by water which greatly facilitates their handling and use. Another important distinction comes from the polarizability of the mercury atom which greatly "softens" the Lewis acidic properties of these derivatives. The purpose of this article is to review the unusual Lewis acidic properties that fluorinated organomercurials display toward neutral substrates.

I.2. Lewis acidic properties of monofunctional organomercurials

As stated in the introduction, evidence for the formation of adducts involving fluorinated organomercurials and neutral Lewis bases was obtained more than half a century ago. While the composition of these adducts was confirmed beyond any doubts, a clear understanding of the coordination geometry of the mercury center could not be provided. The availability of X-ray diffraction methods has now helped to answer some of these questions. Complexes of $(CF_3)_2Hg$ (**1**, Scheme I.1) which have been recently

structurally characterized include the polymeric adduct [**1**•piperazine],[19] and the dimeric adduct [**1**•3,5-dimethyl-4'-amino-triazole] (Figure I.1). [20] Both of these adducts possess four-coordinate mercury centers in heavily distorted tetrahedral coordination geometries. In both structures, the C-Hg-C angle (171° for [**1**•piperazine] and 173° for [**1**•3,5-dimethyl-4'-amino-triazole]) show only a modest deviation from linearity with Hg···N bond distances (2.682 Å for [**1**•piperazine] and 2.72-2.74 Å for [(**1**•3,5-dimethyl-4'-amino-triazole]) that are commensurate with the presence of secondary interactions. A stronger complexation of the mercury center is observed in the 2,2':6',2"-terpyridyl adduct of $(CF_3)_2Hg$ ([**1**•terpy], Scheme I.2) which displays increased bending of the C-Hg-C angle (164.2°) and shorter Hg···N distances (2.62-2.70 Å).[21] Another structure which deserves comment is that of a dimethylbiphenyl crown-6 ether adduct of **1** (denoted as [**1**•crown-6], Scheme I.2) in which the mercury center interacts with the oxygen atoms of the ligands via weak Hg···O secondary interactions ranging from 2.84 to 3.12 Å.[22, 23] Because of the symmetry of these interactions, the C-Hg-C angle (177.9°) remains essentially linear.

Scheme I.1.

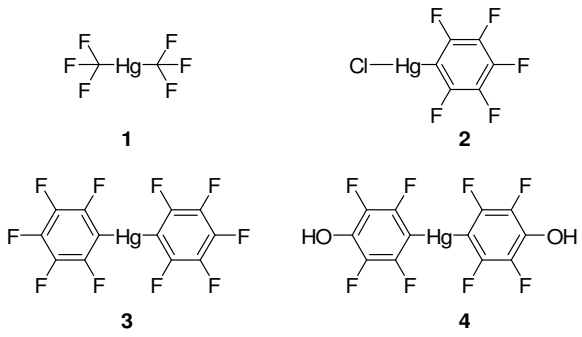

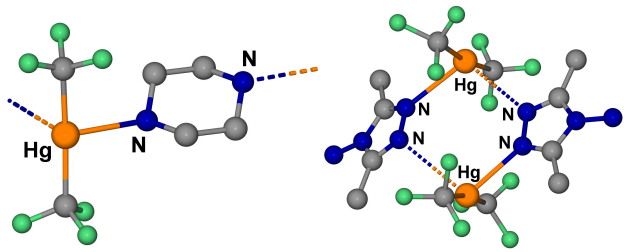

Figure I.1. Structure of [**1**•piperazine] and [**1**•3,5-dimethyl-4'-amino-triazole].

Scheme I.2. [**1**•terpy] (left) and [**1**•crown-6] (right).

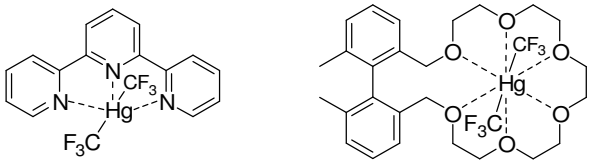

The formation of adducts also occurs with fluorinated aryl mercury compounds such as pentafluorophenyl mercury chloride (**2**, Scheme I.1) which complexes both dimethylformamide (DMF) and DMSO.[24] The DMSO adduct [**2**•DMSO] has a T-shaped structure, with a relatively short Hg···O bond of 2.542(4) Å (Figure I.2). Formation of this short bond is accompanied by a distinct deviation of the C-Hg-Cl angle (169.7(2)°) from linearity. The adduct [(**2**)$_2$•DMF] has also been structurally characterized. In this case, however, the DMF molecules bridge two mercury centers via elongated Hg···O interactions in the 2.66-2.85 Å range. In both adducts, intermolecular Hg···Cl secondary interactions connect the individual molecules into extended polymeric structures. These secondary Hg···Cl interactions partly neutralize the Lewis acidity of the mercury centers and can be regarded as competing with the DMSO or DMF ligands. Nonetheless, the coordination of the oxygen to the mercury center results in a noticeable weakening of the sulfoxide (1019 cm^{-1} in [**2**•DMSO] vs 1057 cm^{-1} in free DMSO) and carbonyl (1654 cm^{-1} in [(**2**)$_2$•DMF] vs 1675 cm^{-1} in free DMF) IR stretching bands. A few Lewis adducts of bis(pentafluorophenyl)mercury (**3**, Scheme I.1) have also been

reported. These include a 2:1 adduct which involves the bis(diphenylarsino)methane ligand (Scheme I.3). In this adduct, the arsenic atoms of the ligand are each coordinated to a molecule of **3** via As-Hg interactions of 3.40 Å..[25] This distance can be compared to the Hg···Se distance of 3.48 Å found in the adduct involving $(C_6F_5)_2Hg$ and 2,2'-dipyridyl diselenide (Scheme I.3).[26] The formation of a water adduct of $Hg(C_6F_4OH\text{-}p)_2$ (**4**, Scheme I.1) has also been recently reported (Figure I.3).[27] In this adduct, the water ligand forms an Hg···O distance of 3.13 Å which by far exceeds the Hg···O distances observed in $[C_6F_5HgCl•DMSO]$ and $[(C_6F_5HgCl)_2•DMF]$. This long distance indicates that the water molecule, which happens to be hydrogen-bonded to the hydroxyl group of a neighboring $(C_6F_4OH\text{-}p)$ ligand, only interacts weakly with the mercury center.

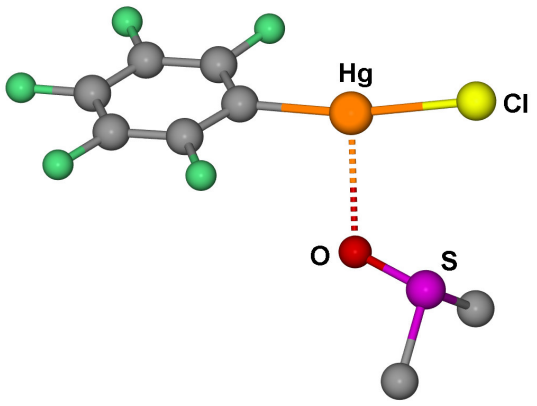

Figure I.2. Structure of **[2**•DMSO**].**

Scheme I.3

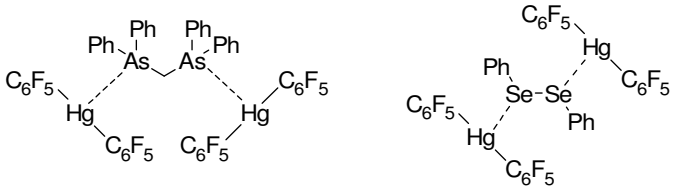

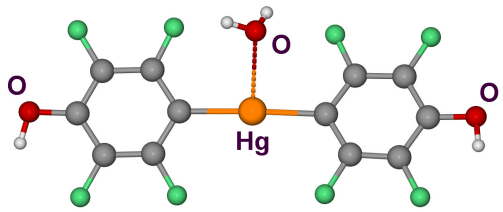

Figure I.3. Structure of **[4•H_2O]**.

I.3. Lewis acidic properties of 1,2-bis(chloromercurio)tetrafluoro benzene and related compounds

Polydentate Lewis acids have attracted a great deal of attention for the multiple electrophilic activation of organic substrates in various reactions.[28-33] Although such an activation mode has often been proposed, indubitable proof of the concomitant coordination of an organic substrate to two or more Lewis acids remained extremely scarce until Wuest showed that compounds containing the 1,2-bis(mercury)benzene motifs crystallize from formamide solvents to yield complexes in which the carbonyl oxygen atom is coordinated to two and sometimes four mercury centers.[34-41] Since non-fluorinated monofunctional organomercurials do not form isolable adducts with Lewis bases such as formamides, these original results clearly established that the Lewis acidity of polydentate organomercurials is increased by cooperative effects. Analogous results in the chemistry of 1,8-bis(chloromercurio)naphthalene confirmed these findings.[42] Unfortunately, these non-fluorinated bidentate Lewis acids did not form stable adducts with more synthetically useful substrates such as aldehydes and ketones. These limitations led several groups to consider multidentate mercury Lewis acids whose acceptor properties are increased by fluorination of the organic backbone.[12, 43]

Scheme I.4

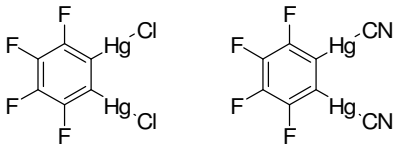

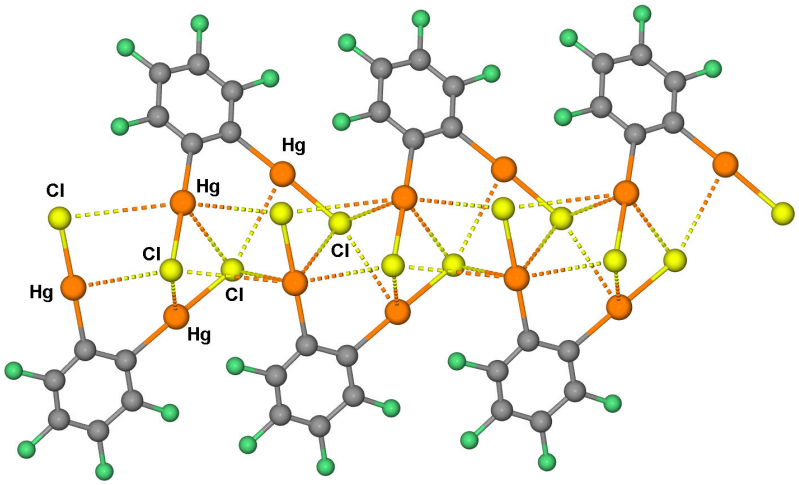

Figure I.4. Structure of the base-free form of the pure of **5.**

1,2-Bis(chloromercurio)tetrafluorobenzene (**5**, Scheme I.4) may be the simplest fluorinated organomercurial that has been carefully investigated. This compound can be crystallized in a base free form from acetaldehyde.[44] It possesses two mercury centers separated by about 3.67 Å and forms extended chains connected by secondary intermolecular Hg···Cl interactions (Figure I.4). Titration experiments monitored by ^{199}Hg NMR spectroscopy indicate that this derivative forms weak 1:1 complexes with DMF and DMSO in acetone.[45] The weakness of these complexes may be due to the acetone solvent which competes for the Lewis acidic mercury sites. In fact, the complex [**5**•μ_2-acetone] can be obtained by slow evaporation of an acetone solution of **5** (Chart 5, Figure I.5).[45] Similar crystallization techniques can be used to obtain [**5**•μ_2-DMF]

(Scheme I.5). Structural characterization of these complexes confirms that the oxygen atom is bound to both mercury centers. The resulting Hg···O bonds (2.679(13) and 2.776(14) Å for [**5**•μ_2-acetone]; 2.653(4) Å) and 2.746(4) Å for [**5**·μ_2-DMF]) are shorter than the sum of the van der Waals radii of oxygen and mercury (3.2 Å) and comparable to those observed in [(**2**)$_2$•DMF]. Chelation of the carbonyl oxygen atom results in a weakening of the carbonyl IR stretching frequency by 23 cm^{-1} for [**5**•μ_2-acetone] and 40 cm^{-1} for [**5**•μ_2-DMF]. $^{13}C\{^1H\}$ MAS NMR spectroscopy shows a downfield shift of the carbonyl carbon resonance by 10 ppm for [**5**•μ_2-acetone] and 5 ppm for [**5**•μ_2-DMF] when compared to neat acetone and DMF, respectively.

Scheme I.5. 1:1 and 2:1 chelate complexes formed by **5**.

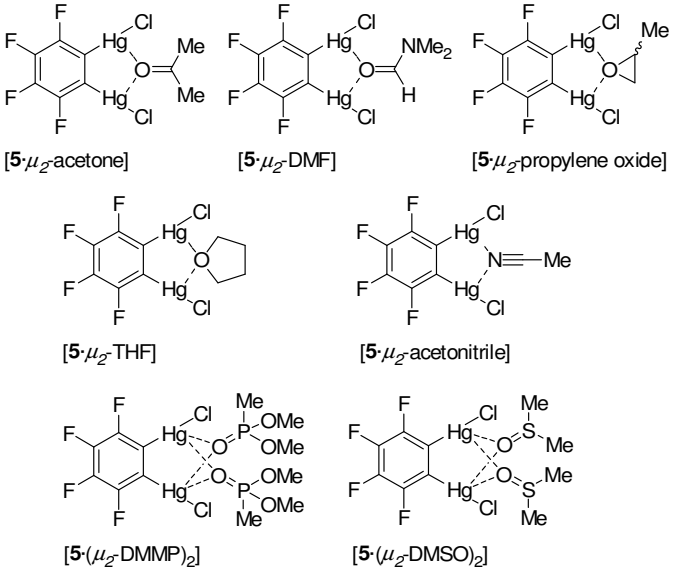

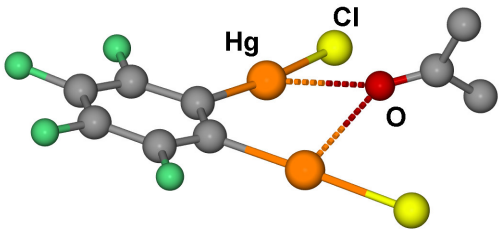

Figure I.5. Structure of **[5**•μ_2-acetone**].**

Crystalline 1:1 complexes of **5** have also been obtained with cyclic ethers such as propylene oxide[44] and THF (Scheme I.5).[46, 47] In both cases, the oxygen is coordinated to both mercury centers. The resulting Hg···O bonds, which fall in the 2.71-2.80 Å range, are slightly longer than those found in the acetone and DMF adducts. Another weak complex is formed with acetonitrile (Scheme I.5).[44] This complex, which features long Hg···N distances of 2.82(1) Å and 2.93(1) Å and an essentially unaffected ν_{CN} of 2255 cm^{-1}, is labile and rapidly loses acetonitrile when exposed to air. Interestingly, all aldehyde adducts characterized thus far do not adopt chelate structures. While acetaldehyde does not form any adducts with **5**, the complex [**5**·benzaldehyde] only shows terminal ligation of the carbonyl functionality to one of the mercury atoms via an Hg···O bond of 2.68 Å (Figure I.6).[44] Complexes of 2:1 stoichiometry have also been observed with **5** and dimethylmethylphosphonate (DMMP)[48] and DMSO[49] as substrates (Scheme I.5, Figure I.7). In these complexes, the donor ligands are positioned on either side of the approximately planar bidentate Lewis acid. The presence of two donors does not influence the Hg···O bond lengths (av 2.79 Å for [**5**•(μ_2-DMMP)$_2$]); av 2.70 Å for [**5**·(μ_2-DMSO)$_2$]) which are comparable to those observed in 1:1 adducts such as [**5**•μ_2-acetone]. As observed for [**2**•DMSO] and [(**2**)$_2$•DMF], the individual molecules of all adducts shown in Scheme I.5 interact via secondary Hg···Cl interactions and form extended structures. In the case of [**5**•(μ_2-DMSO)$_2$], these intermolecular Hg···Cl interactions lead to the formation of a microporous molecular lattice whose channels are filled with solvate DMSO molecules (Figure I.8).[49]

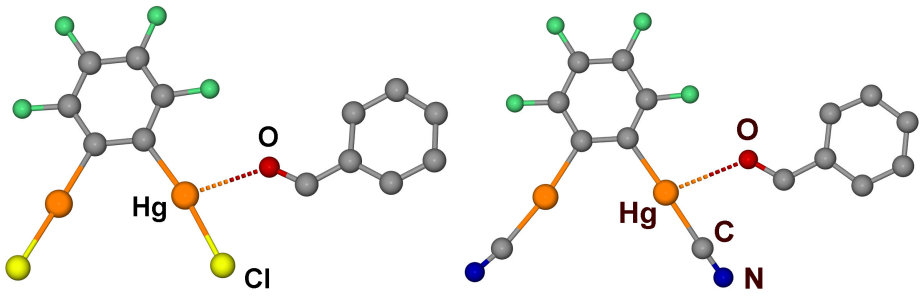

Figure I.6. Structure of [**5**•benzaldehyde] (left) and [**6**•benzaldehyde] (right).

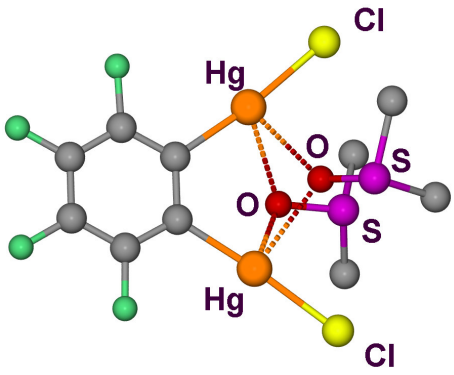

Figure I.7. Structure of [**5**·(μ_2-DMSO)$_2$].

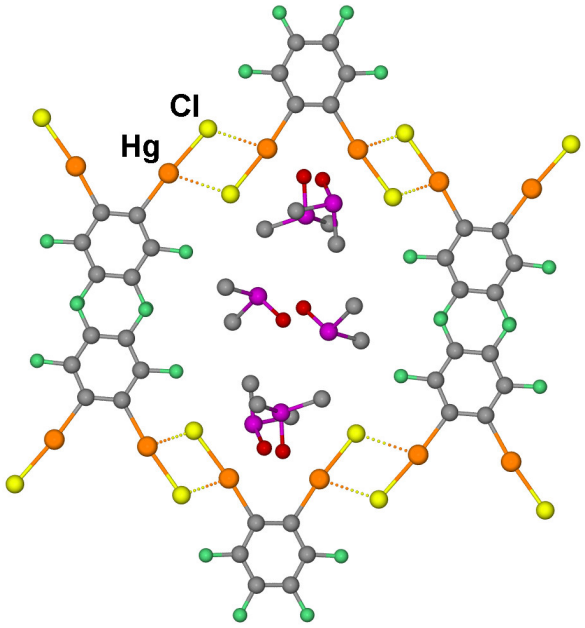

Figure I.8. View of a micropore formed in the structure of [**5**•(μ_2-DMSO)$_2$]-DMSO**.**

1,2-Bis(cyanomercurio)tetrafluorobenzene (**6**, Scheme I.4) reacts with aldehydes to afford complexes such as [**6**•acetaldehyde] and [**6**•benzaldehyde] in which the aldehyde is terminally ligated to one of the mercury centers.[50] The Hg···O bond in [**6**•benzaldehyde] (3.009(12) Å, Figure I.6) is noticeably longer than that found in [**5**•benzaldehyde] (2.68 Å). This difference suggests that the cyanide ligand is less electronegative than chloride. The ability of compound **6** to catalyze the cyanosilylation of benzaldehyde has also been investigated. The results of these studies suggest that bidentate organomercurials such as **6** are not involved in the double electrophilic activation of aldehydes but instead assist in the formation of an activated Lewis acidic silicon species by anion complexation.[50]

A geometry optimization of **5** using DFT methods (bp86 functional, basis set: 6-31g for C and F atoms, 6-31g(d') for Cl and Stuttgart RSC 1997 ECP for Hg) affords a structure close to that experimentally observed.[51] These calculations also indicate that the LUMO (Figure I.9) bears a large contribution from the C-Hg-Cl σ* orbital and

features a large lobe spanning the two heavy atoms. In addition, the electrostatic potential surface shows an accumulation of positive charge on the mercury atoms. These theoretical investigations suggest that the formation of adducts of **5** results from electron donation from the filled orbitals of the donor into the LUMO of **5**. However, since coordination does not significantly affect the structure of the organomercurial and only results in long bonds between the mercury centers and the electron rich donor atoms, the extent of orbital mixing between the donor and the acceptor must be somewhat small. In turn, bonding in these adducts most likely bears an important contribution from favorable electrostatic interactions.

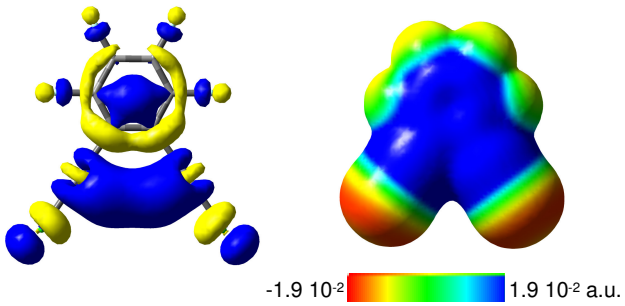

Figure I.9. LUMO (isodensity 0.03) and electrostatic potential surface of **5**.

I.4. Lewis acidic properties of trimeric perfluoro-*ortho*-phenylene mercury

Trimeric perfluoro-*ortho*-phenylene mercury (**7**, Scheme I.6.)[52] has been widely investigated as a host for a variety of anions.[12, 53-59] This molecule, which can be obtained in a base free form by recrystallization from CH_2Cl_2 or sublimation,[60] features a planar structure with readily accessible mercury centers.

Scheme I.6.

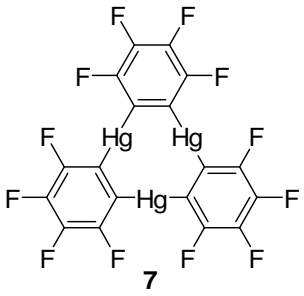

7

Although this compound was reported to form various adducts by Massey over 20 years ago,[61] it is not until recently that a number of structural studies have shed light on the coordination chemistry of this derivative. These studies have confirmed that this derivative exhibits a rich coordination chemistry toward neutral electron rich substrates including aldehydes,[62] ketones,[62, 63] amides,[64-66] nitriles,[66, 67] phosphoramides[64] and sulfoxides[64] with which it usually forms discrete [**7**•μ_3-L], [**7**•(μ_3-L)$_2$] and [**7**•(μ_3-L)$_2$(L)] complexes. In the [**7**•(μ_3-L)$_2$] complexes, two molecules of the donor are coordinated to the mercury centers of **7** on either side of the molecular plane (Scheme I.7). A similar situation is encountered in [**7**•(μ_3-L)$_2$(L)] where an additional ligand is terminally ligated to one of the mercury centers. [**7**•μ_3-acetone][63] and [**7**•(μ_3-acetonitirile)$_2$][67] are representative examples of [**7**•μ_3-L] and [**7**•(μ_3-L)$_2$] adducts, respectively (Figure I.10). In the case of [**7**•μ_3-acetone], the molecules form co-facial dimers which are held by two mercuriophilic interactions of 3.51 Å (Figure I.10).

Scheme I.7. Structures and stoichiometry adopted by adducts of **7** with aldehydes, ketones, amides, nitriles, phosphoramides and sulfoxides.

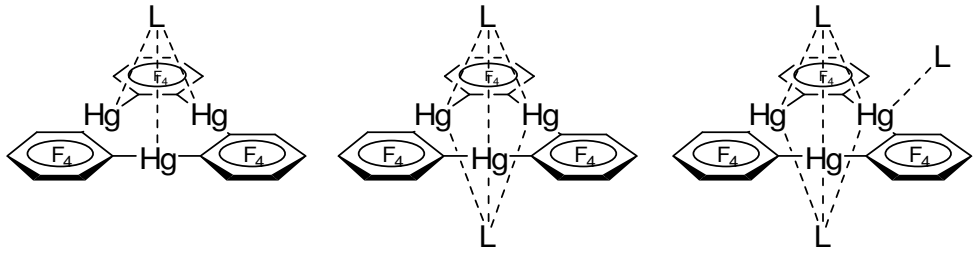

[**7**·μ_3-L] [**7**·(μ_3-L)$_2$] [**7**·(μ_3-L)$_2$(L)]

L =	*n*PrCN,[66]	MeCN,[67]	Me_2CO,[62]
	CH_2CHCN,[67]	PhMeCO,[62]	MeCOOEt,[64]
	MeCHCO,[62]	$Me_2N(H)CO$,[64,]	Me_2SO.[64]
	Me_2CO,[63]	[65] Me_2NMeCO,[66]	
	Ph_2CO.[62]	$(Me_2N)_3PO$.[64]	

For all carbonyl adducts, the Hg···O distances involving the triply bridging substrates fall within a relatively narrow range of 2.8-3.1 Å and do not show any strong dependence on the stoichiometry of the adducts. For example, the Hg···O distances involving the triply bridging acetone molecules in [**7**•μ_3-acetone] (av. 2.90 Å)[63] are close to those in [**7**•(μ_3-acetone)$_2$(acetone)] (av. 2.88 Å)(Figure I.10).[62] The basicity of the ligand also appears to have little influence on the Hg···O distances. For example, the Hg···O bonds in [**7**•(μ_3-DMF)$_2$] (av 2.87 Å)[64] are close to those observed in [**7**•(μ_3-acetone)$_2$(acetone)]. It remains that these Hg···O bonds are distinctly longer than those measured in [**5**•μ_2-acetone] (av 2.73 Å) and [**5**•μ_2-DMF] (av 2.70 Å)[45] which is in agreement with the triply rather than doubly bridging location of the carbonyl ligands. Another interesting feature concerns the terminal ligands of [**7**•(μ_3-acetone)$_2$(acetone)] which form relatively long Hg···O bonds of 3.09 Å. This structural feature may be correlated to the lability of the complex which loses acetone at room temperature.

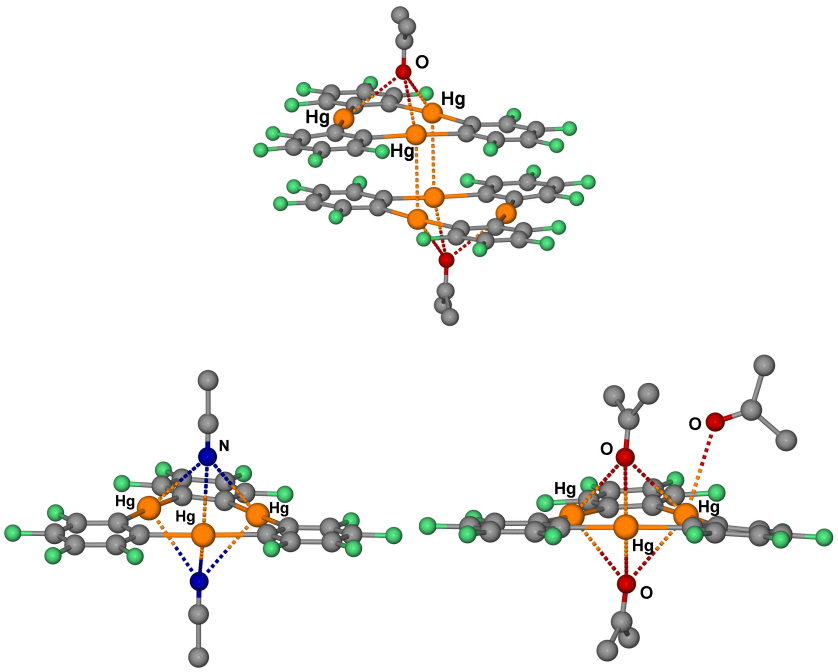

Figure I.10. Structure of [**7**•μ_3-acetone] (top), [**7**•(μ_3-acetonitrile)$_2$] (middle), [**7**•(μ_3-acetone)$_2$(acetone)] (bottom).

For all carbonyl adducts reported thus far, coordination to the mercury centers results in a detectable weakening of the carbonyl IR stretching bands. In the acetone and DMF adduct, the weakening effect is more acute than in [**5**•μ_2-acetone] and [**5**•μ_2-DMF][45] suggesting that the triple coordination of the carbonyl functionality results in an increased polarization of the C=O bond (Table I.1). In the case of the nitriles adduct of **7**, coordination leads to an increase in the energy of the nitrile IR stretch. For [**7**•(μ_3-acetonitirile)$_2$], this stretch appears at 2266 cm-1 as opposed to 2255 cm^{-1} in [**5**·μ_2-acetonitrile] and 2254 cm^{-1} in free acetonitirle (Table I.1).[44, 67] Such an increase has often been observed in Lewis adducts of acetonitrile and is caused by a ligation induced stabilization of the C≡N σ and π bonding orbitals.[68] In turn, the largest deviation observed in [**7**•(μ_3-acetonitirile)$_2$] can be correlated to the triple rather than double coordination of the nitrile functionality.

Table I.1. IR data for selected adducts of **5** and **7**.

	$\nu_{C=O}$ of Me_2CO[45, 63]	$\nu_{C=O}$ of DMF[45, 64, 65]	$\nu_{C\equiv N}$ of MeCN[44, 67]
5	1693 cm^{-1}	1654 cm^{-1}	2266 cm^{-1}
7	1683 cm^{-1}	1646 cm^{-1}	2255 cm^{-1}
free	1716 cm^{-1}	1675 cm^{-1}	2254 cm^{-1}

As expected, this trinuclear complex shows a great affinity for sulfur containing substrates including dimethylsulfide. Crystallization of **7** from neat dimethyl sulfide yields [**7**•(μ_3-Me_2S)$_2$(Me_2S)$_2$] in which four molecules of dimethylsulfide are bound to the trifunctional Lewis acids via Hg···S bond ranging from 3.2-3.5 Å.[69] This complex is quite labile and loses three equivalents of dimethylsulfide upon exposure to dry air thus suggesting the formation of a stable 1:1 adduct. In fact, an adduct of the same stoichiometry can be isolated from 1,2-dichloroethane solutions containing **7** and Me_2S**.** This adduct, [**7**•μ_6-Me_2S]$_n$, adopts a polymeric structure and contains sandwiched dimethylsulfide molecules (Figure I.11). The sulfur atom of the latter interacts simultaneously with the mercury centers of two neighboring molecules of **7** and thereby achieves hexacoordination. The Hg···S bonds (3.571(3) and 3.543(7) Å) are slightly longer than those observed in [**7**•(Me_2S)$_2$(μ_3-Me_2S)$_2$] for the triply coordinated dimethylsulfide molecules but remain within the sum of the van der Waals radii. Compound **7** also interacts with bis(2-hydroxyethyl)sulfide to form a 1:1 adduct with a single and relatively short Hg···S bond of 3.14 Å. [70] Several Hg···O interactions also add to the stability of this adduct. Other adducts involving sulfur containing substrates include [**7**•(μ_3-S=P(OMe)$_2$(p-$C_6H_4NO_2$))$_2$][70] and [(**7**)$_2$•TTF].[71] The latter features a sandwiched TTF molecule held by multiple Hg···S interactions ranging from 3.47-3.53 Å.

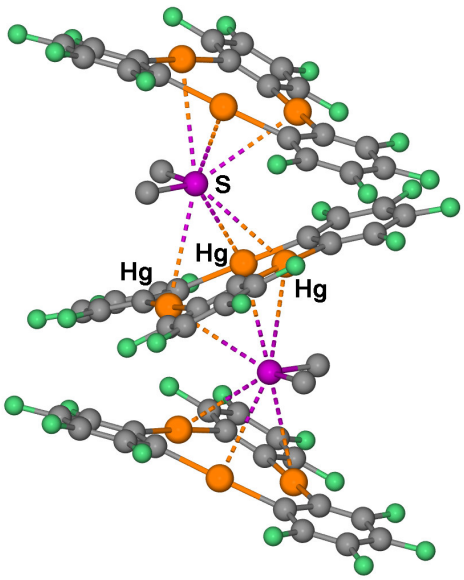

Figure I.11. Portion of the coordination polymer observed in [**7**•μ_6-Me_2S]$_n$.

Substrates with at least two accessible Lewis basic sites tend to form more complex aggregates. For example, 2-(phenyl)-4,4,5,5-tetramethylimidazoline-1-oxyl-3-oxide (NIT-Ph) forms either [**7**•NIT-Ph•**7**] or [**7**•NIT-Ph]$_n$ (Figure I.12) depending on the stoichiometry of the reaction.[72] In these adducts, each of the oxygen atoms of the NIT-Ph molecule interact with the mercury centers of an adjacent molecule of **7**. The Hg···O bonds present in these two structures (2.85-3.02 Å) are comparable to those discussed for the carbonyl adducts. Despite the presence of these relatively short bonds, the NIT-Ph molecules of the polymer [**7**·NIT-Ph]$_n$ do not appear to be coupled to one another as indicated by magnetic susceptibility measurements. This observation suggests that the bonding in such adducts is dominated by electrostatic rather than covalent interactions.

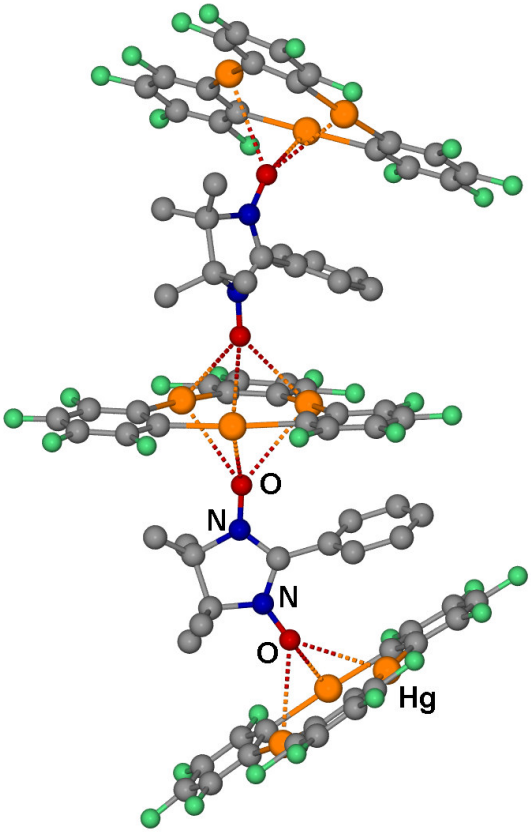

Figure I.12. Portion of the coordination polymer observed in [**7**•NIT-Ph]$_n$.

Sandwich structures are also observed for the *p*-benzoquinone and maleic anhydride.[73] The *p*-benzoquinone adduct features two molecules of **7** which are each coordinated to one of the carbonyl functionalities (Figure I.13). The structure of the maleic anhydride adducts is more complicated. In this adduct, two molecules of maleic anhydride are sandwiched between two molecules of **7**. Each molecule of maleic anhydride is triply coordinated via one of its carbonyl functionality to one of the molecules of **7** and singly coordinated via its remaining carbonyl functionality to the second mercury complex. The Hg···O bonds present in these two structures (2.92-3.12 Å) are once again comparable to those observed in other adducts of oxygen containing ligands. Remarkably, trinuclear **7** is able to stabilize the keto form of acetylacetone (2,4-pentanedione) with which it forms a 2:1 sandwich adduct which has been structurally

characterized (Figure I.13). In chloroform solution, dissociation of the adduct occurs and is accompanied by a transformation of the keto form of acetylacetone into a mixture of its tautomers.[74]

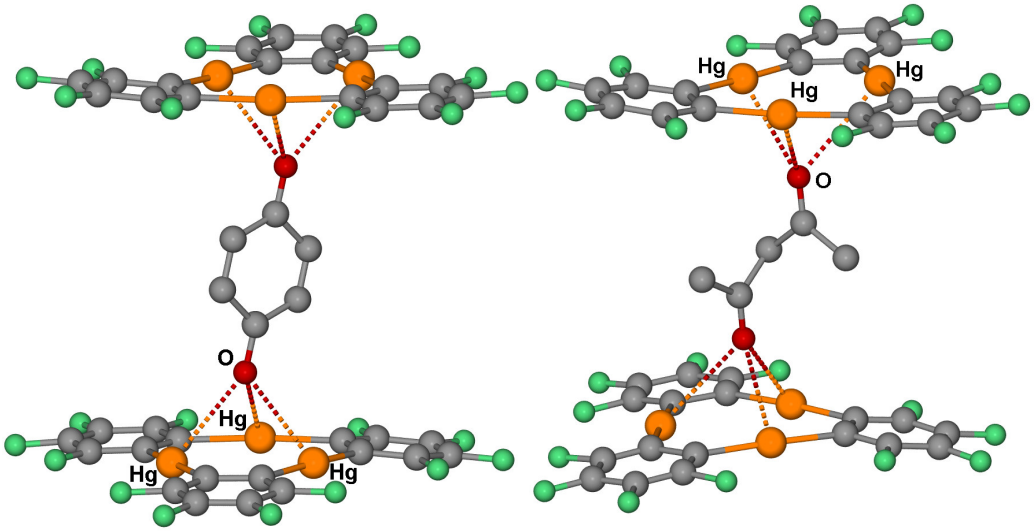

Figure I.13. Structure of [(**7**)$_2$•benzoquinone] (left) and [(**7**)$_2$•2,4-pentanedione] (right).

Compound **7** has been studied computationally (bp86 functional, basis set: 6-31g for C and F atoms, 6-31g(d') for Cl and Stuttgart RSC 1997 ECP for Hg).[51] These calculations indicate that the LUMO spans the three mercury centers and forms a large lobe that protrudes above and below the plane defined by the three mercury atoms (Figure I.14). Calculations using all-electron basis sets with the ADF program show that the LUMO bears a large contribution from the mercury 6p orbitals (44%).[72] The presence of this large lobe in the middle of the three mercury centers suggests that this particular region of the molecule where the Lewis acidity is at a maximum. In agreement with this view, this large lobe appears directly aligned with the direction along which Lewis basic substrates approach the molecule. This simple consideration suggests that formation of adducts possessing triply bridging ligands results from the

simultaneous electron donation from the ligand to the three mercury atoms resulting in four center-two electron interactions. However, the computed magnitude of the HOMO-LUMO gap, which is equal to 3.36 eV,[72] indicates that the LUMO might be too high in energy to efficiently mix with the donor orbitals of the ligand. This conclusion is also supported by the cyclic voltammogram of **1** in THF using $^{n}Bu_4PF_6$ as a supporting electrolyte which does not show any reduction in the solvent window.[72] As a result, the bonding in these adducts may in fact be dominated by electrostatic rather than covalent interactions. This conclusion is in agreement with the work of Fackler who showed that the electrostatic potential surface at the center of the trinuclear macrocycle is positive while the periphery is negative (Figure I.14).[75] In the case of soft donor atoms such as sulfur, dispersion forces probably add to the stability of the adducts.

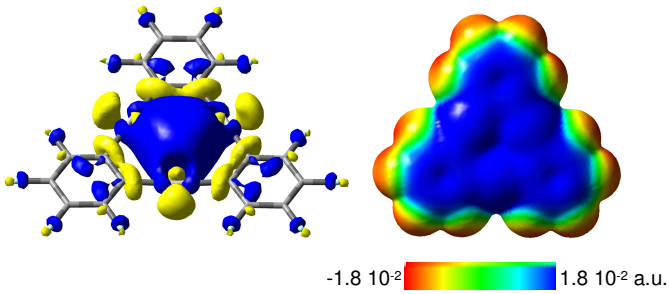

Figure I.14. LUMO (0.03 isodensity surface) and electrostatic potential surface of **7.**

I.5. Interaction of fluorinated organomercurials with aromatic hydrocarbons

Arene mercurations are electrophilic substitution reactions which result from the strong interactions that can occur between Hg(II) ions and aromatic substrates. Similar conclusions can be derived from the the isolation and structural characterization of arene-mercury π-complexes.[76-83] In these complexes, the arene is typically coordinated to the mercury atom in an η^2-fashion via Hg···C_{arene} bonds which range from 2.3 to 2.7 Å. Longer Hg···π interactions are also often observed in neutral organomercurial

derivatives which bear arene ligands.[84] With Hg···C_{arene} distances in the range of 3 to 3.4 Å, these interactions are inherently weak and have been found to occur mainly in an intramolecular fashion. Examination of the literature shows that simple organomercurials such as Ph_2Hg do not form complex with arenes. As documented in the following paragraphs, this situation can be altered in the presence of fluorinated ligands (Scheme I.8).

Scheme I.8. Aromatic hydrocarbons reported to form 1:1 adducts with the organomercurials **2**, **3**, and **7**.

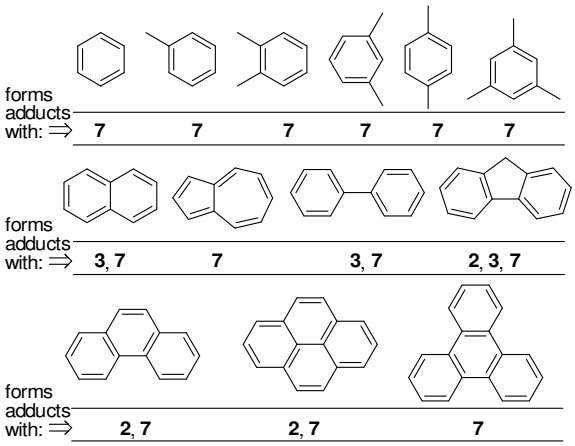

Some of the simplest adducts reported to date involve the organomercurial **5** which forms the adduct [**5**-1.5(benzene)] from a propylene oxide solution containing **5** and benzene.[47] The structure of this adduct has been determined and shows the presence of a η^1-μ-benzene molecule which bridges the mercury centers of adjacent molecules of **5** (Figure I.15). The resulting Hg···C distances of 3.16 and 3.24 Å confirm the presence of an interaction. Examination of the packing diagram also suggests the absence of significant benzene-fluoroarene interactions.

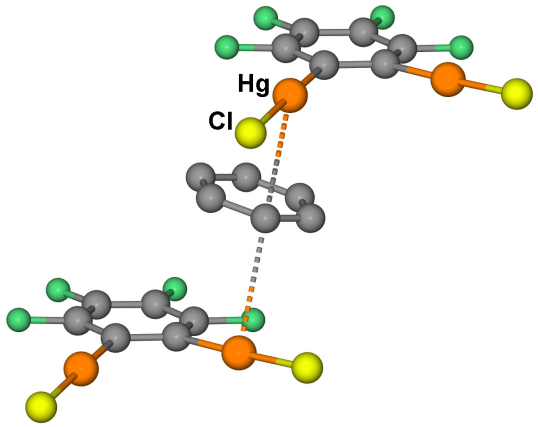

Figure I.15. Stick and ball representation of a portion of the structure of [**5**•1.5(benzene)].

The presence of a mercury chloride moiety does not appear to be a prerequisite for the formation of arene complexes. In fact, a recent study has shown that **3** forms crystalline adducts with a variety of arenes including naphthalene, biphenyl and fluorene (Chart 8).[85] The solid state structures of these adducts reveal the existence of supramolecular binary stacks where molecules of **3** alternate with the aromatic substrate. The shortest short Hg···C contacts (3.21-3.49 Å) are detected for [**3**•naphthalene] in which the naphthalene interacts with the mercury centers in a bis(trihapto) fashion (Figure I.16). Cohesion of the stacks in adducts [**3**•biphenyl] and [**3**•fluorene] can be attributed to both secondary Hg–π and perfluoroarene–arene interactions.

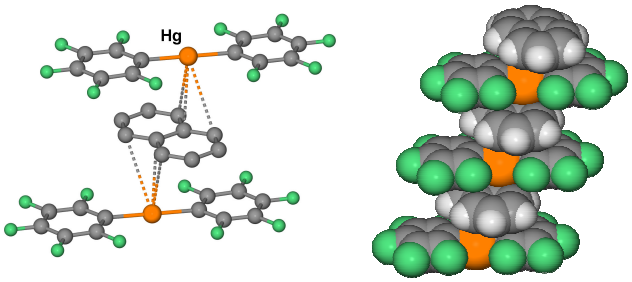

Figure I.16. Stick and ball (left) and space filling representation (right) of the structure of [**3**•naphthalene].

Similar properties are also displayed by the trinuclear complex **7** which shows a marked affinity for many arenes. For example, **7** crystallizes from benzene to afford extended binary stacks where molecules of **7** alternate with molecules of benzene (Figure I.17, Chart 8).[86] These stacks are rather compact (centroid-centroid distance of 3.24 Å) so that secondary π-interactions can be invoked between the benzene molecule and the mercury centers. Each of the six C-C bonds of the benzene molecule interacts with one of the six mercury centers of the two juxtaposed molecules of **7**. The Hg···C contacts must be relatively weak as no significant differences in the C-C bond lengths of benzene were noted. As indicated by wideline deuterium NMR, the sandwiched benzene molecules undergo an in-plane 60° reorientation with an activation energy of 52 ± 4 kJ/mol.[43] The magnitude of this activation energy suggests the presence of directional interactions between the mercury atoms of **7** and the benzene molecules.

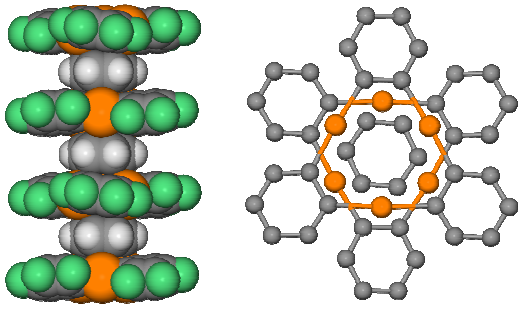

Figure I.17. Side and top views of a stack in the structure of [**7**•C_6H_6].

In order to assess how the bulk of the arene influences the structure of such stacked assemblies, the adducts of **7** with toluene, *o*-, *m*-, and *p*-xylenes, and mesitylene have been synthesized and structurally characterized (Chart 8).[87] In all cases these adducts form extended binary stacks similar to those found in [**7**•benzene]. The substituted benzene molecules adopt an apparently random orientation with respect to the trinuclear core of **7** thus suggesting that the binding might be largely dispersive and/or electrostatic. Complex **7** also forms adducts with larger aromatic substrates including biphenyl,[88] naphthalene,[88] pyrene,[89] triphenylene,[88] fluorene,[85] azulene,[90] and phenanthrene (Chart 8).[91] As for the benzene and substituted benzene adducts, the structure of the arene derivatives consists of extended stacks where molecules of **7** alternate with the aromatic substrate (Figure I.18). In the case of [**7**•triphenylene], arene-fluoroarene contacts between the two components are also present, thus adding to the stability of the stacks. Clues to the formation of some of these adducts in solution can be obtained from fluorescence quenching experiments. For example, addition of **7** to a solution of naphthalene quenches the emission of naphthalene with a Stern Volmer constant of 159±6 M^{-1}.

In all cases, donor-acceptor interactions between the arene and the Lewis acidic mercury centers may be responsible for the formation of these adducts. Keeping in mind that mercury is polarizable, the involvement of intense van der Waals interactions cannot be neglected and most certainly contribute to the formation of these supramolecules.

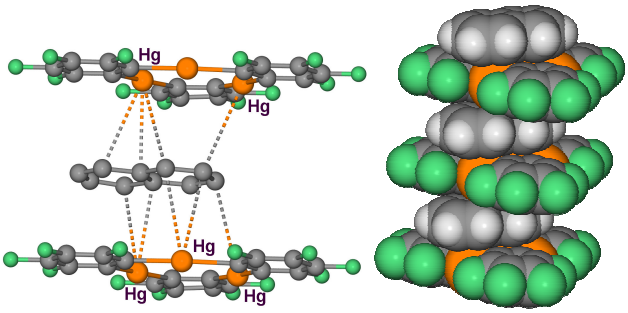

Figure I.18. Stick and ball (left) and space filling representation (right) of part of the structure of [**7**•naphthalene].

In the solid state, arene adducts of **2**, **3**, and **7** are photoluminescent and show room temperature phosphorescence of the arene. The observed phosphorescence results from the spin orbit coupling provided by the mercury atom which effectively promotes population of the triplet state of the arene via intersystem crossing. Taking into account the fact that the mercury atoms of the organomercurial are coordinated to the π-faces of the arene, such an external heavy-atom effect seems to constitute a valid explanation for the observed phosphorescence. In all cases, the emission lifetimes are shorter than those of the free arenes (Table I.2). Once again, the strong spin-orbit coupling effect caused by the mercury atoms[92] makes the radiative relaxation of the triplet state a more allowed transition, hence leading to shorter lifetimes than those exhibited by the pure organic compounds in which phosphorescence is strongly forbidden. Arene adducts of these organomercurials constitute promising materials for the development of OLED. Because the emission only results from the triplet state of the arene, emission colors can be tuned simply by varying the identity of the arene substrate. As an example, the pyrene, naphthalene, and biphenyl adducts give rise to a red, blue, and green emission, respectively (Figure I.19).

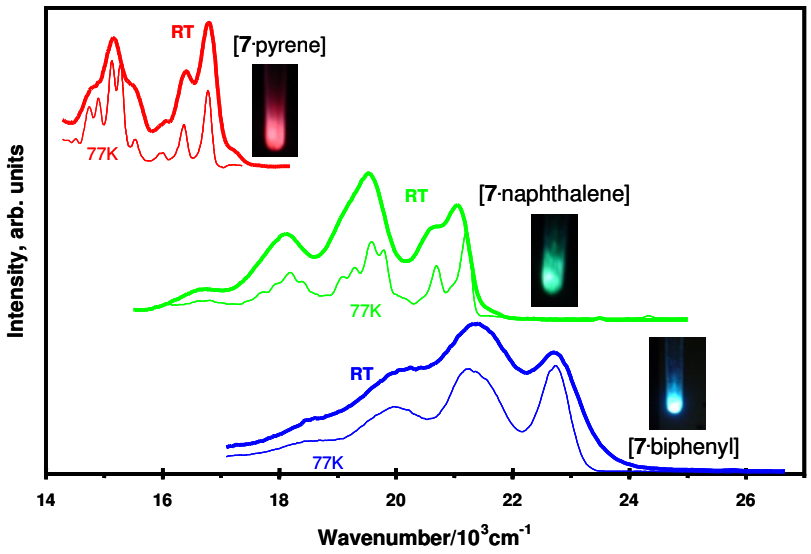

Figure I.19. Photoluminescence spectra for crystalline solids of [**7**•pyrene], [**7**•naphthalene], and [**7**•biphenyl]. Intensities of different spectra were adjusted arbitrarily for clarity. Photographs are shown for the emissions of crystalline solids at ambient temperature.

Comparative studies carried out on the naphthalene, biphenyl, and fluorene adducts **3** and **7** show that the triplet lifetimes measured for adducts involving **7** are distinctly shorter than those recorded for arene adducts of **3**. Accordingly, the triplet radiative decay rate constant of adducts involving **7** are significantly higher than those measured for adducts involving **3** (Table I.2). The drastic shortening in the lifetimes and increase in k_r values for arene adducts of **7** vs. **3** demonstrate cooperative effects between the three mercury centers in **7** that lead to more efficient phosphorescence via external heavy-atom effects.

Table I.2. Radiative Rate Constants and Triplet Lifetimes for Naphthalene, Biphenyl, and Fluorene adducts of **3** and **7**.

	k_r/s^{-1}	τ_{4K}/ms	τ_{77K}/ms*	τ_{RT}/ms
[**3**•naphthalene]	139	7.71	5.15	3.11
[**3**•biphenyl]	209	4.77	2.96	2.60
[**3**•fluorene]	264	3.32	1.56	0.976
[**7**•naphthalene]	669	1.42	0.985	0.712
[**7**•biphenyl]	1091	0.891	0.337	0.454
[**7**•fluorene]	1469	0.657	0.436	0.265
[**7**•pyrene]	-	-	0.423	0.568

*For comparison, the triplet lifetimes of pyrene, naphthalene, biphenyl and fluorene in frozen glasses are 0.7, 2.3, 4.4 and 6.3 *seconds*, respectively.

I.6. Interaction of fluorinated organomercurials with *N*-heterocycles

The use of triplet emitters in OLED has become an efficient way to improve the electroluminescence efficiency of the device.[93] Unfortunately, triplet liftimes are typically long and do not always allow for the rapid on/off switching of the emission required in displays. For these reason, strategies that would afford lifetimes in the μs range are receiving considerable attention.[94] Since chromophores with internal spin-orbit perturbation are typically more sensitive to external heavy-atom effects,[95] recent efforts have focused on the synthesis and properties of complexes involving **7** and *N*-methylcarbazole or *N*-methylindole wherein the nitrogen atom acts as an internal spin-orbit coupling perturber.[96] These recent studies build on an earlier report which clearly established the affinity of **7** for other *N*-heterocyclic substrates including 4-phenylpyridine.[61]

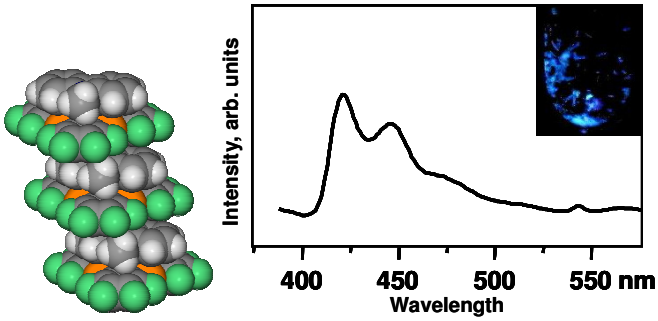

Figure I.20. Space filling view and room temperature photoluminescence spectrum of [**7**•N-methylcarbazole]. The photograph shows the emissions of the solid at ambient temperature under a hand held UV light**.**

Binary adducts containing **7** and *N*-methylcarbazole or *N*-methylindole can be readily crystallized from CH_2Cl_2. The structure [**7**•*N*-methylcarbazole] has been experimentally determined (Figure I.20).[97] It resembles the structure of arene adducts of **7** and consists of extended alternating stacks where the individual components interact via long Hg···N and Hg···C interactions. The emission spectrum of the adducts correspond to monomer phosphorescence of the *N*-heterocycles with lifetimes below 100 μs at room temperature and 77K (Figure I.20). Remarkably, the lifetimes at 77 K are shortened by five orders of magnitude when compared to those of the free *N*-heterocycles in EPA glass (Table I.3). Such lifetime reductions are unusual and most likely result from the synergy of the external mercury and internal nitrogen heavy atom effects.

Table I.3. Triplet lifetimes for *N*-heterocycles and their adducts with **7**.

	Pure	Complexed to **7**	
	EPA	Solid, 77 K	Solid, RT
N-methylindole	6.7 s	57 μs	29 μs
N-methylcarbazole	7.5 s	99 μs	49 μs

The trinuclear mercury derivative **7** also complexes carbazole to form a binary adduct whose structure has not been elucidated.[98] Interestingly, when **7** and carbazole are combined in the presence of a Lewis base such as THF or NEt_3, the ternary adducts [**7**•($C_{12}H_8NH$•THF)] and [**7**•($C_{12}H_8NH$•NEt_3)] (Figure I.21), respectively, can be isolated.[98] In these adducts, the carabazole is hydrogen bonded to the Lewis base. Both adducts have extended structures that exhibit supramolecular binary stacks where molecules of **1** and the carbazole-Lewis base complex alternate. Since carbazole alone does not form adducts with THF or NEt_3, these results suggest that complexation to **7** increases the acidity of the carbazole substrate.

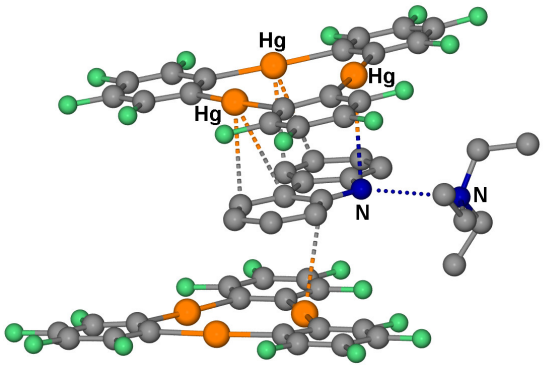

Figure I.21. View of part of the structure of [**7**•($C_{12}H_8NH$•NEt_3)].

I.7. Interaction of fluorinated organomercurials with neutral inorganic and organometallic complexes

Simple mixing of **7** with ferrocene or nickelocene results in the formation of supramolecular electrophilic double-sandwiches in which each cyclopentadienide ring of the metallocene is capped by a molecule of **7** (Figure I.22). The shortest Hg···C distances range from 3.20–3.24 Å and indicate that the carbon atoms of the Cp rings are in close contact with the mercury centers.[99] Unlike pure nickelocene, which is air

sensitive and displays a green color, the nickelocene adduct [(**7**)$_2$•NiCp$_2$] is air-stable and dark red. The unusual color of this complex results from an increase in the intensity of the formally spin forbidden $^3A_{2g} \rightarrow {}^1E_{1g}$ transition indicating the occurrence of a mercury heavy atom effect.

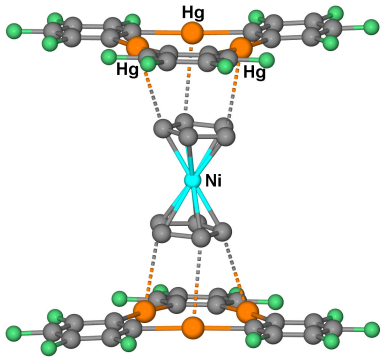

Figure I.22. Molecular structure of [(**7**)$_2$•NiCp$_2$].

Trinuclear **7** also shows a marked affinity of electron rich gold complexes including [Au(μ-C$_2$,N$_3$-bzim)]$_3$ (bzim = 1-benzylimidazolate) with which it interacts in solution as indicated by ^{19}F/^{1}H-HOESY and PGSE NMR measurements. [75, 100] The trinuclear organomercurial **7** crystallizes with two molecules of [Au(μ-C$_2$,N$_3$-bzim)]$_3$ to form extended chains in which the organomercurial is sandwiched by two molecules of the gold complex (Figure I.23).[75] Examination of the structure of these complexes shows the presence of metallophilic Hg···Au interactions of 3.27 and 3.24 Å which appear to be complemented by electrostatic interactions between the π-basic gold complex and the π-acidic mercury derivative.

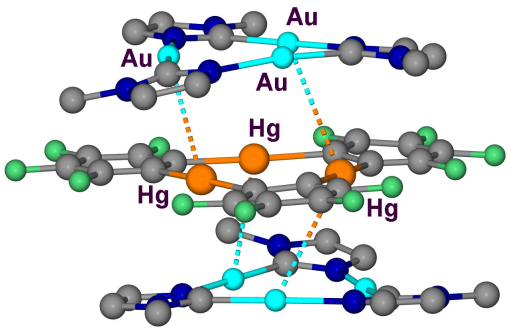

Figure I.23. Molecular structure of the 2:1 adduct formed by $[Au(\mu\text{-}C_2,N_3\text{-bzim})]_3$ and **7**. The phenyl groups of the benzylimidazolate ligands are omitted.

I.8. Conclusion

The results discussed in this review show that the introduction of fluorinated ligands into organomercurials has a dramatic effect on their Lewis acidic properties. This effect most likely results from an increase in the positive charge developed by the mercury atoms along with a lowering of the energy of the vacant orbitals. As a result, fluorinated organomercurials form Lewis adducts with numerous bases. Similar effects can be invoked in the chemistry of mercuracarborands which also possess Lewis acidic mercury centers.[101, 102]

Surprisingly, fluorinated organomercurials also have an affinity for aromatic substrates, alkynes and *N*-heterocycles with which they form unusual π-complexes. In addition to possessing unprecedented structures, these π-complexes show a set of distinctive properties imparted by the presence of the mercury atoms. Specifically, the mercury atoms act as spin orbit coupling perturbers and trigger the phosphorescence of the π-complexed substrates. This approach is extremely general and is likely to find application in the design of light emitting devices.

CHAPTER II

TRIMERIC PERFLUORO-*ORTHO*-PHENYLENE MERCURY: REACTIVITY, PURE AND SOLVATED STRUCTURES, AND LEWIS ACIDIC SUPRAMOLECULAR CHEMISTRY

II.1. Introduction

Trimeric *ortho*-phenylene mercury [103, 104] and its derivatives [52, 105] have been studied extensively in the past five decades. Such compounds constitute valuable starting materials for the synthesis of other organometallic compounds that posses the *ortho*-phenylene backbone. The fluorinated derivative [*o*-$C_6F_4Hg]_3$ (**7**, Scheme II.1) has unusual Lewis acidic properties and forms adducts with a variety of electron-rich substrates.

In this chapter, recent results which add to the understanding of the chemistry of **7** will be detailed.

Scheme II.1

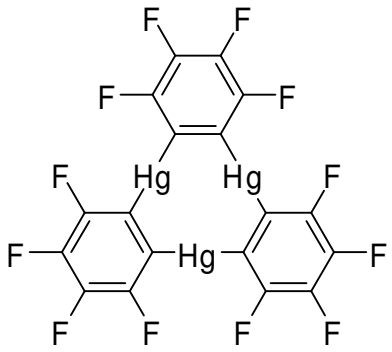

II.2. Solvated structure of $[o\text{-}C_6F_4Hg]_3$ and 1,2-dichloroethane

The trimeric nature of **7** was firmly established by Massey, [106, 107] and a variety of polymorphic forms of **7** were investigated by Gabbaï *et al.*[60] The latter study notes that all of the different polymorphs of **7** display very similar intramolecular structures; the molecules of **7** are co-planar and self-assemble with Hg-Hg distances of 3.5 Å and greater. The extended packing observed in the structures was rationalized by invoking electrostatic, mercuriophilic, and mercury-π secondary interactions.

In the majority of cases when solvents are co-crystallized with **7**, the more Lewis basic atoms of the solvent are conspicuously close to multiple mercury sites. Polar solvents such as DMF, [53, 65, 66] acetone, [62, 63] DMSO, [64] and ethylacetate form complexes where the terminal oxygen atom of the substrate engages in secondary contacts with the three mercury atoms. In turn, the whole of the substrate is positioned above the molecular plane of **7**. Solvents such as acetonitrile [53, 66] and THF [108] that do not have terminal oxo-functionalities form similar complexes with **7** as well.

When **7** is crystallized from 1,2-dichloroethane (DCE), the resulting solvated structure [$\mathbf{7}_2$•DCE] (**8**, Figure II.1) is realized. The types of interactions present in the structure seem to be intermediate between those present in the pure crystals of **7** and the adducts described above. The chlorine atoms of DCE interact with only one mercury center and intermolecular mercuriophilic contacts between molecules of **7** are still prominent.

Compound **8** crystallizes as large rectangular blocks from saturated dichloroethane solutions. The crystals belong to the monoclinic space group $P2_1/c$. The asymmetric unit contains one molecule of **7** and half of a molecule of dichloroethane that straddles an inversion center. Neither **7** nor the dichloroethane display any notable intramolecular distortions. The molecules of **7** form extended stacks. These stacks, which are tilted by 45.8º from the normal, consist of eclipsed molecules of **7** whose planes are parallel. The stacking motif adopted by the molecules of **7** in **8** is similar to that observed in the orthorhombic modification in pure **7**.[60] There are intermolecular Hg-Hg contacts (Hg(1)-Hg(2A) 3.79 and Hg(1)-Hg(3A) 3.90 Å) which are close to those

found in the polymorphs of **7**. The chlorine atoms of DCE have a close contact of 3.303(6) Å with a single mercury atom, Hg(1). Unlike many other adducts of **7** and molecules featuring terminal Lewis basic atoms, the chlorines do not interact with all three Lewis acid sites of **7**. Instead they sit to the "side" of two different molecules of **7** and terminally ligate to a single mercury atom in a manner similar to one of the acetone molecules in the compound [**7**•(μ_3-acetone)$_2$(acetone)]. [62]

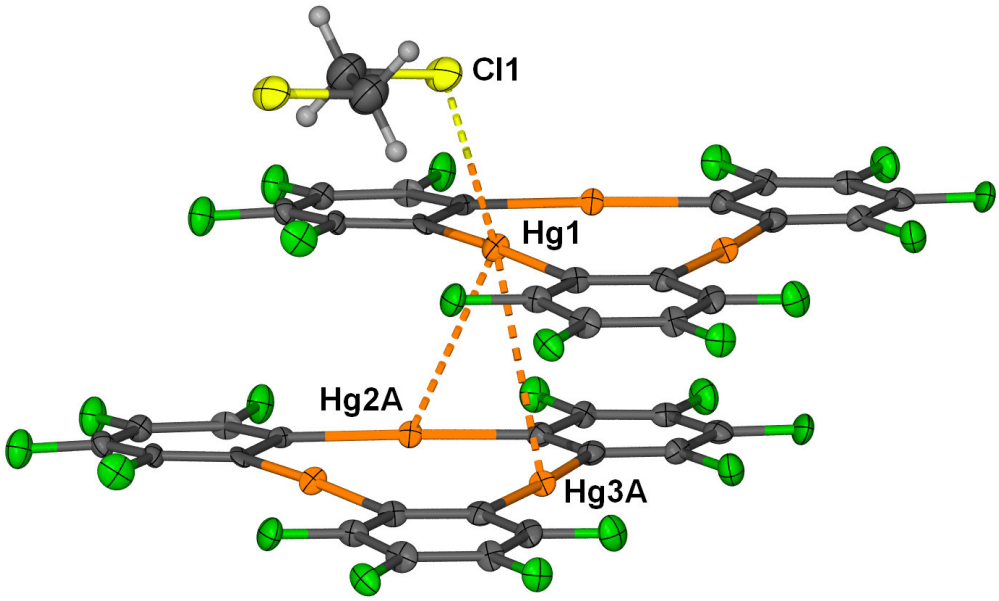

Figure II.1. ORTEP view (50% ellipsoid) of the intermolecular interactions in **8**. Representative intermolecular distances (Å): Hg(1)-Cl(1) 3.30, Hg(1)-Hg(2A) 3.79; Hg(1)-Hg(3A) 3.90.

II.3. Adducts of [*o*-$C_6F_4Hg]_3$ and molecules featuring Lewis basic heteroatoms: triphenylphosphine oxide and 2-phenyl-5-(4-biphenylyl)-1,3,4-oxadiazole

Scheme II.2

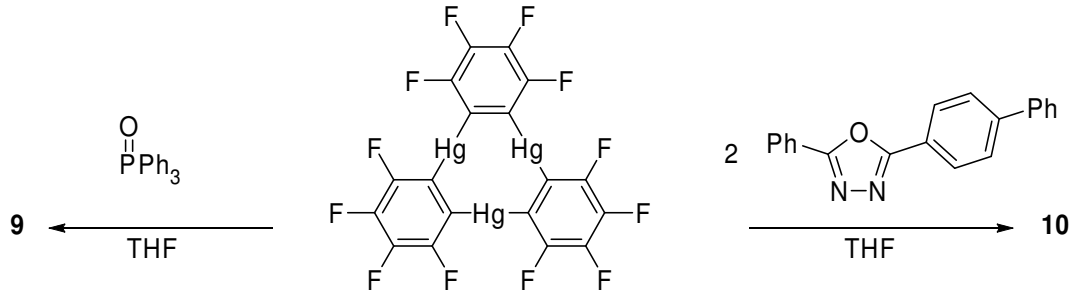

Adducts containing **7** and organic substrates with Lewis basic oxygen atoms, in particular acetone and hexamethylphosphoramide, often have the oxygen atom directly bound to the three mercury centers of **7**. [62-64] Additionally, some of these adducts [63] self-assemble to form cofacial dimers featuring two molecules of **7** with close intermolecular Hg-Hg interactions, described as "mercurophilic." While hexamethylphosphoramide (HMPA) forms a 2:1 complex with **7**, [**7**•$(HMPA)_2$], with a donor ligand on either side of the molecular plane of **7**, experiments carried out as part of this thesis show that **7** and triphenylphosphine oxide form a 1:1 adduct.

Slow concentration of a THF solution of **7** containing a 5-fold excess of triphenylphosphine oxide affords small clear crystals of **9**. Compound **9** crystallizes in the monoclinic space group $P2_1/c$ with one molecule of **7** and triphenylphosphine oxide in the asymmetric unit. The phosphoryl oxygen is pointing toward the molecular plane of **7** and is simultaneously coordinated to the three mercury centers. The Hg-O distances range from 2.77 to 2.83 Å and are within the sum of the van der Waals distances for oxygen (r_{vdw} = 1.54 Å) [109] and mercury (r_{vdw} = 1.75 Å). [110, 111] They approach the Hg-O distances found in the triply bridging acetone molecules of [**7**•μ_3-acetone] (av. 2.90 Å),

[63] [**7**•(μ_3-acetone)$_2$(acetone)] (av. 2.88 Å),[62] and [**7**•(μ_3-DMF)$_2$] (av 2.87 Å).[64] In fact, the oxygen atom sits 1.90 Å from the plane defined by the three mercury sites. The O=P distance is slightly longer (0.03 Å) than the normal 1.48 Å in the pure compound. Additionally, there is appears to be a further interaction, namely an arene-fluoroarene between the tetrafluoroarene moiety containing C(7) and the phenyl group containing C(25) with a distance of 3.53 Å between the centroids of the two rings.

Further analysis of the structure reveals that the molecules of [**7**•μ_3-O=PPh$_3$] are associated with one another as cofacial dimers (Figure II.2). The molecular planes of the two molecules of **7** in a given dimer are separated by 3.49 Å and are offset from one another. This arrangement leads to a significant Hg(1) – Hg(3A) intermolecular contact of 3.59 Å.

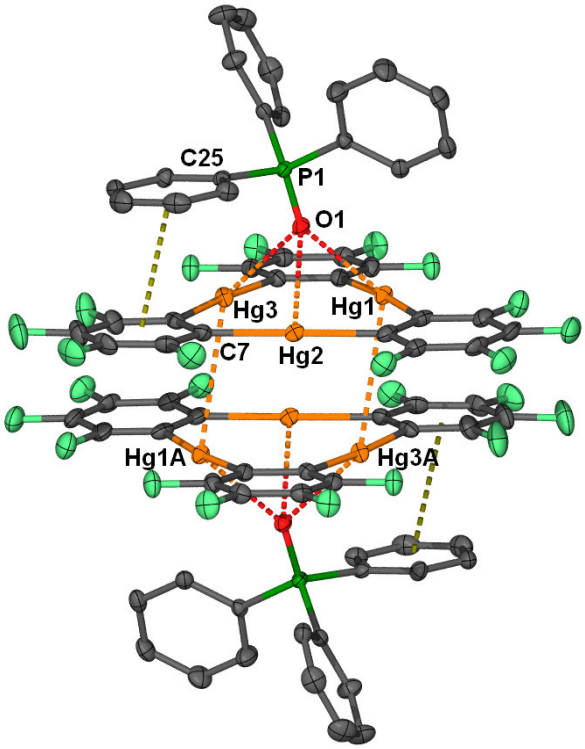

Figure II.2. ORTEP view (50% ellipsoid) of the intermolecular interactions in **9** displaying a centroid–centroid interaction of 3.53 Å. Representative intermolecular distances (Å): Hg(1)-O(1) 2.77, Hg(2)-O(1) 2.83 Hg(3)-O(1) 2.83, Hg(1)-Hg(3A) 3.59.

While **9** features a terminal Lewis basic atom, this is not a prerequisite for adduct formation with **7**. In fact, heterocycles have been noted to also interact with **7** to form binary adducts. Documented examples include [**7**•4-phenylpyridine], [61] [**7**•*N*-methylcarbazole], [**7**•*N*-methylindole] [97] and [**7**•carbazole]. [98] The compound 2-phenyl-5-(4-biphenylyl)-1,3,4-oxadiazole (PBD), [112] which has been used extensively as an additive in electroluminescent displays, forms a 2:1 adduct with **7** (**10**) where the nitrogen atoms of the central oxadiazole ring form the closest contacts with the mercury centers.

Compound **10** (Figure II.3) crystallizes in the orthorhombic space group *P*ca2_1. The space group is chiral, and the crystals appear to be 1:1 racemates (Flack parameter of 0.48). [113] There are two molecules of PBD and one of **7** in the asymmetric unit. There are no abnormal intramolecular distances with any of the components. The nitrogens of the two oxadiazole rings of the PBD molecules approach the molecular plane of **7** and each of the nitrogen atoms has a close contact with a mercury atom at distances ranging from 2.92-3.23 Å. These distances are well within the van der Waals radii of mercury[110, 111] and nitrogen (limit 3.7 Å) [114] indicating the presence of secondary Hg-N interactions. Surprisingly, the lone oxygen atoms are not engaged in any similar secondary contacts. This may be a consequence of the steric congestion arising from the 2,5-substitution of the heterocycle of PBD that precludes any close approach. There appears to be no perfluoroarene/arene interactions in the crystal, and both the phenyl and biphenyl arms do not engage in any significant contacts.

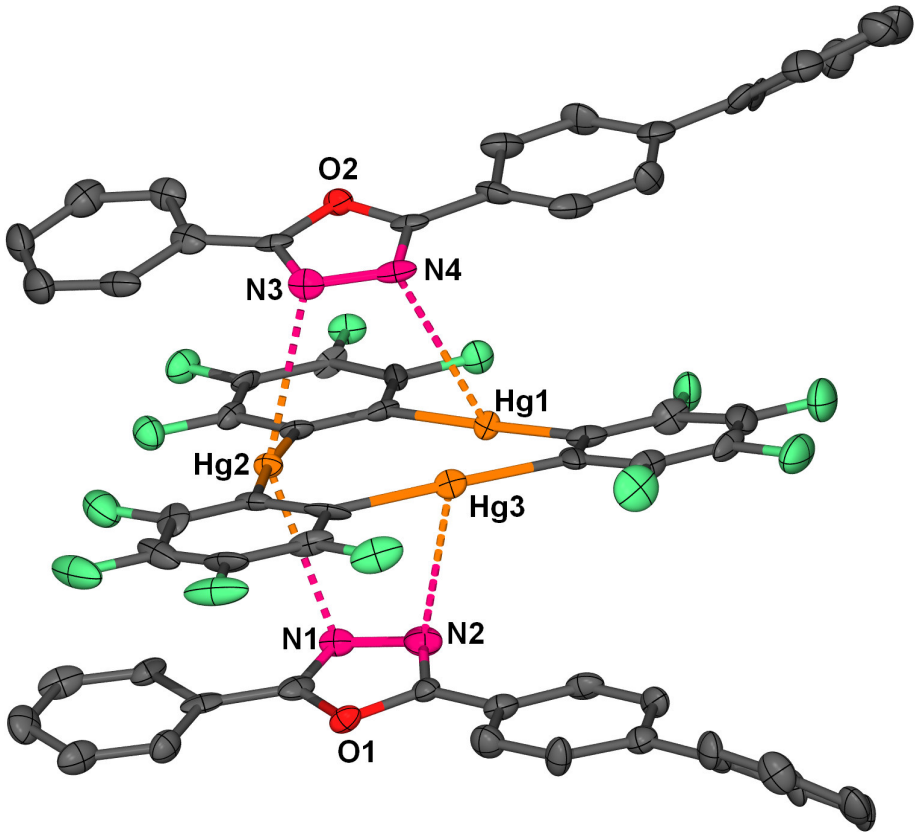

Figure II.3. ORTEP view (50% ellipsoid) of the intermolecular interactions in **10**. Representative intermolecular distances (Å): N(1)-Hg(2) 2.94, N(2)-Hg(1) 3.23, N(3)-Hg(2) 2.92, N(4)-Hg(3) 3.22.

II.4. Transmetallation of $[o\text{-}C_6F_4Hg]_3$ by $Zn(0)/ZnCl_2$

Transmetallation reactions using organomercurials with low-valent main group compounds are often used to gain access to the chemistry of organo-main-group derivatives. For example, *ortho*-phenylene zinc can be prepared from trimeric *ortho*-phenylene mercury and elemental zinc in THF. [115] Interestingly, analogous reactions with **7** have not been investigated. Bearing in mind that **7** reacts with InBr to afford 9,10-dibromo-9,10-dihydro-9,10-diindaoctafluoroanthracene, [116] we decided to investigate its reactivity with zinc.

It was discovered that **7** does not react in THF with only zinc metal or zinc dichloride. Surprisingly, **7** reacts with a mixture of zinc powder and zinc dichloride in anhydrous THF to afford the tetranuclear complex **11** (Scheme II.3). This compound is very insoluble and its characterization by NMR has not been successful. It is isolated from the residue in the form of single crystals that are typically coated with zinc dust and zinc chloride. Its identity has been established solely on the basis of X-ray diffraction studies (*vide infra*).

Scheme II.3

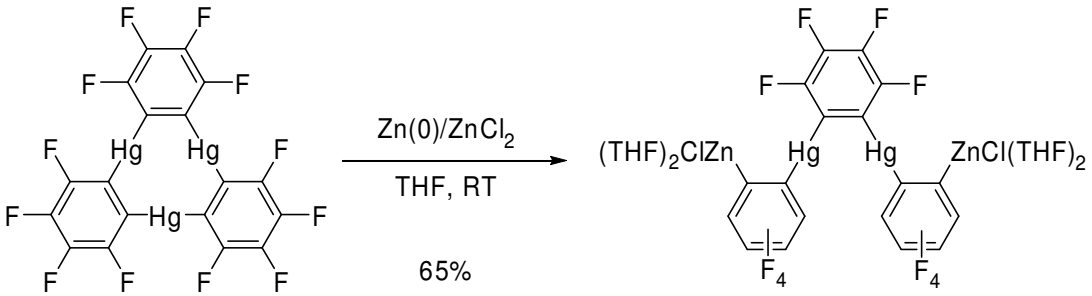

The mechanism leading to the formation of this derivative remains somewhat obscure because **7** fails to react with zinc metal or zinc dichloride exclusively. Because of the complication associated to the isolation and purification of this derivative, its chemistry has not been pursued to date.

Compound **11** crystallizes in the orthorhombic space group *P*bcn with four C_2 symmetric molecules in the unit cell. With a C(1)-Hg(1)-C(7) angle of 176.6(2)°, the coordination geometry around the mercury center remains essentially linear (Figure II.4). The zinc atom of the phenylene zinc chloride moiety is coordinated to two THF ligands and adopts a distorted tetrahedral geometry. This distortion, which most likely results from the hindered structure of this derivative, leads to a O(1)-Zn(1)-O(2) angle of 90.93(15)° which is much smaller than the expected 109 °. The chloride ligand Cl(1)

forms secondary interactions with the two symmetry related mercury atoms Hg(1) and Hg(1A). These interactions (Hg(1)-Cl(1) = 3.1645(15), Hg(1A)-Cl(1) = 3.236(3) Å) are within the limit of the sum of the van der Waals radii (r_{vdw}(F) = 1.30-1.38 Å, r_{vdw}(Cl) = 1.58-1.78 Å, [109] r_{vdw}(Hg) = 1.73-2.00 Å), [110, 111] and do not affect the Zn(1)-Cl(1) bond (2.2364(14) Å) which falls in the expected range. Finally, it is worth noting that the C(1)-C(2) bond formed by the two metallated carbons of the *ortho*-phenylene ring linking the zinc and mercury atoms is significantly elongated (1.440(7) Å) when compared to the other C-C bonds of the phenylene ring (av. 1.38 Å). We propose that this distortion results from the steric crowding present in this derivative.

There is also another solid state structure of **11** that crystallizes in the monoclinic space group $P2_1/c$ but there appears to be adventitious solvent and the structure does not model satisfactorily. These results are included in Table II.2 as $\mathbf{11}_{Mono}$.

II.5. Experimental

General. Extra care was taken at all times to avoid contact with solid, solution, and airborne particulate mercury compounds. **7** was prepared according to the reported procedures.[52] 1,2-dichloroethane (Fisher Scientific) and tripenyphosphine oxide (Aldrich) were used as received. THF was distilled over Na/K amalgam. Zinc chloride (granular, EM Science) was dried with heat gun under vacuum prior to use, and zinc metal (dust, Aldrich) was stirred with 2% HCl, 3 washes of water, 2 washes ethanol, and then diethyl ether prior to drying under vacuum. Air-sensitive compounds were handled under N_2 atmosphere using standard Schlenk and glovebox techniques. The crystallographic measurements were performed using a Siemens SMART-CCD area detector diffractometer, with a graphite-monochromated Mo-K_α radiation (λ = 0.71069 Å). Specimens of suitable size and quality were selected and mounted onto glass fiber with apiezon grease. The structures were solved by direct methods, which successfully located most of the non-hydrogen atoms. Subsequent refinement on F^2 using the SHELXTL/PC package (version 5.1) allowed location of the remaining non-hydrogen atoms. Further crystallographic details can be found in Table II.1 and Table II.2.

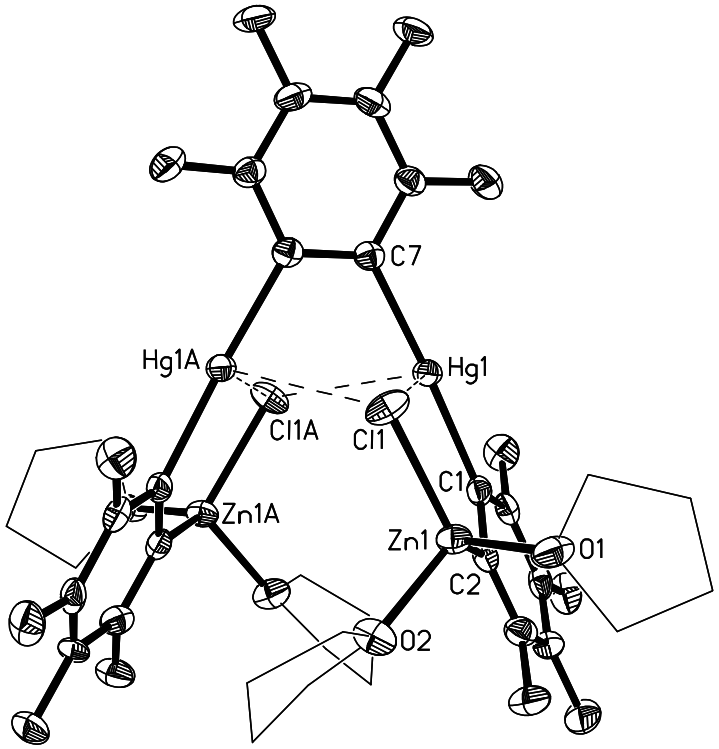

Figure II.4. ORTEP view of **11** (50% ellipsoid, C_{THF} and H atoms omitted for clarity). Selected distances (Å) and angles (deg): Zn(1)-C(2) 1.955(5), Zn(1)-O(2) 2.034(3), Zn(1)-O(1) 2.044(3), Zn(1)-Cl(1) 2.2364(14), Hg(1)-C(1) 2.080(5), Hg(1)-C(7) 2.096(5), Hg(1)-Cl(1) 3.1645(15), Hg(1A)-Cl(1) 3.236(3) Å, Hg(1)-Hg(1A) 3.4384(10), C(1)-C(2) 1.440(7), O(2)-Zn(1)-O(1) 90.93(15), C(2)-Zn(1)-Cl(1) 117.62(15), C(1)-Hg(1)-C(7) 176.6(2).

Table II.1. Crystal data, data collection, and structure refinement for **8**, **9**, and **10**.

Crystal data	**8**	**9**	**10**
Formula	$C_{19}H_2ClF_{12}Hg_3$	$C_{36}H_{15}F_{12}Hg_3OP$	$C_{58}H_{28}F_{12}Hg_3N_4O_2$
M_r	1095.43	1324.22	1335.42
Crystal size (mm^3)	0.20 × 0.18 × 0.07	0.10 × 0.08 × 0.07	0.28 × 0. 22 × 0.08
Crystal system	Monoclinic	Monoclinic	Orthorhombic
Space group	$P2_1/c$	$P2_1/c$	$Pca2_1$
a (Å)	20.538(4)	11.4075(9)	13.732(6)
b (Å)	4.8259(10)	20.8596(16)	12.344(5)
c (Å)	22.342(5)	14.0225(11)	29.426(13)
β (°)	114.04(3)	97.443(2)	90
V ($Å^3$)	2022.3(7)	3325.2(4)	4988(4)
Z	4	4	4
ρ_{calc} (gcm^{-3})	3.598	2.645	2.187
μ (mm^{-1})	22.968	13.964	9.306
F(000) (e)	1924	2408	3072
Data Collection			
T/K	110(2)	110(2)	110(2)
Scan mode	ω	ω	ω
hkl range	-23→21, -5→5, -25→25	-15→15, -27→27, -18→18	-17→17, -16→15, -37→38
Measured refl.	12373	38507	41349
Unique refl., [R_{int}]	3180 [0.0560]	8115 [0.0346]	11339 [0.1006]
Refl. used for refinement	3180	8115	11339
Absorption Correction	SADABS	SADABS	SADABS
T_{min}/T_{max}	0.348128	0.541271	0.325441
Refinement			
Refined parameters	304	478	707
R_1,[a] wR_2[b] [I>2σ (I)]	0.0682, 0.1512	0.0218, 0.0416	0.0583, 0.1020
ρ_{fin} (max/min) ($eÅ^{-3}$)	9.628, -3.507	3.597, -1.521	2.330, -2.219

[a] $R1 = (F_o - F_c)/ F_o$.[b] $wR2 = \{[w(F_o^2 - F_c^2)^2]/ [w(F_o^2)^2]\}^{1/2}$; $w = 1/[\sigma^2(F_o^2) + (ap)^2 + bp]$; $p = (F_o^2 + 2F_c^2)/3$; *a* = 0.1350 (**8**), 0.0135 (**9**), 0.0384 (**10**); *b* = 0.0 (**8**), 3.2432 (**9**), 0.0 (**10**)

Table II.2. Crystal data, data collection, and structure refinement for **11** and **11$_{Mono}$**.

Crystal data	**11**	**11$_{Mono}$**
Formula	$C_{34}H_{32}Cl_2F_{12}Hg_2O_4Zn_2$	$C_{34}H_{32}Cl_2F_{12}Hg_2O_4Zn_2$
M_r	1335.42	1299.87
Crystal size (mm^3)	0.22 × 0. 21 × 0.19	0.20 × 0.20 × 0.08
Crystal system	Orthorhombic	Monoclinic
Space group	*P*bcn	$P2_1/c$
a (Å)	16.551(4)	13.577(3)
b (Å)	12.491(3)	18.268(4)
c (Å)	18.844(5)	20.917(4)
β (°)	90	104.61(3)
V ($Å^3$)	3895.8(17)	5020.1(17)
Z	4	4
ρ_{calc} (gcm^{-3})	2.277	1.720
μ (mm^{-1})	9.306	6.165
F(000) (e)	2520	2536
Data Collection		
T/K	110(2)	110(2)
Scan mode	ω	ω
hkl range	-17→18, -14→14, -19→21	-14→15, -20→20, -23→23
Measured refl.	25039	15512
Unique refl., [R_{int}]	3059 [0.1143]	3644[0.0317]
Refl. used for refinement	3059	3644
Absorption Correction	PSI-SCAN	SADABS
T_{min}/T_{max}	0.3271/0.8304	0.643611
Refinement		
Refined parameters	253	316
R_1,[a] wR_2[b] [I>2σ(I)]	0.0277, 0.0664	0.0210, 0.0529
ρ_{fin} (max/min) ($eÅ^{-3}$)	1.633, -1.773	0.561, -0.596

[a] $R1 = (F_o - F_c)/ F_o$.[b] $wR2 = \{[w(F_o^2 - F_c^2)^2]/ [w(F_o^2)^2]\}^{1/2}$; $w = 1/[\sigma^2(F_o^2) + (ap)^2 + bp]$; $p = (F_o^2 + 2F_c^2)/3$; *a* = 0.1350 (**11**), 0.0500 (**11$_{Mono}$**); *b* = 0.0 (**11**), 3.2432 (**11$_{Mono}$**).

Synthesis of [(7)$_2$•1,2-dichloroethane] (8). Compound **7** (15 mg, 0.014 mmol) was dissolved in 1,2-dichloroethane (5 mL). Upon slow evaporation large rectangular blocks of **8** formed at the bottom the vial in 95% yield (14.5 mg, 0.007 mmol).

Synthesis of [7•triphenylphosphine oxide] (9). Compound **7** (10 mg, 0.009 mmol) and triphenylphosphine oxide (10 mg, 0.033 mmol) were dissolved in 10 mL of CH_2Cl_2. Slow evaporation of the solvent led to the formation of colorless blocks which were washed twice with *n*-pentane to afford **9** in 80% yield (9.5 mg, 0.007 mmol).

Synthesis of [7•(2-phenyl-5-(4-biphenylyl)-1,3,4-oxadiazole)$_2$] (10). Compound **7** (15 mg, 0.014 mmol) and 2-phenyl-5-(4-biphenylyl)-1,3,4-oxadiazole (15 mg, 0.050 mmol) were dissolved in 10 mL of CH_2Cl_2. Slow evaporation of the solvent led to the formation of colorless blocks of mixed material with both starting material and **10** (this did not change even with excess **7**) and the crystals had to be extracted manually. Yield: 30% yield (7 mg, 0.004 mmol).

Synthesis of transmetallation products (11 and 11$_{Mono}$). In a glovebox under an argon atmosphere, **7** (0.006 g, 0.006 mmol) and an excess of zinc chloride (20 mg, 0.148 mmol) were dissolved in a THF (5 mL) suspension of zinc metal (10 mg, 0.154 mmol). Without any further agitation, colorless, highly air and water-sensitive block crystals of **11** formed on the sides and bottom of the reaction vial within 2 hr. Compound **11** was isolated in 65% yield (5mg) and washed with more THF.

CHAPTER III

SUPRAMOLECULAR STABILIZATION OF α,ω -DIPHENYLPOLYYNES BY COMPLEXATION TO THE TRIDENTATE LEWIS ACID TRIMERIC PERFLUORO-*ORTHO*-PHENYLENE MERCURY*

III.1. Introduction

Infinitely repeating sp-hybridized carbon atoms, known as "carbyne", is a much discussed one-dimensional allotrope of carbon whose instability has complicated isolation and definitive characterization. [117-119] Similar complications are also encountered in the synthesis and isolation of short chains of sp-hybridized carbon atoms, namely polyynes. Owing to these limitations, recent efforts have been directed to the development of methods allowing for the stabilization of polyynes. [120-123] Although the incorporation of electropositive end-groups has enabled the isolation of complexes featuring up to 28 consecutive sp-carbon atoms, [124] the exposed nature of the polyyne chain is often associated with the instability of such compounds which tend to undergo photochemically or thermally induced polymerization and oxidation reactions. [125] As a result, the incorporation of covalently bound end-groups which can protect and thus insulate the more exposed part of the molecule has often been considered. Such an approach is nicely illustrated by the work of Gladysz who reported a series of diplatinum polyynediyl complexes in which the polyyne is shielded by the alkanediyl chains of two bridging diphosphines. [126] Using a different approach, Hirsch was able to prepare a stable decayne bearing aromatic polyether dendrimers as end-groups. [127] As shown by some of our recent work, trimeric perfluoro-*ortho*-phenylene mercury (**7**, [*o*-$C_6F_4Hg]_3$)

---

* Reprinted in part with permission from Taylor, T. J.; Gabbaï, F. P. "Supramolecular stabilization of α,ω-diphenylpolyynes by complexation to the tridentate Lewis acid [*o*-$C_6F_4Hg]_3$" *Organometallics*, *127*, 12166, Copyright 2005 by the American Chemical Society.

"sticks" to the π-face of aromatic substrates to form extended binary supramolecules in which both components alternate. [43, 97, 99] In all cases, the mercury centers of the trinuclear mercury complex approach the π-face of the substrate and engage in polyhapto secondary Hg-C interactions in the 3.3-3.6 Å range. Taking into account the affinity that mercury(II) cations display for alkynes, [128] we decided to determine if **7** could also form supramolecular adducts with polyynes. If successful, it occurred to us that such an approach may serve to enhance the stability of otherwise highly reactive substrates.

Scheme III.1

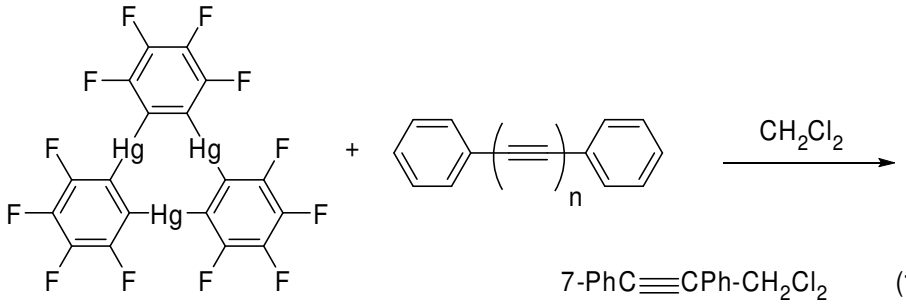

7-PhC≡CPh-CH_2Cl_2 (**12**)
$(7)_2$-Ph$(C{\equiv}C)_2$Ph (**13**)
7-Ph$(C{\equiv}C)_3$Ph (**14**)
$(7)_2$-Ph$(C{\equiv}C)_4$Ph (**15**)
$(7)_2$-Ph$(C{\equiv}C)_6$Ph-CH_2Cl_2 (**16**)
7-(Ph$(C{\equiv}C)_6$Ph)$_2$ (**17**)

III.2. Preliminary investigation with diphenylacetylene and $[o\text{-}C_6F_4Hg]_3$

In order to provide initial evidence for the affinity of **7** for alkynes, we first studied its interaction with diphenylacetylene. Combination of **7** with diphenylacetylene in CH_2Cl_2 followed by slow evaporation of the solvent leads to the crystallization of **[7•**diphenylacetylene•CH_2Cl_2**]** (**12**). Elemental analysis indicated that compound **12** eventually decomposes due to solvent loss.

Compound **12** crystallizes in the triclinic space group *P*-1 with one molecule of each component present in the asymmetric unit. The compound forms canted binary stacks with alternating molecules of **7** and diphenylacetylene (Figure III.1). The stacks are bordered by CH_2Cl_2 molecules on one side which fill the gap that are present due to the size difference of **7** and diphenylacetylene. The Ph-Ph dihedral angle of the tolane is 5.9 °. The molecule of **7** exhibits a slight deviation from planarity as well, where two of the phenylene rings are co-planar while one phenylene ring has a dihedral angle of 6.0 ° with respect to the plane of the other phenylene rings. There are no short perfluoroarene–arene interactions. The diphenylacetylene molecule interacts with the mercury centers of **7** via Hg-$C_{aromatic}$ and Hg-C_{alkyne} interactions in the range of 3.22 – 3.34 Å (Figure III.1). The formation of these stacks may be attributed to these secondary interactions which are largely dispersive in nature.

III.3. Synthesis and characterization of the adducts **13**-**17**

The formation of adducts involving **7** and α,ω-diphenylpolyynes with 4, 6, 8, and 12 sp-carbon atoms was originally surveyed by mixing equimolar quantities of **7** with the corresponding α,ω-diphenylpolyynes in CH_2Cl_2 (Scheme III.1). Slow evaporation of the solvent resulted in the crystallization of **7**•$Ph(C{\equiv}C)_3Ph$ (**14**) as a 1:1 adduct and (**7**)$_2$•$Ph(C{\equiv}C)_2Ph$ (**13**), and (**7**)$_2$•$Ph(C{\equiv}C)_4Ph$ (**15**) as 2:1 adducts. In most cases, varying the ratio of **7** to the α,ω-diphenylpolyynes in the starting mixtures did not affect the composition of the adducts. In order to optimize the yields of the 2:1 adducts, their synthesis were repeated by mixing two equivalents of **7** with one equivalent of the corresponding α,ω-diphenylpolyyne. Crystals of (**7**)$_2$•$Ph(C{\equiv}C)_6Ph$•CH_2Cl_2 (**16**) were obtained by chilling a 2:1 mixture of **7** and $Ph(C{\equiv}C)_6Ph$ in CH_2Cl_2. The solution decomposition of the polyyne prior to crystallization is partly responsible for the low isolated yields of **14-16** which do not exceed 40%. Saturated solutions of excess $Ph(C{\equiv}C)_6Ph$ and minimal **7** also formed a second molecular crystal compound upon extending chilling at -20 ºC. This compound, [**7**•$(Ph(C{\equiv}C)_6Ph)_2$], (**17**), was formed in very low (< 10%) yield as dense yellow flakes at the interface of the saturated solution.

Due to the small amount of material available, only structural characterization was possible. Adducts **13** and **14** are colorless while adducts **15-17** display yellow hues which, *a priori*, correspond to the color of the pure polyynes. All adducts are air stable with the exception of **16**, which decomposes by loss of CH_2Cl_2.

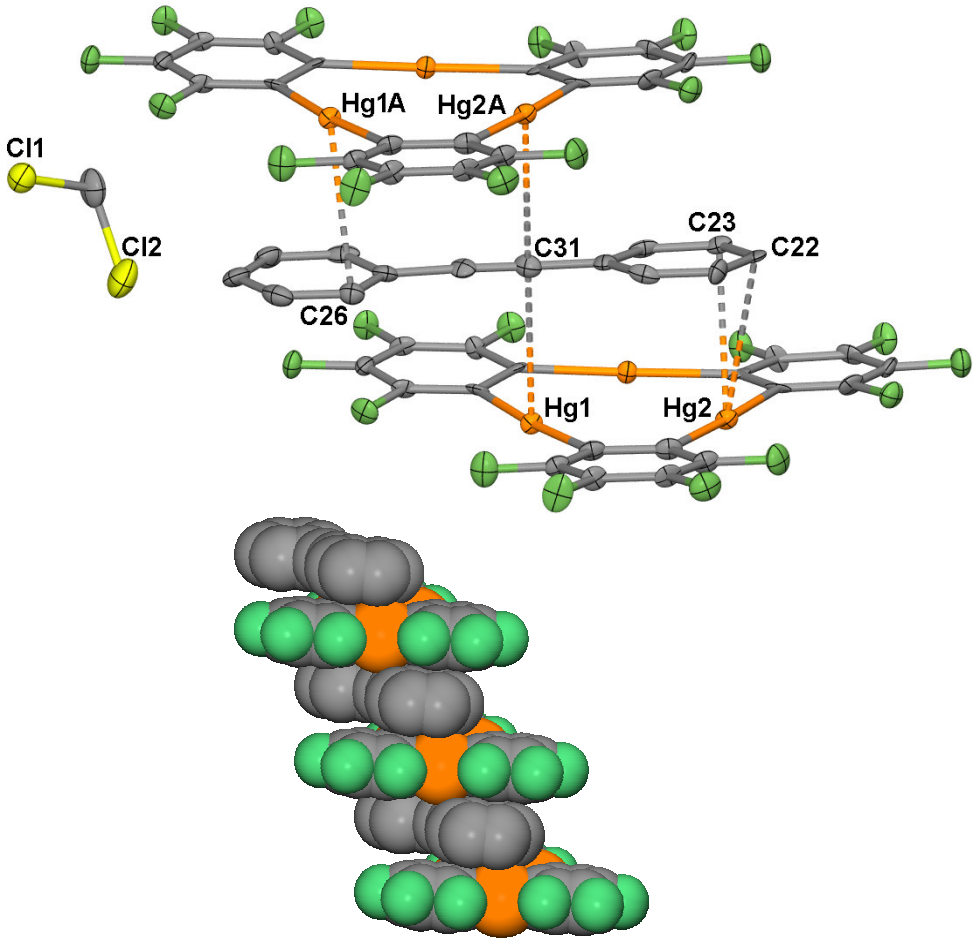

Figure III.1. (above): ORTEP view (50% ellipsoids) of compound **12** (H atoms omitted). Representative intermolecular distances (Å): Hg(1)-C(31) 3.235, Hg(2)-C(22) 3.395, Hg(2)-C(23) 3.223, Hg(1A)-C(26) 3.299, Hg(2A)-C(31) 3.355. (below): Space filling model of the binary stack present in **12.**

The structures of **13-17** have been determined by X-ray crystallography (Table III.1, Table III.2, and Figure III.2). In all cases, the α,ω-diphenylpolyynes, which are approximately planar, are associated to molecules of **7** on either side of the molecular plane. As depicted in Figure III.2, some of the phenyl and alkynyl carbon atoms of the polyynes are in contact with the mercury centers of **7**. The resulting Hg-C distances (3.18-3.47 Å) are within the sum of the van der Waals radii of mercury (1.7-2.0 Å) [110, 111] and carbon (1.7 Å) [129] thus indicating the presence of secondary Hg-π interactions. Secondary Hg-π interactions of comparable length have been previously observed in arene adducts of **7**[43, 97, 99] and in the solid state structure of various alkynylmercury derivatives. [130, 131] These interactions are complemented, in the case of **13,** by an arene-fluoroarene interaction involving the phenyl rings of $Ph(C{\equiv}C)_2Ph$ and a tetrafluorophenylene ring of **7**. While the solid state structure of 13 consists of $(\mathbf{7})_2{\bullet}Ph(C{\equiv}C)_2Ph$ "sandwiches" piled on top of each other (Figure III.3a), the supramolecular structure of **14** reveals the formation of extended stacks in which molecules of **7** and $Ph(C{\equiv}C)_3Ph$ alternate regularly (Figure III.3b). In **15** and **16**, which also adopt stacked structures, a molecule of the α,ω-diphenylpolyyne alternates with two molecules of **7** (Figure III.3c,d). These two molecules of **7** reside side by side and decorate the faces of juxtaposed molecules of polyyne. In the case of **16**, the increased length of the polyyne chain leads to the generation of a gap which is filled by two molecules of dichloromethane (Figure III.2d, Figure III.3d).

In **13-16**, the arrangement of the adjacent stacks is such that the poylyne chains are entirely surrounded by molecules of **7** (Figure III.3c). In **15** and **16**, the polyyne chain slightly deviates from linearity to exhibit an S-shaped conformation which has been observed in the structural chemistry of such compounds. [132] Within the error of the X-ray measurement, the structures of the α,ω-diphenylpolyynes do not seem to be affected by their complexation to **7**, which is indicative of the weakness of the Hg-C interactions.

Compound **17** crystallizes in the triclinic space group *P*-1 with one molecule of **7** and two molecules of $Ph(C{\equiv}C)_6Ph$ in the asymmetric unit. There are numerous Hg-

$C_{aromatic/alkyne}$ interactions between the molecule of **7** and the two hydrocarbons. There is also an infinite arene-perfluoroarene stack which involves the phenyl ring containing C(43) and the tetrafluorophenyl ring containing C(1). The resulting centroid-centroid distances are equal to 3.57 and 3.80 Å. The molecule of **7** remains planar and no significant intramolecular angles or distances are observed (Figure III.4). The two $Ph(C{\equiv}C)_6Ph$ molecules, however, both display noticeable bending along the nominally "straight" polyyne chain: the $Ph(C{\equiv}C)_6Ph$ containing C(19) shows a kink in the chain, while the molecule containing C(43) displays an S-type confirmation similar to those previously reported in the polyyne chain of **15** and elsewhere. [132] Additionally, as opposed to the α,ω-diphenylpolyynes in **13-16**, the intramolecular phenyl groups are not coplanar and display dihedral angles of 35.6 and 108.8 °.

The acetylenic stretches ($\nu_{C\equiv C}$) of **13-16** measured by IR spectroscopy are essentially identical to those of the free polyyne (Figure III.5). The largest frequency difference is observed for 13 whose $\nu_{C\equiv C}$ is red-shifted by 8 cm^{-1} when compared to $Ph(C{\equiv}C)_2Ph$. In order to gather additional information concerning the electronic structure of the polyynes, adducts **13-16** have been studied by luminescence spectroscopy. The luminescence spectrum of **13** indicates complete quenching of the fluorescence and displays an emission whose energy and vibronic progression is identical to that reported for the phosphorescence of the pure diyne (Figure III.6). [133] This observation is in agreement with a mercury heavy atom effect as observed in arene adducts of **7**. [97] Adducts **14-16** give rise to only faint emissions. Taken collectively, these spectroscopic studies corroborate the conclusion derived from the crystallographic studies and indicate that **7** acts as an innocent synthon which does not significantly alter the geometry or electronic structure of the polyyne.

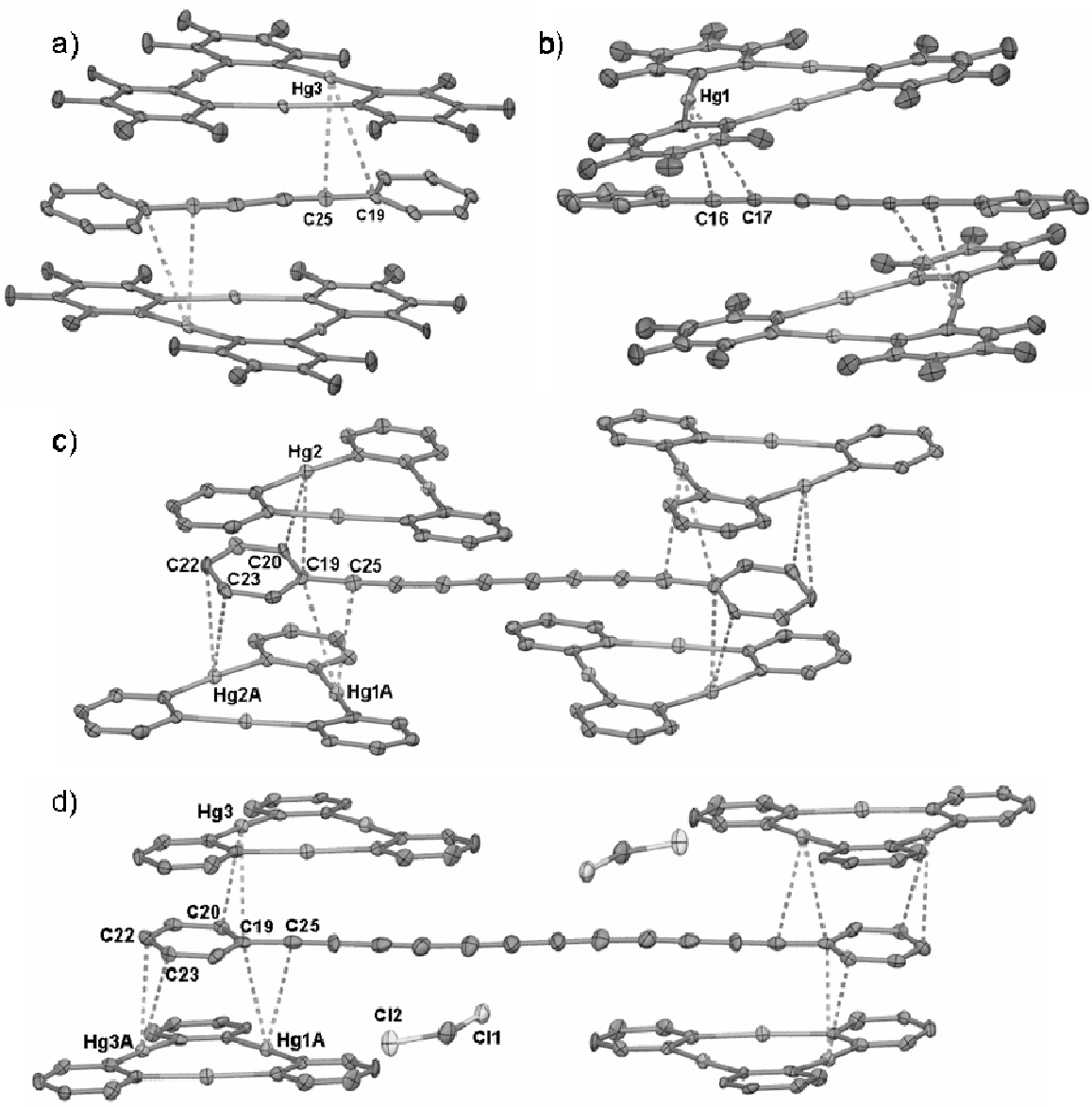

Figure III.2. Structures of (a) **13**, (b) **14**, (c) **15**, and (d) **16** (50% ellipsoids). Short intermolecular distances are represented by dotted lines. H atoms are omitted for **13**-**16**; F atoms are omitted for **15** and **16**. Selected intermolecular bond distances (Å): (a) Hg(3)-C(19)3.45, Hg(3)-C(25) 3.29; (b) Hg(1)-C(16) 3.25, Hg(1)-C(17) 3.42; (c) Hg(1)-C(27) 3.34, Hg(2)-C(19) 3.35, Hg(2)-C(20) 3.42, Hg(1)-C(27) 3.34, Hg(1A)-C(19) 3.47, Hg(1A)-C(25) 3.26, Hg(2A)-C(22) 3.39, Hg(2A)-C(23) 3.32; (d) Hg(1)-C(19) 3.32, Hg(1)-C(25) 3.36, Hg(3)-C(22) 3.32, Hg(3)-C(23) 3.40, Hg(3A)-C(19) 3.35, Hg(3A)-C(20) 3.18.

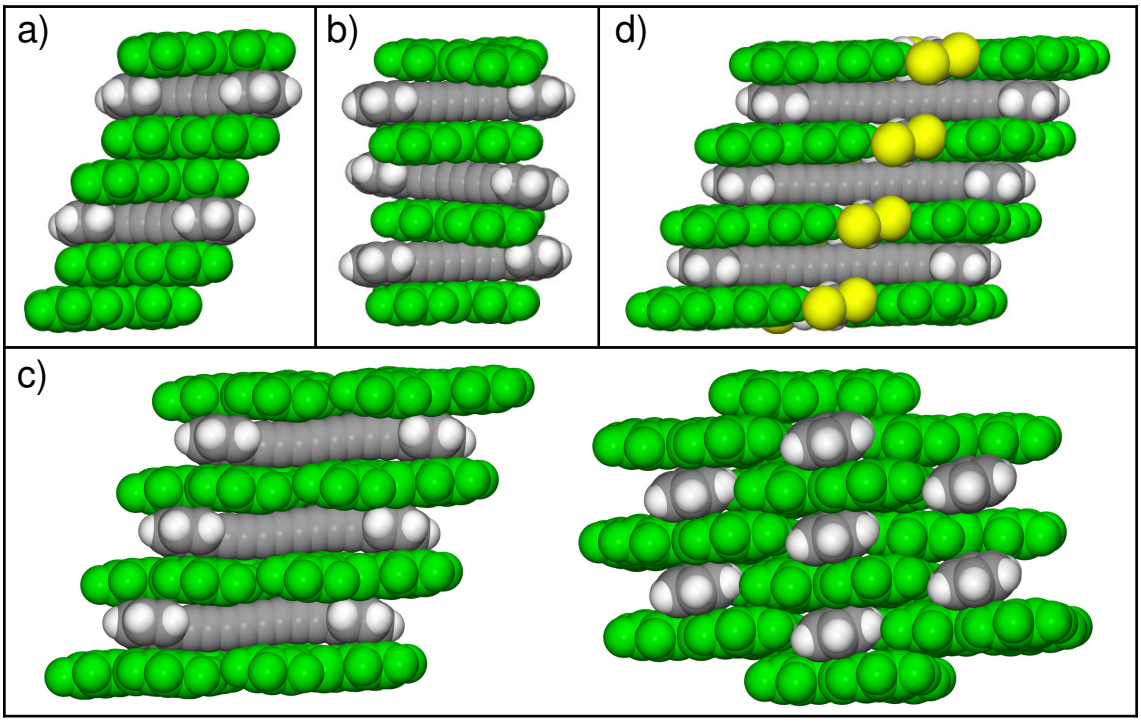

Figure III.3. Supramolecular structure of **13** (a), **14** (b), **15** (c) and **16** (d) (color code: **7**: green; $Ph(C{\equiv}C)_nPh$: C-atoms: grey, H-atoms: off-white; Cl-atoms: yellow). For the structure of **15** shown in c): left: view of a portion of the stacks; right: View of a portion of the molecular lattice showing how the individual molecules of $Ph(C{\equiv}C)_4Ph$ are separated from one another.

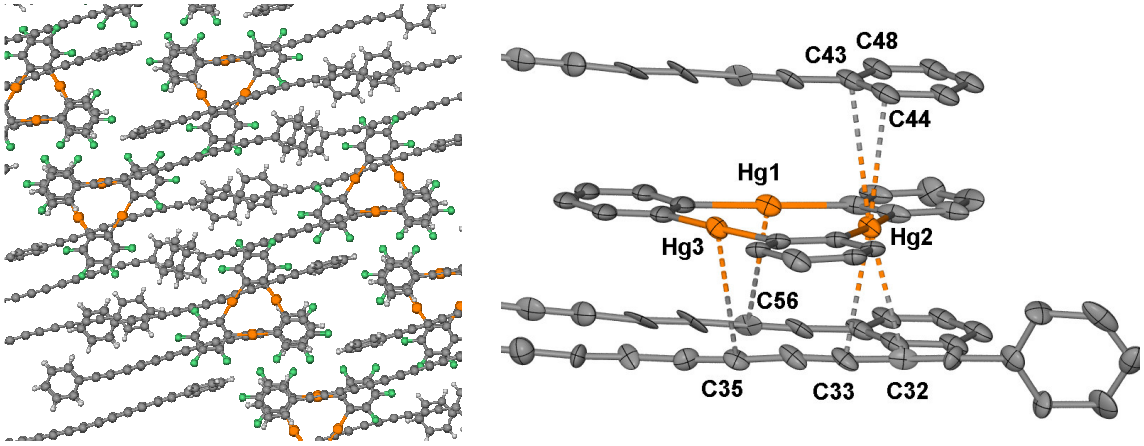

Figure III.4. (Left) Ball and stick view of **17** down the a-axis. (Right) ORTEP view (50% ellipsoid) of the intermolecular interactions in **17**. Representative intermolecular distances (Å): Hg(1)-C(56) 3.59, Hg(2)-C(32) 3.22, Hg(2)-C(33) 3.22, Hg(2)-C(43) 3.56, Hg(2)-C(44) 3.21, Hg(3)-C(35) 3.58.

Table III.1. Crystal data, data collection, and structure refinement for **12 - 14**.

Crystal data	**12**	**13**	**14**
Formula	$C_{33}H_{12}Cl_2F_{12}Hg_3$	$C_{52}H_{10}F_{24}Hg_6$	$C_{36}H_{10}F_{12}Hg_3$
M_r	1309.10	2294.14	1272.21
Crystal size (mm^3)	0.15 x 0.13 x 0.05	0.08 × 0.07× 0.065	0.13 × 0.10 × 0.08
Crystal system	Triclinic	Triclinic	Monoclinic
Space group	P-1	*P*-1	*C*2/c
a (Å)	7.5173(15)	9.0887(18)	12.360(3)
b (Å)	11.890(2)	10.574(2)	30.321(6)
c (Å)	19.305(4)	13.650(3)	9.0688(18)
α(°)	73.89(3)	68.33(3)	90
β (°)	79.21(3)	78.31(3)	108.43(3)
γ(°)	76.00(3)	83.00(3)	90
V ($Å^3$)	1595.1(6)	1192.2(4)	3224.4(11)
Z	2	2	4
ρ_{calc} (g cm^{-1})	2.726	3.195	2.621
μ (mm^{-1})	14.665	19.380	14.435
F(000) (e)	1184	1018	2296
Data Collection			
T/K	110(2)	110(2)	110(2)
Scan mode	ω	ω	ω
hkl range	-8→8, -13→11, -21→21	-10→10, -11→11, -15→15	-16→15, -39→39, -11→11
Measured refl.	9865	6872	13487
Unique refl., [R_{int}]	4602 [0.0338]	3346 [0.0475]	3716 [0.0488]
Refl. used for refinement	4602	3346	3716
Absorption Correction	SADABS	SADABS	SADABS
T_{min}/T_{max}	0.259756	0.342430	0.257089
Refinement			
Refined parameters	451	370	231
R_1,[a] wR_2[b] [I>2σ(I)]	0.0325, 0.0863	0.0599, 0.1583	0.0336, 0.0853
ρ_{fin} (max/min) ($eÅ^{-3}$)	1.094, -2.210	4.300, -4.879	2.056, -2.540

[a] $R_1 = \Sigma (||F_o| - |F_c||)/|F_o|$; [b] $wR_2 = \{\Sigma [w(F_o^2 - F_c^2)^2]/\Sigma [w(F_o^2)^2]\}^{1/2}$; $w = 1/[\sigma^2(F_o^2) + (aP)^2 + bP]$; $P = (F_o^2 + 2F_c^2)/3$. For **12** , $a = 0.075$, $b = 0$, For **13**, $a = 0.1166$, $b = 0$; for **14**, $a = 0.0502$, $b = 0$.

Table III.2. Crystal data, data collection, and structure refinement for **15** - **17**.

Crystal data	**15**	**16**	**17**
Formula	$C_{28}H_5F_{12}Hg_3$	$C_{31}H_7Cl_2F_{12}Hg_3$	$C_{66}H_{20}F_{12}Hg_3$
M_r	1171.09	1280.04	1641.80
Crystal size (mm^3)	0.37 × 0.10 × 0.06	0.10 × 0.035 × 0.025	0.04 × 0.01 × 0.005
Crystal system	Triclinic	Monoclinic	Triclinic
Space group	*P*-1	$P2_1/c$	*P-1*
a (Å)	6.9766(14)	9.6848(19)	7.335(7)
b (Å)	10.317(2)	7.1522(14)	14.611(13)
c (Å)	18.189(4)	43.542(9)	25.47(2)
α (°)	95.01(3)	90	88.611(10)
β (°)	93.27(3)	95.49(3)	81.72
γ(°)	102.36(3)	90	80.313(14)
V ($Å^3$)	1270.1(4)	3002.3(10)	2662(4)
Z	2	4	2
ρ_{calc} (g cm^{-1})	3.062	2.832	2.050
μ (mm^{-1})	18.194	15.580	8.714
F(000) (e)	1042	2300	764
Data Collection			
T/K	110(2)	110(2)	110(2)
Scan mode	ω	ω	ω
hkl range	-7→7, -11→11, -20→20	-12→12, -8→9, -56→56	-8→8, -16→16, -29→28
Measured refl.	8031	23337	16759
Unique refl., [R_{int}]	3641 [.0509]	6954 [0.0718]	8292 [0.1153]
Refl. used for refinement	3641	6954	8292
Absorption Correction	SADABS	SADABS	SADABS
T_{min}/T_{max}	0.230142	0.442009	0.472339
Refinement			
Refined	388	433	730
R_1,[a] wR_2[b] [I>2σ	0.0377, 0.0907	0.0528, 0.0956	0.0857, 0.1240
ρ_{fin} (max/min)	2.265, -1.968	1.750 and -2.320	3.863, -1.946

[a] $R_1 = \Sigma (| F_o | - | F_c |)/| F_o |$; [b] $wR_2 = \{\Sigma [w(F_o^2 - F_c^2)^2]/\Sigma [w(F_o^2)^2]\}^{1/2}$; $w = 1/[\sigma^2(F_o^2) + (aP)^2 + bP]$; $P = (F_o^2 + 2F_c^2)/3$. **15**, *a* = 0.0377, *b* = 5.9144.For **16**, *a* = 0.0252, *b* = 26.1711, for **17**, *a* = 0.0244, *b* = 0.0000.

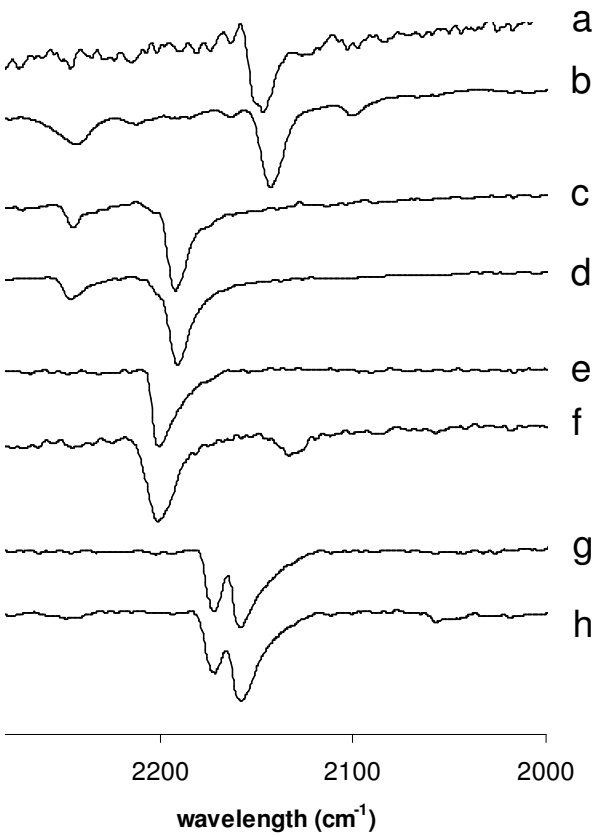

Figure III.5. IR spectra of **13** (a), $Ph(C{=}C)_2Ph$ (b), **14** (c), $Ph(C{=}C)_3Ph$ (d), **15** (e), $Ph(C{=}C)_4Ph$ (f), **16** (g), and $Ph(C{=}C)_6Ph$ (h), showing the acetylenic stretches.

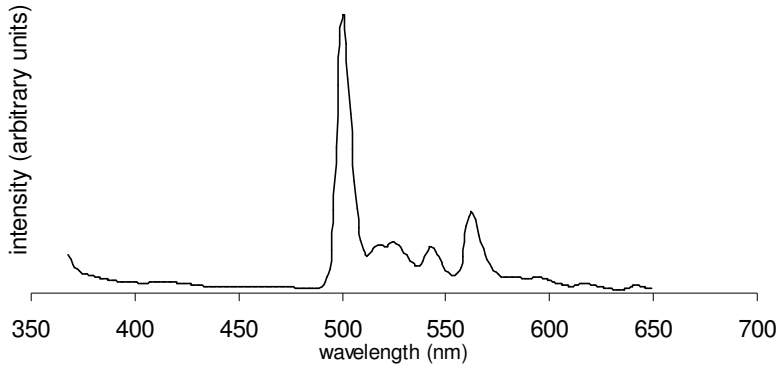

Figure III.6. Emission scan of **13** at 77 K, λ_{ex}= 348 nm.

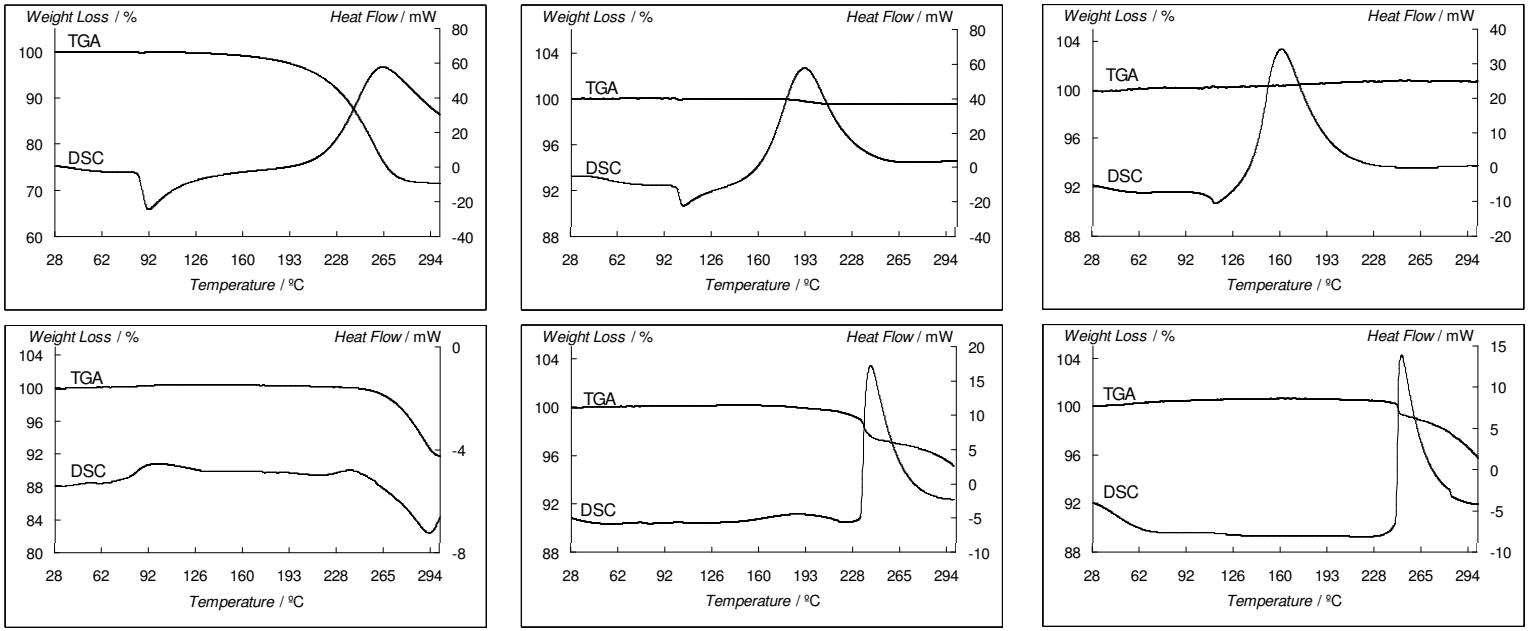

Figure III.7. TGA and DSC traces for $Ph(C{\equiv}C)_2Ph$, $Ph(C{\equiv}C)_3Ph$, $Ph(C{\equiv}C)_4Ph$ (top) and **13-15** (bottom) acquired at a heating rate of 20.0 ºC/min in an open pan.

As indicated in the introduction, the objective of this work is the discovery of a new method allowing for the stabilization of polyynes. Apart from **16** which decomposes within a few days by loss of CH_2Cl_2, adducts **13**-**15** are indefinitely stable under ambient conditions in a laboratory illuminated with fluorescent light. The stability of **14** and **15** is noteworthy since $Ph(C\equiv C)_3Ph$ and $Ph(C\equiv C)_4Ph$ will rapidly decompose under the same conditions. In order to further assess the stabilization resulting from the complexation of the α,ω-diphenylpolyyne by **7**, we surveyed the thermal behavior of the adducts by DSC/TGA and compared them to those of the corresponding pure α,ω-diphenylpolyynes. These measurements were carried out under air to obtain data that relate to the behavior of the solids under ambient conditions. Taking into account the instability of $Ph(C\equiv C)_6Ph$ and **5** which loses solvent at room temperature, measurements were only carried out on $Ph(C\equiv C)_2Ph$, $Ph(C\equiv C)_3Ph$, and $Ph(C\equiv C)_4Ph$ and their corresponding adducts **13-15** (Figure III.7). According to our DSC measurements, the α,ω-diphenylpolyynes $Ph(C\equiv C)_2Ph$, $Ph(C\equiv C)_3Ph$, and $Ph(C\equiv C)_4Ph$ melt at 92, 98, and 111 ºC as indicated by a detectable endotherm. These melting points values correspond to those reported in the literature which attests to the purity of our samples. [134] For $Ph(C\equiv C)_2Ph$, melting is followed by a weight loss assigned to sublimation, which in principle should be endothermic. The DSC response, however, indicates the onset of an exotherm suggesting that sublimation is accompanied by an exothermic polymerization. For $Ph(C\equiv C)_3Ph$ and $Ph(C\equiv C)_4Ph$, melting is followed by a conspicuous exotherm which begins at 135 ºC for $Ph(C\equiv C)_3Ph$, and 120 ºC for $Ph(C\equiv C)_4Ph$. These temperatures most likely correspond to the advent of polymerization since no mass loss is observed. The thermal behavior of the adducts is drastically different. For **13**, a slightly endothermic weight loss is observed at 250 ºC which probably corresponds to sublimation of $Ph(C\equiv C)_2Ph$ and/or **7**. For adducts **14** and **15**, an exothermic decomposition is observed at about 240 ºC. This decomposition is accompanied by a mass loss which can be assigned to sublimation of some of the trinuclear mercury complex or to oxidative decomposition of the polyyne. Altogether, these DSC/TGA studies indicate that the adducts are more thermally stable than the respective free α,ω-

diphenylpolyynes. In the case of $Ph(C\equiv C)_4Ph$, the stability range is increased by almost 120 ºC in an oxidizing atmosphere. Similar conclusions could be derived by monitoring the acetylenic stretch of $Ph(C\equiv C)_4Ph$ and **15** as a function of temperature in KBr (Figure III.8). In the case of $Ph(C\equiv C)_4Ph$, the stretch disappears above 170 ºC while that in **15** persists beyond 250 ºC.

Since binary solids containing directly adjacent polyynes have been shown to polymerize, [135, 136] we propose that the increase in stability of α,ω-diphenylpolyynes in adducts **13-15** results from their entrapment and physical separation in a supramolecular lattice. Paradoxically, the supramolecular forces responsible for the formation of these adducts are weak and do not affect the structure of the polyynes. In contrast to previous efforts, our approach relies on the use of an innocent stabilizing unit which interacts with the polyyne via weak supramolecular interactions.

III.4. Adducts of monofunctional organomercurials and $Ph(C\equiv C)Ph$ and $Ph(C\equiv C)_2Ph$

It has been found that other fluorinated organomercurials are competent for the complexation of diphenylacetylene and α,ω-diphenylpolyynes. This was determined by mixing equimolar quantities of pentafluorophenyl mercury chloride (**2**) and bromide (**18**) with diphenylacetylene and $Ph(C\equiv C)_2Ph$, respectively, in CH_2Cl_2. Slow evaporation of the solvent resulted in the crystallization of [(**2**)$_2$•diphenylacetylene] (**19**) and [(**18**)$_2$•$Ph(C\equiv C)_2Ph$] (**20**) as 2:1 adducts.

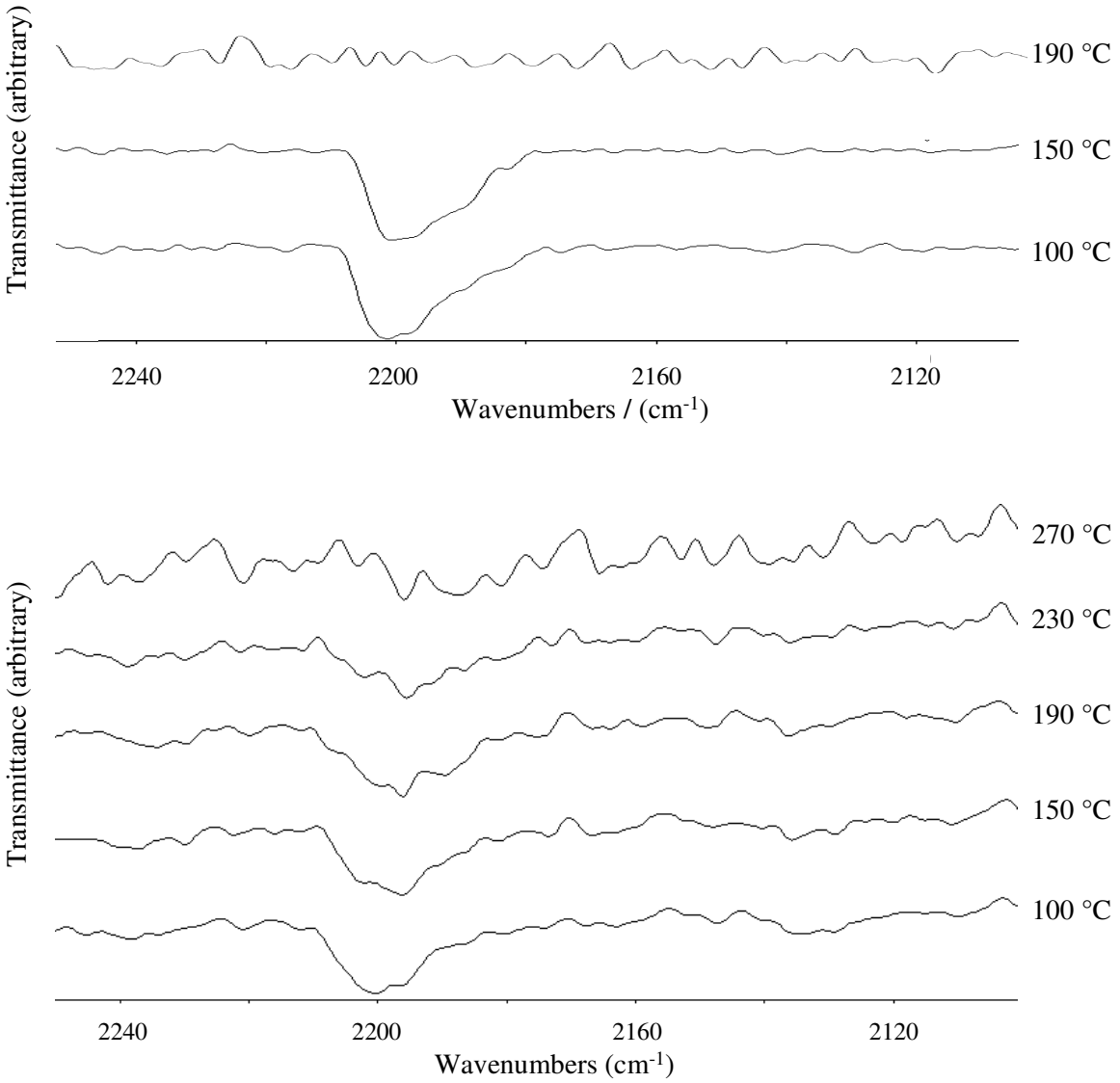

Figure III.8. IR measurements taken at increasing temperatures on KBr samples of $Ph(C{\equiv}C)_4Ph$ (above) and **15** (below).

[(**2**)$_2$•diphenylacetylene] (**19**) crystallizes in the monoclinic space group $P2_1/c$ with one complete molecule of **2** and half of a molecule of diphenylacetylene in the asymmetric unit. As opposed to **12**, no infinite stacks are present. Instead, the diphenylacetylene molecule is sandwiched between two molecules of **2**. These

molecules are almost parallel and a form a dihedral angle of only 5.3 °. There are two equivalent close fluoroarene-arene interactions (centroid-to-centroid distance of 3.603 Å) involving the phenyl groups of the hydrocarbon and the pentafluorophenyl group of the organomercurial. The alkyne functionality bridges the two mercury centers in a bis(dihapto) fashion as depicted in Figure I.1. The resulting Hg-C interactions are equal to 3.46 and 3.50 Å. Additional Hg-C_{arene} interactions of 3.39 and 3.57 Å connect the neighboring [(**2**)$_2$•diphenylacetylene] "sandwiches" together. The structure of **19** is cross-linked throughout by secondary Hg-Cl-Hg bridges with distances of 3.20 and 3.23 Å (Figure III.9, Table III.3). These secondary interactions are common in the chemistry of chloromercurio compounds. [137]

[(**18**)$_2$•Ph(C≡C)$_2$Ph] (**20**) crystallizes in the triclinic space group *P*-1 with two distinct C_6F_5HgBr molecules and one Ph(C≡C)$_2$Ph molecule in the asymmetric unit (Figure III.10, Table III.3). The pentafluorophenyl rings in the two molecules of **18** are not coplanar and form a dihedral angle of 28.9 °. The Ph(C≡C)$_2$Ph molecule is not planar either, and the two rings are twisted by 15.6 °. The Ph(C≡C)$_2$Ph molecule interacts with Hg(1) via Hg-$C_{aromatic}$ interactions ranging from 3.30-3.36 Å. It also interacts with Hg(2) via Hg-C_{alkyne} interactions of 3.41 and 3.58 Å. There do not appear to be any significant arene-fluorarene interactions. Intermolecular Hg-Br interactions lead to the formation of an extended structure. Instead of a two-dimensional ladder motif often seen with mercury-halogen species as noted above, there are additional Hg-Br interactions of 3.46-3.81 Å in the third dimension that create a repeating cage-like structure. The Hg centers are quite crowded when considering all the secondary interactions, and both could be considered to have grossly distorted octahedral coordination environments consiting of the primary phenyl and bromide ligands, three bromine atoms provided by the neighboring molecules, and the intermolecular Hg-$C_{alkyne/aromatic}$ interactions (Figure III.11).

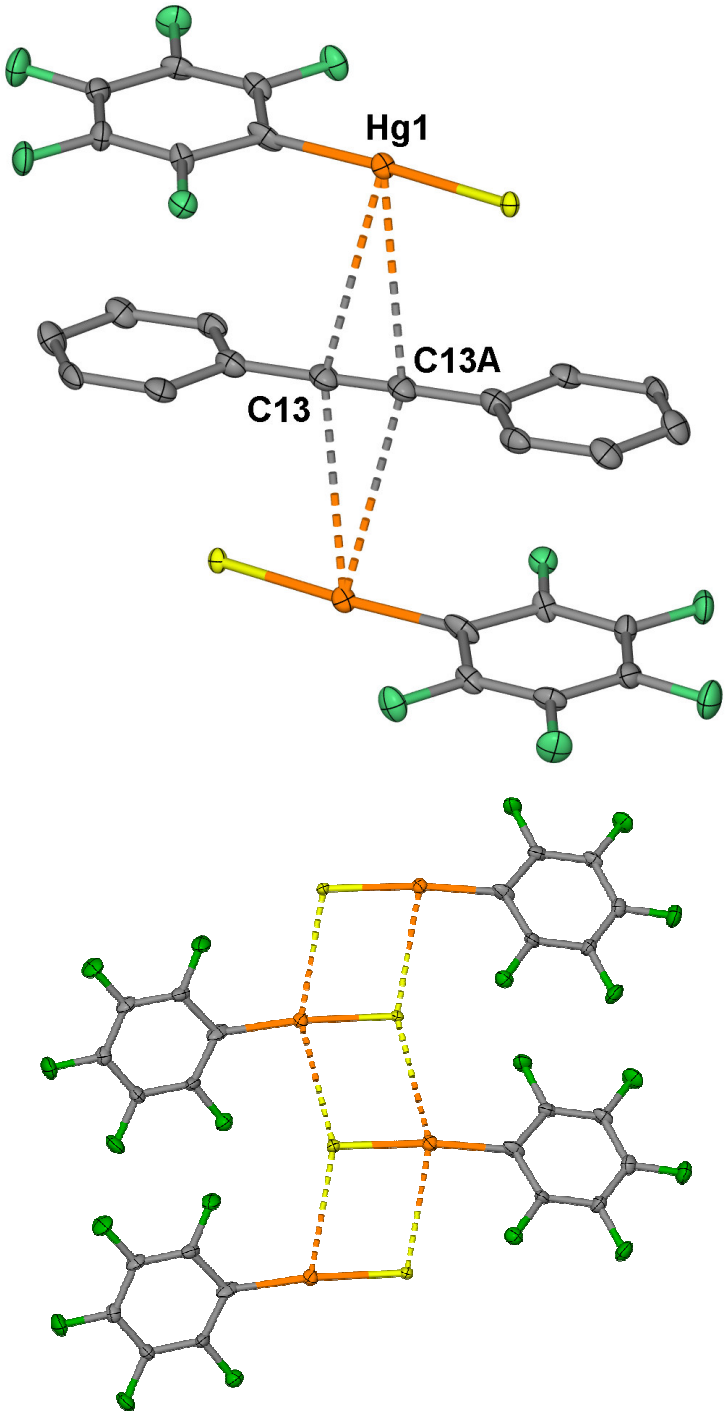

Figure III.9. (above): ORTEP. view (50% ellipsoids) of compound **19**. Representative intermolecular distances (Å): Hg(1)-C(13) 3.500, Hg(1)-C(13A) 3.464, Hg(1A)-C(11) 3.394, Hg(1A)-C(12) 3.565. (below): View of the intermolecular Hg-Cl bridge in **19**.

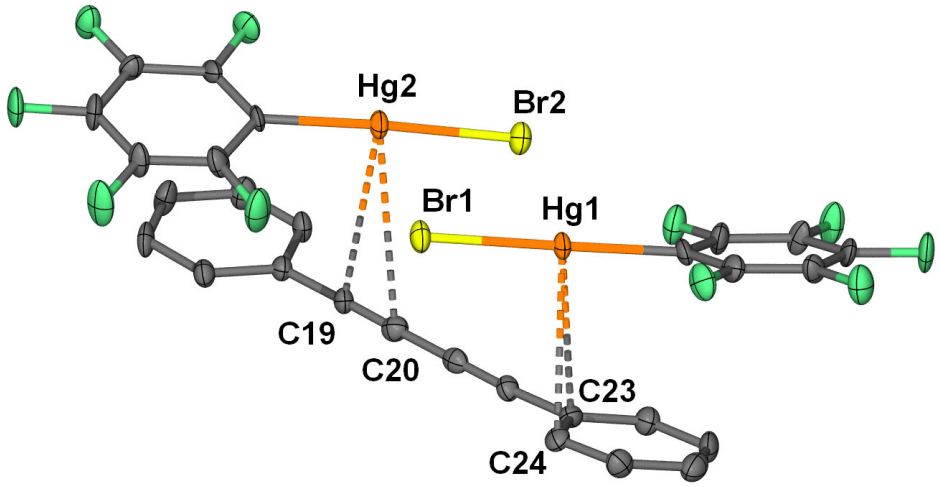

Figure III.10. ORTEP view (50% ellipsoid) of the intermolecular interactions in **20**. Representative intermolecular distances (Å): Hg(1)-C(23) 3.36, Hg(1)-C(24) 3.30, Hg(2)-C(19) 3.41, Hg(2)-C(20) 3.58.

III.5. Experimental

General considerations. Due to the toxicity of the mercury compounds discussed in these studies extra care was taken at all times to avoid contact with solid, solution, and air-borne particulate mercury compounds. Most of the studies herein were carried out in well-aerated fume hoods. Atlantic Microlab, Inc., Norcross, GA, performed the elemental analyses. All solvents were purchased commercially and used as provided for crystallizations. Trimeric perfluoro-*ortho*-phenylene-mercury (**7**),[52] and pentafluorophenyl mercury chloride (**2**)[138] and bromide (**18**) [139] were prepared as described in literature. $Ph(C{\equiv}C)_2Ph$ [1,4-diphenylbutadiyne, (Strem)] was used as provided. $Ph(C{\equiv}C)_3Ph$, $Ph(C{\equiv}C)_4Ph$, and $Ph(C{\equiv}C)_6Ph$ were synthesized using variations of reported literature procedures. [140-142]

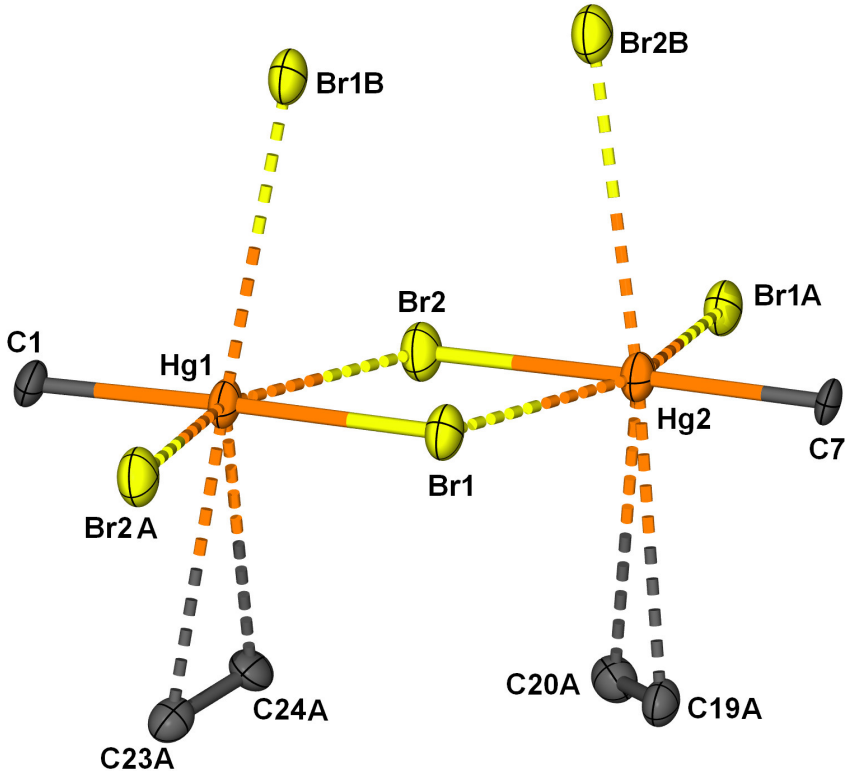

Figure III.11. ORTEP view (50% ellipsoid) of the roughly octahedral environment of the Hg atoms in **20**. Representative Hg-Br intermolecular distances (Å): Hg(1)-Br(2) 3.53, Hg(1)-Br(2A) 3.74, Hg(1)-Br(1B) 3.45, Hg(2)-Br(1) 3.46, Hg(2)-Br(1A) 3.81, Hg(2)-Br(2B) 3.52.

Table III.3. Crystal data, data collection, and structure refinement for **19** and **20.**

Crystal data	**19**	**20**
Formula	$C_{13}H_5ClF_5Hg$	$C_{28}H_{10}Br_2F_{10}Hg_2$
M_r	492.21	1097.36
Crystal size (mm^3)	0.20 × 0.15 × 0.08	0.19 × 0.05 × 0.04
Crystal system	Monoclinic	Triclinic
Space group	$P2_1/c$	P-1
a (Å)	13.062(12)	7.148(3)
b (Å)	6.048(6)	13.425(5)
c (Å)	16.232(15)	15.601(6)
α(°)	90	68.555(6)
β (°)	99.647(17)	78.226(6)
γ(°)	90	80.426(6)
V ($Å^3$)	5020.1(17)	1357.2(9)
Z	4	2
ρ_{calc} (g cm^{-1})	2.586	2.685
μ (mm^{-1})	12.432	14.330
F(000) (e)	900	996
Data Collection		
T/K	110(2)	110(2)
Scan mode	ω	ω
hkl range	-17→16, -7→7, -21→19	-9→9, -17→17, -20→20
Measured refl.	7024	11679
Unique refl., [R_{int}]	2831[0.0465]	6064 [0.0471]
Refl. used for refinement	2831	6064
Absorption Correction	SADABS	SADABS
T_{min}/T_{max}	0.0954/0.6752	0.171637
Refinement		
Refined parameters	181	379
R_1,[a] wR_2[b] [I>2σ(I)]	0.0418, 0.0969	0.0434, 0.0986
ρ_{fin} (max/min) ($eÅ^{-3}$)	2.113, -3.299	1.564 and -2.141

[a] $R_1 = \Sigma (| F_o | - | F_c |)/| F_o |$; [b] $wR_2 = \{\Sigma [w(F_o^2 - F_c^2)^2]/\Sigma [w(F_o^2)^2]\}^{1/2}$; $w = 1/[\sigma^2(F_o^2) + (aP)^2 + bP]$; $P = (F_o^2 + 2F_c^2)/3$.For **19**: $a = 0.0685$, $b = 0.0000$, for **20**: $a = 0.0444$, $b = 0.0000$.

Synthesis of [7•diphenylacetylene•CH_2Cl_2] (12). Compound **7** (0.025 g , 0.024 mmol) and diphenylacetylene (0.0045 g, 0.025 mmol) were dissolved in CH_2Cl_2 (5 mL). Upon concentration by slow evaporation of the solvent, colorless x-ray quality crystals of **12** were formed in 70% yield (0.022 g, 0.0168 mmol). The crystals were collected before complete evaporation of solvent to avoid crystal decomposition from loss of solvent which readily occurs at room temperature. IR (KBr disc, cm^{-1}): 1684, 1771, 1819, 1843, 1896, 1911, 1961, and 1980 Anal., Calcd without residual solvent, $C_{32}H_{10}F_{12}Hg_3$: C, 31.40; H, 0.82. Found: C: 32.14, H: 0.89.

Synthesis of [$(7)_2$•Ph$(C\equiv C)_2$Ph] (13). Compound **7** (24.5 mg, 0.024 mmol) and Ph$(C\equiv C)_2$Ph (2.4 mg, 0.012 mmol) were sonicated in dichloromethane (5 mL) until a clear solution was obtained. Colorless crystals of **13**, which formed upon slow evaporation of the solvent, were washed with hexane. Yield: 22 mg, 80%. Anal. Calcd for $C_{52}H_{10}F_{24}Hg_6$: C, 27.22; H, 0.44. Found: C, 27.20; H, 0.30. m.p. 295 °C (decomp.)

Synthesis of [7•Ph$(C\equiv C)_3$Ph] (14). Compound **7** (42 mg, 0.040 mmol) and Ph$(C\equiv C)_3$Ph (10.0 mg, 0.042 mmol) were mixed in dichloromethane (5 mL). Slightly yellow crystals of **14**, which formed upon slow evaporation of the solvent in the absence of light, were washed with hexane. Yield: 20.6 mg, 40%. Anal. Calcd for $C_{36}H_{10}F_{12}Hg_3$: C, 33.99; H, 0.79. Found: C, 34.05; H, 0.65. m.p. 299-300 °C (decomp.)

Synthesis of [$(7)_2$•Ph$(C\equiv C)_4$Ph] (15). Compound **7** (47 mg, 0.045 mmol) and Ph$(C\equiv C)_4$Ph (6 mg, 0.024 mmol) were mixed in dichloromethane (15 mL). The resulting solution was cooled to -10 °C which resulted, after four days, in the formation of yellow crystals of adduct **15**. These crystals were isolated by filtration and rinsed with a small amount of cold hexanes. Yield: 13 mg, 25%. Anal. Calcd for $C_{56}H_{10}F_{24}Hg_6$: C, 28.72; H, 0.43. Found: C, 28.71; H, 0.33. m.p. 320 °C (decomp.)

Synthesis of [$(7)_2$•Ph$(C\equiv C)_6$Ph•CH_2Cl_2] (16). Compound **7** (40 mg, 0.039 mmol) and Ph$(C\equiv C)_6$Ph (6 mg, 0.020 mmol) were mixed in dichloromethane (10 mL). The resulting solution was cooled to -10°C which resulted, overnight, in the formation of bright yellow crystals of adduct **16**. These crystals were isolated by filtration and rinsed

with a small amount of cold hexanes. Yield: 10 mg, 20%. Elemental analysis was not feasible as samples decomposed rapidly in the absence of solvent.

Synthesis of [7•(Ph(C≡C)$_6$Ph)$_2$] (17). Compound **7** (10 mg, 0.010 mmol) and Ph(C≡C)$_6$Ph (6 mg, 0.020) were mixed in dichloromethane (5 mL). The resulting solution was cooled to -10 °C which resulted, over a period of two weeks, in the formation of bright yellow crystals of adduct **17**. The crystals were isolated by manual selection since they were highly soluble. Yield < 2 mg, < 12%.

Synthesis of [(2)$_2$•diphenylacetylene] (19). Compound **2** (40 mg, 0.048 mmol) and diphenylacetylene (9 mg, 0.05 mmol) were dissolved in CH_2Cl_2 (15 mL). Upon concentration by slow evaporation of the solvent, clear blocks of **19** were formed in 90% yield (0.026 g, 0.022 mmol). mp 312 ° C (decomp). Anal. Calcd for $C_{26}H_{10}Cl_2F_{10}Hg_2$: C, 31.72; H, 1.02. Found: C, 31.93; H, 0.98.

Synthesis of [(18)$_2$•Ph(C≡C)$_2$Ph] (20). Compound **18** (15 mg, 0.034 mmol) and Ph(C≡C)$_2$Ph (3.4 mg, 0.017 mmol) were mixed in dichlormethane (5 mL). Colorless crystals of **20**, which formed upon slow evaporation of the solvent, were washed with hexane. Yield: 16 mg, 85%.

Single-crystal X-ray analysis. X-ray data for **13-15, 19,** and **20** were collected on a Bruker SMART 1000 CCD diffractometer, while data for **16** and **17** were collected on a Bruker SMART APEX CCD diffractometer, all using graphite-monochromated radiation from a Mo sealed X-ray tube (K_α = 0.70173Å). Specimens of suitable size were mounted on glass loops with mineral oil. The structures were solved by direct methods, which successfully located most of the non-hydrogen atoms. Subsequent refinement on F^2 using the SHELXTL/PC package (version 5.1) allowed location of the remaining non-hydrogen atoms.

Infrared spectroscopy. IR spectra were recorded with a ATI-Mattson Genesis series FTIR Spectrometer with the samples prepared as compressed KBr discs. The bands were compared to reported values when available. [143-146] Variable temperature measurements with **15** and Ph(C≡C)$_4$Ph were made using one sample of each which

were heated in an oven at 100 ºC and then from 130 ºC at 20 ºC increments until no band was observed at 2200 cm^{-1} (Figure III.8).

DSC/TGA measurements. Experiments were performed with a TA Instruments Q600 SDT under an air purge at heating rates of 10 to 20 ºC/min.

Luminescence. The luminescence spectra were recorded with a SLM/AMINCO Model 8100 spectrofluorometer equipped with a xenon lamp. Low-temperature measurements were made in a cryogenic device of local design, and liquid nitrogen used to obtain the 77 K measurements.

CHAPTER IV

HYDROCARBON UPTAKE IN THE ALKYLATED MICROPORES OF A COLUMNAR SUPRAMOLECULAR SOLID*

IV.1. Introduction

Microporous self-assembled materials are attracting a great deal of interest for the storage of gases. Selective uptake and retention of small gaseous molecules such as dihydrogen are particularly attractive goals which may lead to novel storage strategies. [147-155] In principle, similar strategies could be extended to gaseous alkanes whose separation, transport and storage continues to pose problems. Despite these important applications, limited effort has been devoted to the study of alkane sorption in microporous self-assembled materials. Available studies include the use of microporous metal-organic frameworks and van der Waals crystals for the storage, [156] size selective encapsulation, [157] or gas chromatographic separation of alkanes. [158] In all of these cases, the walls of the micropores are lined by aromatic groups which interact with the guest hydrocarbon by CH···π or van der Waals interactions. [156-161] Keeping in mind that strong van der Waals attractions occur between saturated hydrocarbons, it occurred to us that microporous solids with alkylated cavity walls may be well suited for the storage of alkanes. Despite the simplicity of this paradigm, [162] the synthesis of such microporous solids remains unprecedented.

We have shown that trimeric perfluoro-*ortho*-phenylene-mercury ([*o*-$C_6F_4Hg]_3$, **7**) [12, 43, 52] interacts with benzene via secondary Hg-π interactions to form extended stacks that propagate in a direction perpendicular to the molecular plane. [86]

---

* Reprinted in part with permission from *Angew. Chem., Int. Ed. Engl., 45,* Taylor, T. J.; Bakhmutov, V. I.; Gabbaï, F. P. "Hydrocarbon Uptake in the Alkylated Micropores of a Columnar Supramolecular Solid," 7030, Copyright 2006 by Wiley-VCH Verlag GmbH&Co. KGaA.

Additionally, we have observed close contacts between **7** and unsaturated substrates in supramolecular adducts. [163] In this communication we describe how these assembly principles can be used for the construction of columns with alkylated exteriors. We also demonstrate that such columns can self-assemble to form a microporous solid which traps light alkanes in its alkylated cavities.

Scheme IV.1.

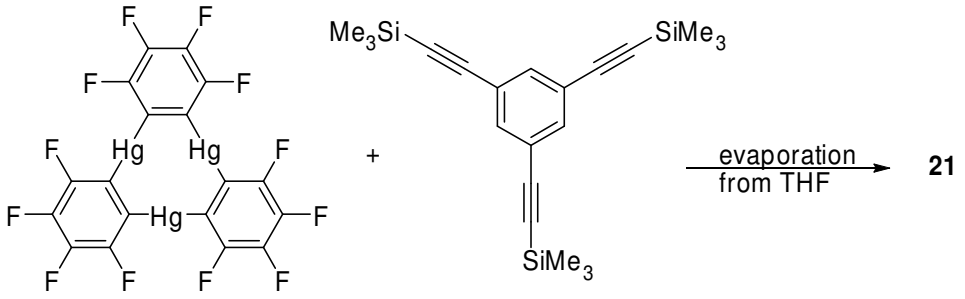

IV.2. Synthesis and characterization of $[o\text{-}C_6F_4Hg]_3$•1,3,5-$(TMSC{\equiv}C)_3C_6H_3$]

Reaction of **7** with 1,3,5-tris(trimethylsilylethynyl)benzene in THF leads to the formation of a crystalline adduct (Scheme IV.1), which, after washing with CH_2Cl_2 and drying, has been identified as [**7**•1,3,5-$(TMSC{\equiv}C)_3C_6H_3$] (**21**) as indicated by X-ray and elemental analysis (Figure IV.1). This adduct dissociates in polar solvents. ^{1}H NMR in d_6-acetone indicates that **21** does not contain any THF or CH_2Cl_2 molecules. Crystals of **21** belong to the hexagonal space group $P6_3/mmc$ (Figure IV.1, Table IV.1). Examination of the structure reveals the formation of extended columns that run parallel to the *c*-axis. These columns consist of binary stacks in which molecules of **7** and 1,3,5-$(TMSC{\equiv}C)_3C_6H_3$ alternate (Figure IV.2). These molecules interact via secondary Hg-π and Hg-$C_{acetylenic}$ interactions (Hg(1)-C(5) = 3.349(4) Å, Hg(1)-C(6) = 3.363(5) Å) whose distances are within the sum of the van der Waals radii of mercury (1.7-2.0 Å) [110, 111] and carbon (1.7 Å) [129] (Figure IV.1). These stacks are rather compact as indicated by

the distance of 3.28 Å separating the centroids of the two components. This centroid distance can be compared to the 3.24 Å distance found in [**7**•benzene] which adopts a comparable stacked structure. [86] In **21,** the neighboring columns are interdigitated and run parallel to one another to generate a three-dimensional honeycomb structure with large cylindrical channels parallel to the *c*-axis (Figure IV.3). The trimethylsilyl groups of the 1,3,5-tris(trimethylsilylethynyl)benzene molecules are oriented toward the center of the channels and decorate the walls with non-polar methyl groups. Probing these channels with a 1.2 Å sphere afforded a void volume of 200.0 $Å^3$/unit cell. This volume corresponds to 8.9% of the total volume of the crystal. [164] Assuming that the channels are perfectly cylindrical, their internal effective diameter is 6.2 Å. The channels appear to be essentially empty as the samples show negligible weight loss (< 0.1%) upon application of a vacuum, and thermogravimetric measurements do not show any weight change until 190 ºC where the adduct starts decomposing. As expected, these channels are hydrophobic and do not show any affinity for water.

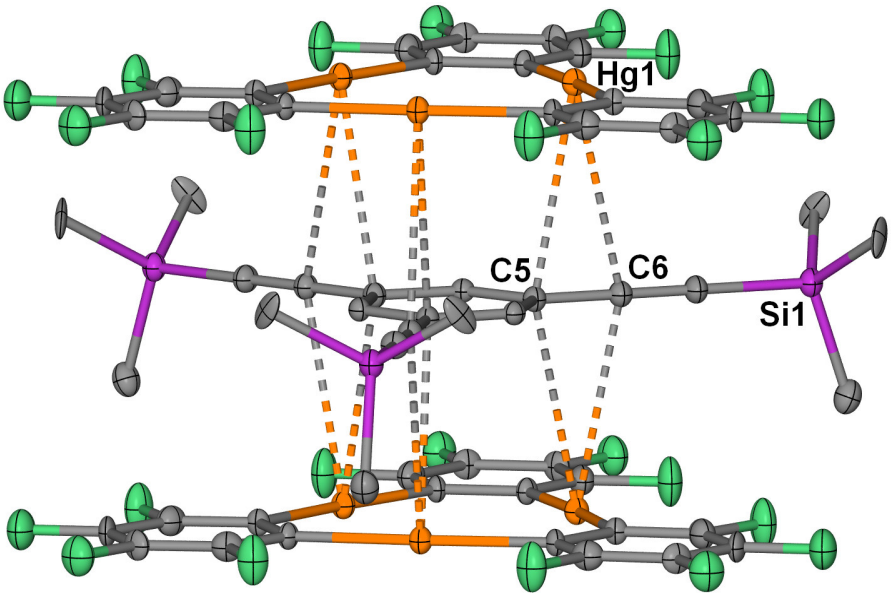

Figure IV.1. ORTEP view (50% ellipsoid) of the intermolecular interactions in **21**. H atoms are omitted, only one conformation of the disordered $SiMe_3$ groups is shown. Representative intermolecular distances (Å): Hg(1)-C(5) 3.35, Hg(1)-C(6) 3.36.

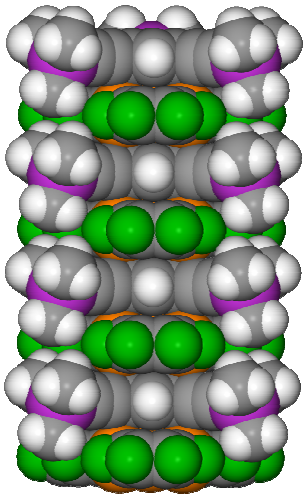

Figure IV.2. Space filling view of a stack of **21** with four repeating units.

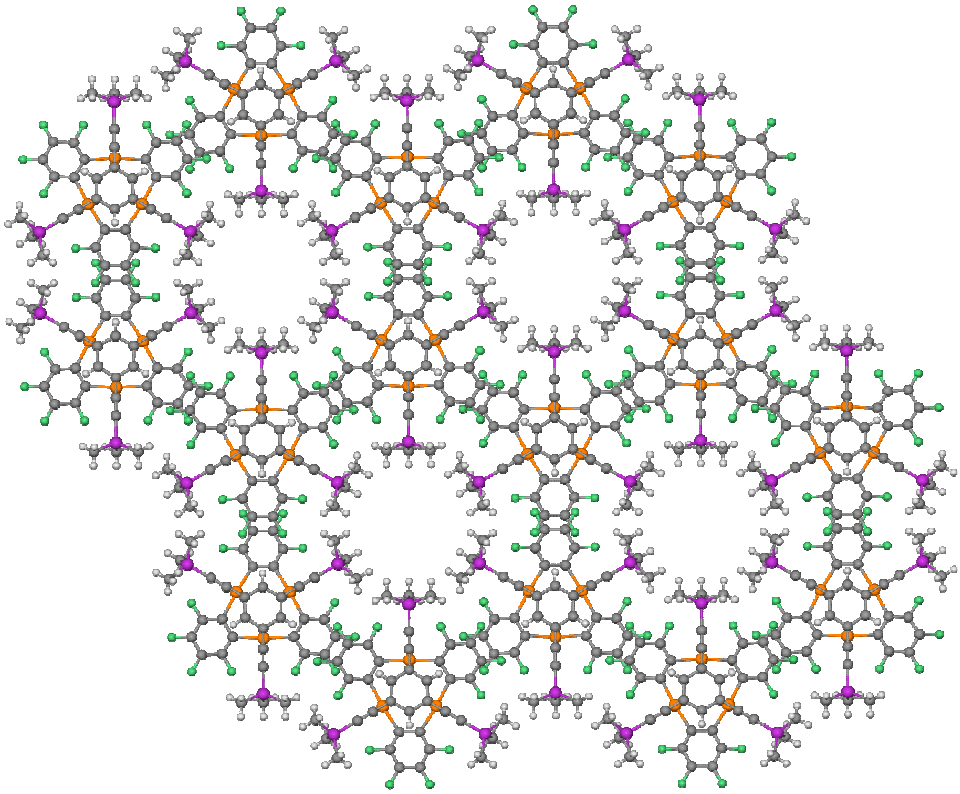

Figure IV.3. Ball-and-stick view of the honeycomb structure of **21** down the *c*-axis.

IV.3. Solvent and gas adsorption studies

In order to study the robustness of this microporous solid, we decided to determine if it would retain its structure upon guest incorporation in the channels. A single crystal of **21** was indexed and subsequently immersed in neat bromoform. After 12 hours, analysis of the crystal indicated encapsulation of bromoform and formation of **21**⊃0.82-$CHBr_3$. Remarkably, this single crystal to single crystal transformation occurs with retention of the $P6_3/mmc$ space group and essentially negligible changes of the unit cell parameters (Table IV.1). The structure of **21**⊃0.82-$CHBr_3$ only differs from that of **21** by the presence of bromoform molecules that are located in the channels and whose occupancy was refined at 82%. A similar occupancy was derived by integration of the ^{1}H NMR spectrum of **21**⊃0.82-$CHBr_3$ dissolved in d_6-acetone.

Encouraged by these results which attest of the structural robustness of **21**, we decided to investigate its affinity for volatile alkanes. Alkane uptake was investigated gravimetrically by exposure of solid **21** to an atmosphere of the corresponding alkane (Figure IV.5). Remarkably, alkane uptake is observed not only for *n*-hexane and *n*-pentane but also for *n*-butane, propane and ethane which are all gases under ambient conditions. For methane, however, the uptake was less than 0.5%. While ethane is still accumulating at a pressure of 1 bar, the sorption isotherms of propane and *n*-butane, recorded at room temperature, display plateaus which indicate saturation of the pores. The total gas uptakes at $P/P_0 = 1$ are equal to 1.2, 2.1, and 2.9 weight % for ethane, propane and butane respectively. For *n*-pentane and *n*-hexane, uptakes of 2.2 and 2.5 % are observed at $P/P_0 = 0.25$. Further adsorption studies were performed with *n*-heptane, which plateaued at 2.5 wt %. For these three liquid alkanes, additional weight gain is observed at higher pressure which is assigned to condensation on the external surface of the crystals. [165, 166] Conversion of these weight % uptakes into molar ratios indicates formation of **21**⊃0.57-ethane, **21**⊃0.67-propane, **21**⊃0.71-*n*-butane, **21**⊃0.45-*n*-pentane, **21**⊃0.41-*n*-hexane, and **21**⊃0.35-*n*-heptane.

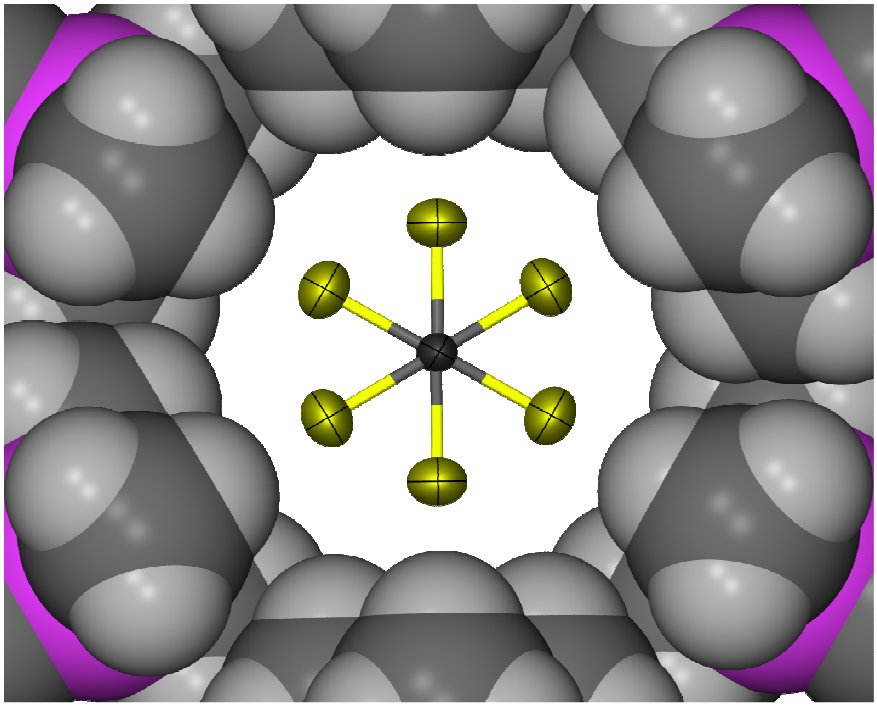

Figure IV.4. ORTEP view (50% ellipsoid) of **21**⊃0.82-$CHBr_3$ down the *c*-axis displaying the two disordered positions of the bromoform molecule in the cavity of **21** (space-filling with one orientation of the $SiMe_3$ groups).

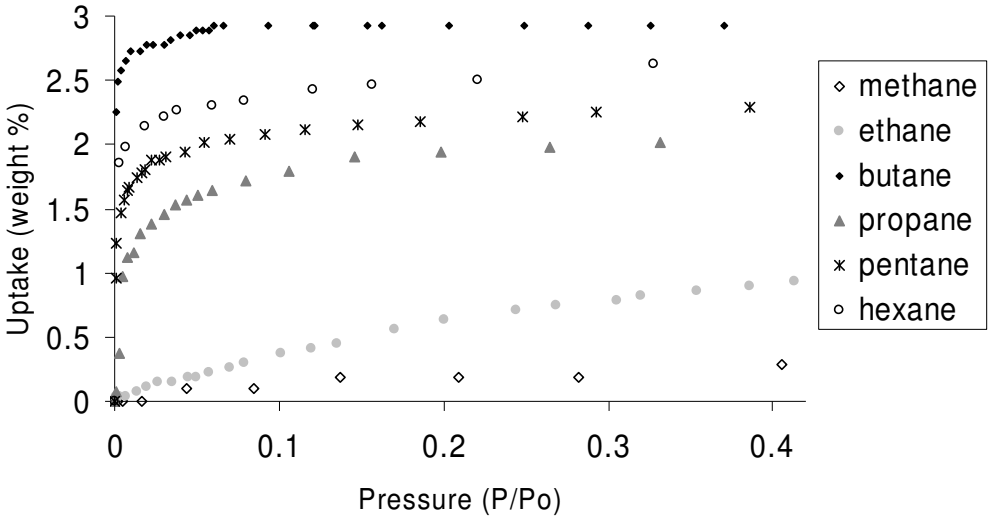

Figure IV.5. *n*-Alkane sorption isotherms for **21** at room temperature.

Correlating these uptakes with the molecular volume of each alkane [167] indicates that ethane, propane, *n*-butane, *n*-pentane and *n*-hexane occupy 38, 57, 74, 55, and 57% of the cavity space, respectively. The relatively low occupancy observed for ethane and propane can be correlated to the weakness of the van der Waals attraction in which these small molecules can engage. It is not directly obvious why the uptake observed for *n*-butane is greater than that for *n*-pentane and *n*-hexane. However, keeping in mind that two linear alkanes placed side by side necessitate more than 7.5 Å in width, the narrow channels of **21** most probably force the longer alkanes *n*-pentane and *n*-hexane to pack on top of one another leading to a somewhat inefficient occupation of the space. Molecular mechanics simulations (MM2 force field) seem to confirm this hypothesis. *n*-Pentane and *n*-hexane are predicted to lay in the channels with their main molecular axis aligned with *c*-axis. By contrast, *n*-butane in the gauche conformation is small enough to lay sideways in the channels (Figure IV.6) thus leading to a more efficient occupation of the channels. This difference is probably at the origin of the higher uptake observed for *n*-butane.

We were curious to determine at what point volatile hydrocarbons become too sterically demanding to enter the cavities of **21**. We investigated whether branched aliphatics would adsorb by exposing **21** to vapors of 3,3-dimethylbut-1-ene. There was a rapid uptake that plateaued at 1.5 wt % indicating formation of **21**⊃0.26 C_6H_{12}. At higher partial pressures additional uptake was observed and assigned to surface adsorption. Thus we concluded that branched aliphatics can be accommodated by the cavities.

Looking for other bulky candidates, we investigated aromatic hydrocarbons and measured the uptake of benzene and some of its simple methyl-substituted derivatives. Benzene readily fills the pores and appears to fit very well inside of the cavities. The 3.8 wt % is the highest weight gain of the hydrocarbons measured. The stoichiometry of this adduct is **21**⊃0.69-C_6H_6, which is similar to the stoichiometry of the *n*-butane adduct (Figure IV.7).

Toluene and *meta*-xylene were also found to go into the cavities, both at 3.5 wt %. A ^{1}H NMR experiment on a sample of **21** exposed to 1,3,5-triisopropyl benzene overnight and then dissolved in d_6-acetone showed no presence of any peaks arising from this benzene derivative, indicating no uptake had occurred. 1,3,5-Triisopropyl benzene is probably too big to enter the cavities.

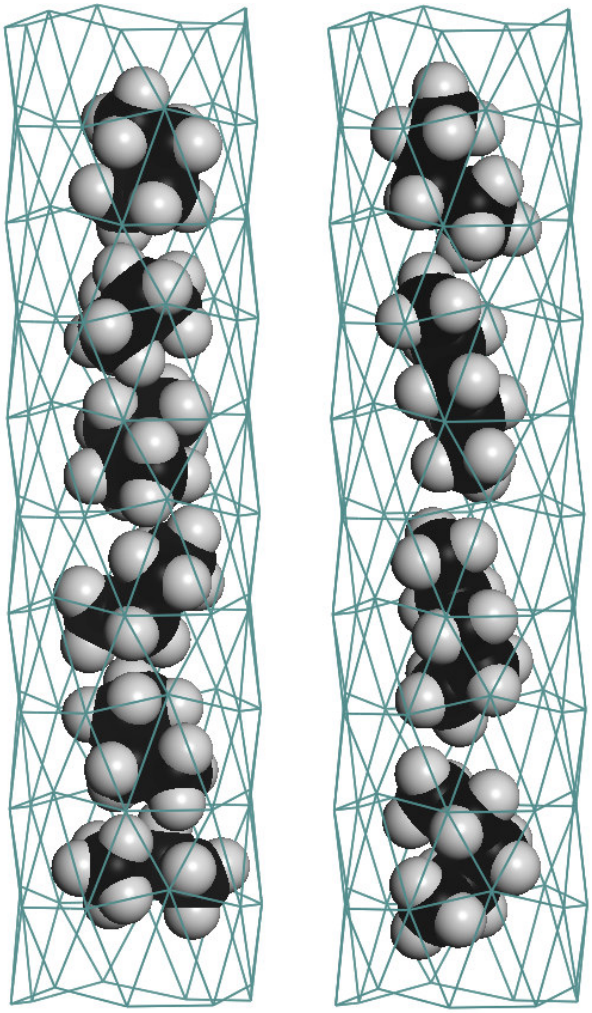

Figure IV.6. Arrangements and conformations of *n*-butane and *n*-pentane molecules in the channels of **21** as determined by molecular mechanics simulations. The walls of the channels are approximated by the H atoms of the $SiMe_3$ groups.

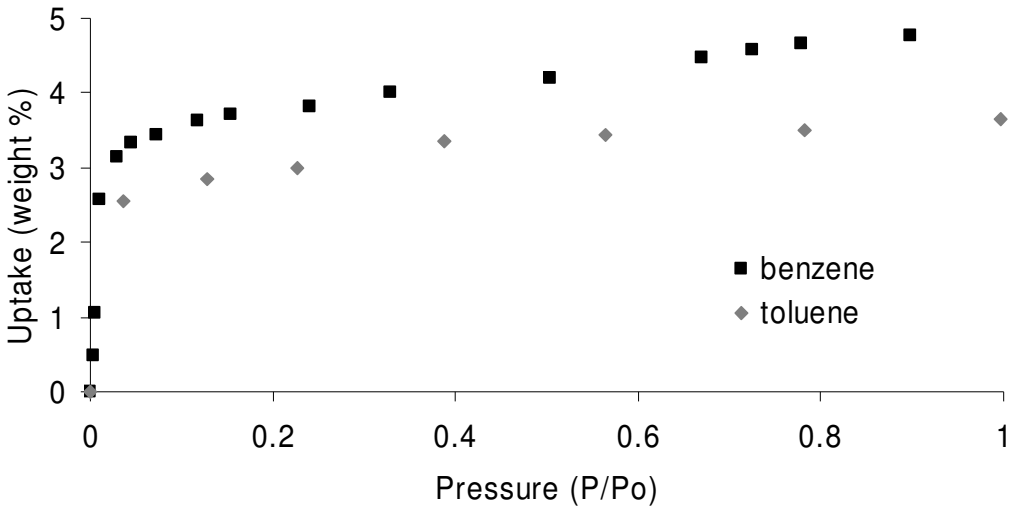

Figure IV.7. Benzene and toluene sorption isotherms for **21** at room temperature.

In order to evaluate the stability of the adducts containing the alkanes, we have studied guest release under vacuum (Figure IV.8). Although ethane is rapidly removed from the pores in vacuum, the propane and *n*-butane adducts show a more gradual weight loss as the vacuum is applied. This behaviour attests of the strength of the host-guest interactions. X-ray powder diffraction data collected after uptake and guest release shows retention of the original structure indicating that **21** displays permanent microporosity, as will be described in the following pages.

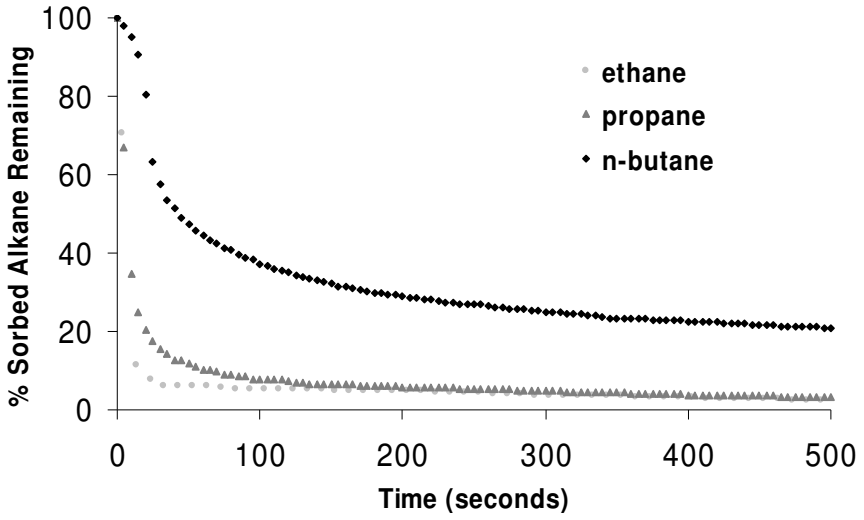

Figure IV.8. Desorption of alkanes under vacuum as a function of time for **21**⊃0.57-ethane, **21**⊃0.67-propane, and **21**⊃0.71-*n*-butane.

Microporous solid **21** does not immediately release the trapped alkanes upon removing the *n*-alkane atmosphere. In fact, the samples are sufficiently stable to be analyzed by ^{1}H MAS NMR (Figure IV.9). [168] Before exposure, **21** shows two resonances corresponding to the methyl groups (0.18 ppm) and the aromatic CH proton (6.29 ppm) of 1,3,5-(TMSC≡C)$_3$C$_6$H$_3$. After exposure to ethane, an additional resonance assigned to the methyl group of the entrapped ethane molecules appears at 0.90 ppm. The spectrum also displays a sharp resonance at 0.59 ppm which corresponds to free ethane caught in the headspace of the rotor. It is interesting to note that the entrapped ethane resonance is only slightly shifted with respect to the free gas. This observation indicates that the walls of the channels do not generate significant magnetic anisotropy within the internal space of the channels. The spectrum of **21** after exposure to propane results in the appearance of two new signals at 1.15 and 0.75 ppm which are respectively assigned to the methylene and methyl group of the entrapped hydrocarbon. The spectra of **21** after exposure to *n*-butane, *n*-pentane and *n*-hexane show an increase in the intensity of the methylene signal with respect to the methyl signal. It is important to

note that in the spectra of the *n*-pentane and *n*-hexane samples the two different types of methylene groups are not resolved and are detected as a single resonance. [169-172]

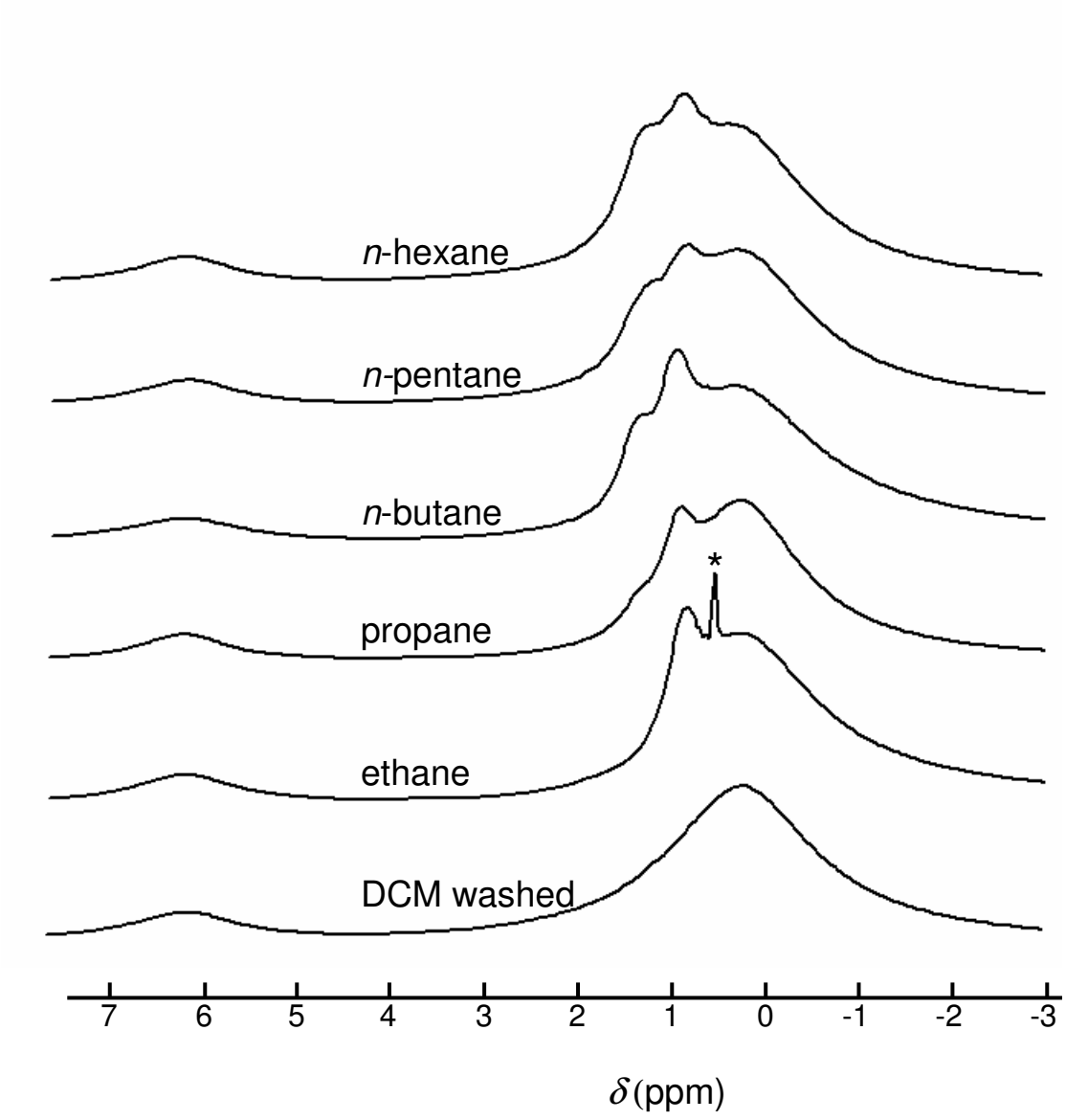

Figure IV.9. ^{1}H MAS NMR spectra of **21** before and after alkane adsorption. The peak assigned to free ethane gas is indicated (*).

As mentioned previously, the interior of the pores is nonpolar, leading to the enhanced uptake of similarly nonpolar solvents and gases while excluding moisture. To follow up on this contention, we investigated the uptake of other volatile molecules containing heteroatoms that range from non-polar to polar.

The uptake profiles of both methanol and ethanol are substantially different from those of the hydrocarbons. From the initial introduction of methanol up to a pressure of 100 mm Hg of pressure, no significant uptake (< 0.5 wt %) was observed. However a rapid uptake was recorded once the pressure reached 100 mm Hg. This uptake leveled off at 3.3 wt % (Figure IV.10). The gain in weight corresponds to the uptake of 1.5 equivalents of methanol, and may indicate the formation of a new adduct of methanol and **7**. [46] A sample of **21** was also exposed to methanol to determine if the odd uptake characteristics had anything to do with breaking apart the crystal lattice of **21**. In fact, while many of the peaks remained, there is a new broad peak growing in at 4.92 º, at a lower angle than the sharp 100 peak. Additionally, the 200 peak is conspicuously absent in the diffraction pattern (Figure IV.10). While the chemical changes associated with this uptake will not be elaborated upon, there does appear to be some type of degradation of the original crystal structure upon the prolonged exposure of methanol to **21**. Exposure of **21** to ethanol does not show the abrupt weight change observed with methanol, but the profile of the uptake does appear significantly different from the hydrocarbon samples (Figure IV.12).

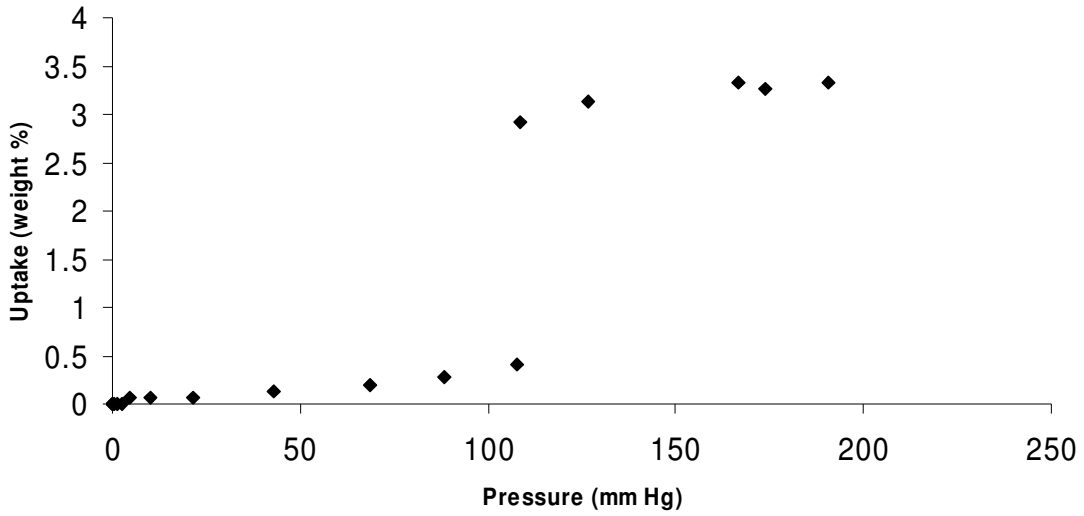

Figure IV.10. Methanol sorption into **21** at room temperature.

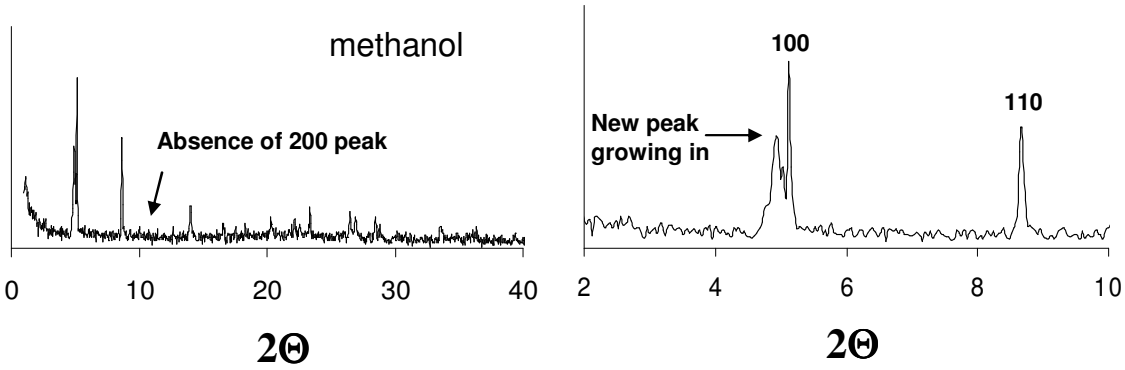

Figure IV.11. XRD pattern of **21** exposed to the vapors of methanol (left), with an expanded view of the low-angle region (right).

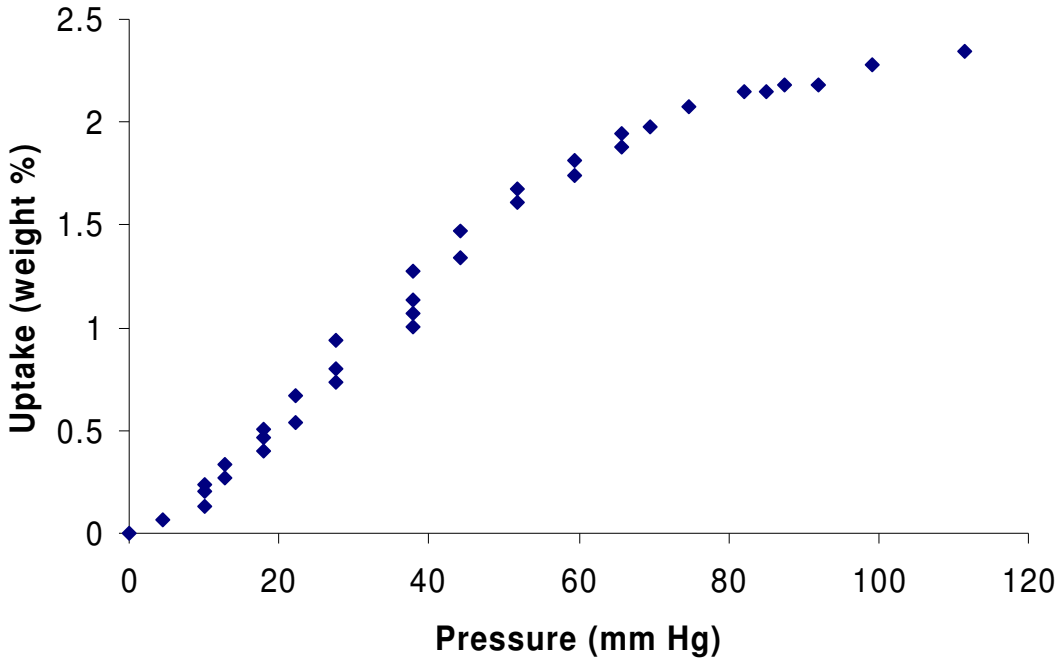

Figure IV.12. Ethanol sorption into **21** at room temperature. Multiple readings were taken at given pressures during the sorption, the largest value is the final value.

The adsorption of dichloromethane into **21** proceeded by a rapid uptake of solvent up to 4 wt % and then followed by a rapid weight loss to just above the starting weight of the sample. These results have not been rationalized as of this time, but may offer a reason why cleaning the adduct **21** with dichloromethane prior to further experimentation leaves an "empty" framework as further confirmed by TGA and gravimetric experiments.

The *apo*-compound **21**, dried in air after washing with dichloromethane, was investigated by X-ray powder diffraction. The diffraction patterns showed a series of peaks which correspond to those predicted based on the single crystal diffraction data of **21**. In order to assess the stability of the structure upon guest inclusion, the postion of the *hkl* reflections 100, 110, 200, 101, 400, and 510 were monitored.

Full x-ray diffraction patterns for samples of **21** exposed to saturated atmospheres of ethane, *n*-butane, *n*-pentane, and *n*-hexane were collected. The patterns

show the same diagnostic reflections at the same angles, which confirms the retention of the structure (Figure IV.13). Additionally, the *n*-butane sample was removed and placed under vacuum overnight and run again as a desorbed sample. This pattern has no significant differences with the other patterns. This shows that the adsorption and desorption processes are reversible with these lighter hydrocarbons.

To confirm that the alkane uptakes we had recorded were not artifacts of a persistent experimental error, thermogravimetric analyses were performed. Two samples were run: a sample of **21** saturated with *n*-pentane and a DCM-washed sample of **21** (Figure IV.14). The *n*-pentane-saturated sample began losing weight above 100 ºC and more and more rapid weight loss was recorded until 196.5 ºC. At this point, the weight loss slowed, and a new weight decrease associated with decomposition of **21** and concomitant sublimation of **7** emerged. [163] The total weight loss at 196.5 ºC was 2.84 % for the *n*-pentane sample, which exceeds the amount of uptake calculated for the interior of the alkylated cavities, but this may be rationalized by noting that upon saturating the atmosphere with *n*-pentane the crystalline solid is capable of additional surface uptake of hydrocarbon.The DCM-washed material showed a negligible weight loss of 0.24 % under 195 ºC, indicating that the cavities are essentially empty.

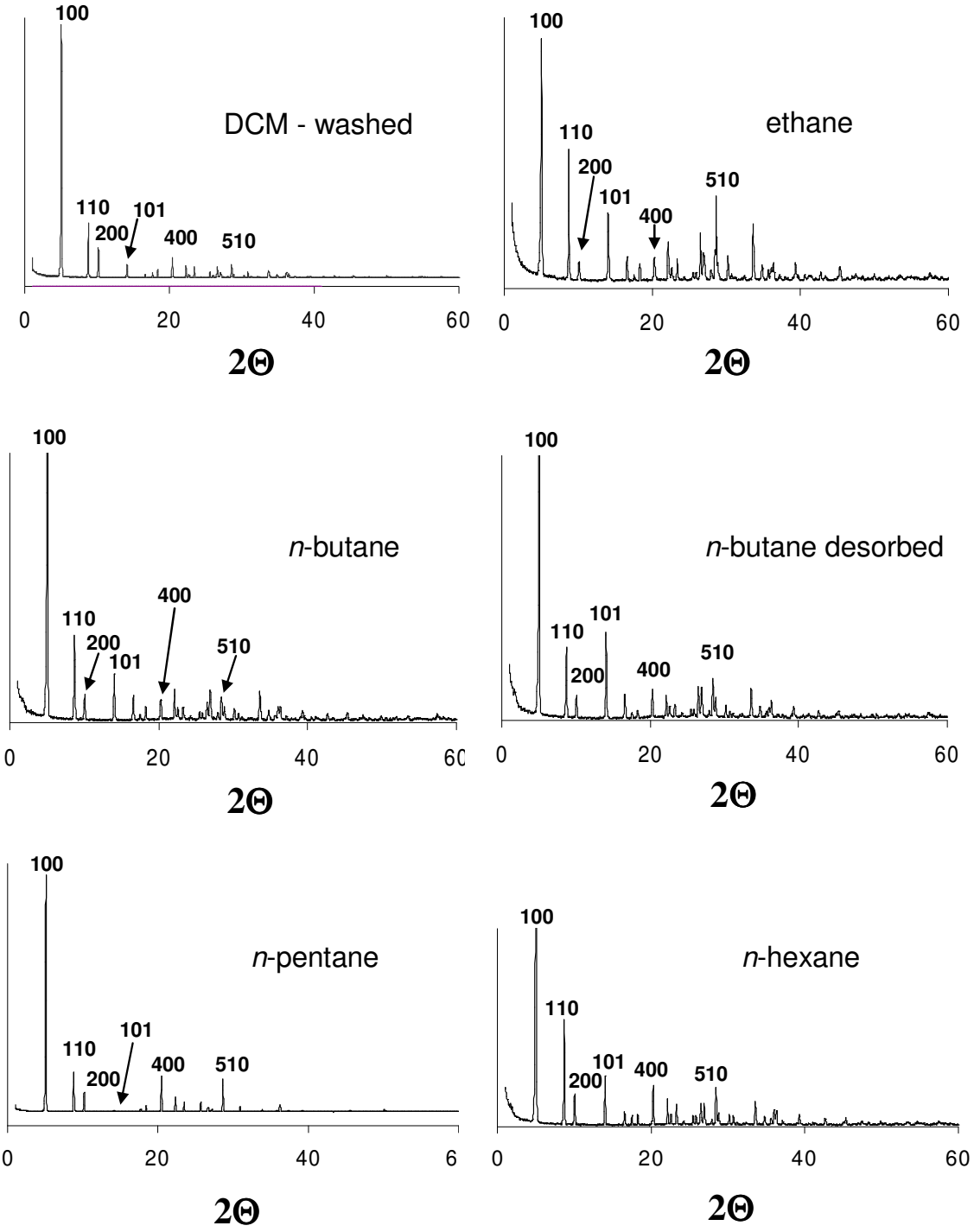

Figure IV.13. XRD patterns of **21** washed with dichloromethane and exposed to different alkanes.

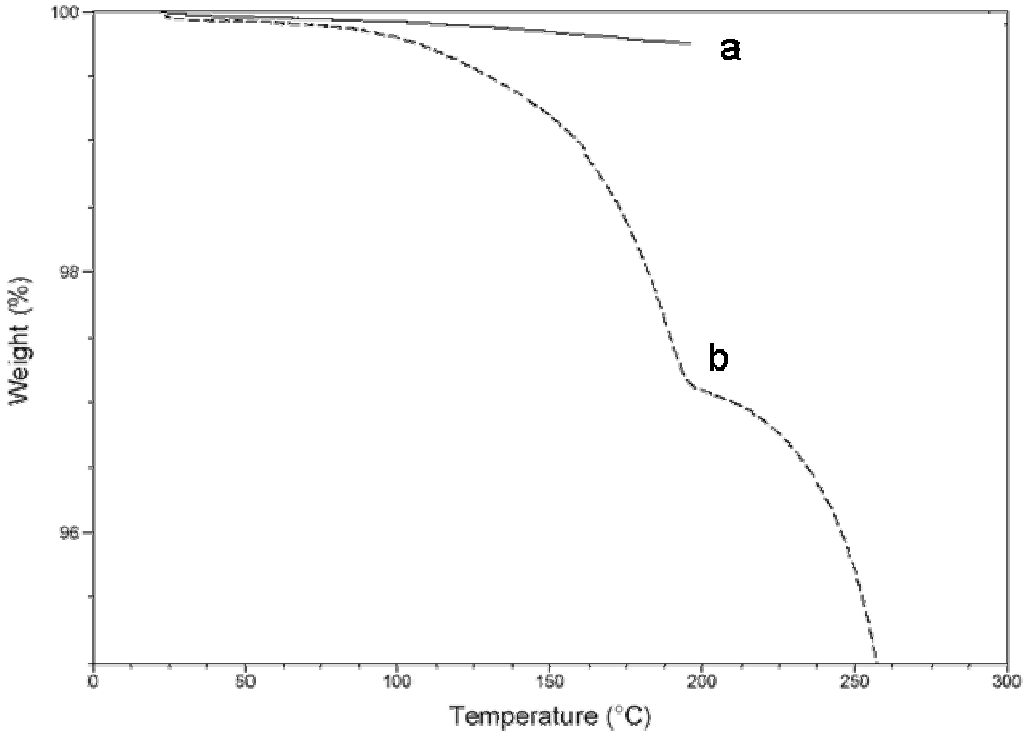

Figure IV.14. TGA traces for dichlormethane washed **21** (a) and a sample of **21** exposed to a saturated atmosphere of *n*-pentane overnight.

In conclusion, we describe how secondary Hg-π and Hg-$C_{acetylenic}$ interactions can be harnessed for the construction of supramolecular columns. Control over these unusual supramolecular interactions allows for the design of a porous compound which traps hydrocarbons in its alkylated interior.

Table IV.1. Crystal data, data collection, and structure refinement for **21, 21⊃0.82-$CHBr_3$**, and **21⊃0.73-C_6H_6**.

Crystal data	**21**	**21⊃0.82-$CHBr_3$**	**21⊃0.73-C_6H_6**
Formula	$C_{39}H_{30}F_{12}Hg_3Si_3$	$C_{39.81}H_{30.82}Br_{2.44}F_{12}Hg_3Si_3$	$C_{43.4}H_{34.4}F_{12}Hg_3Si_3$
M_r	1412.67	1619.88	1469.69
Crystal size (mm^3)	0.12 × 0.03× 0.03	0.13 × 0.10 × 0.08	0.09 × 0.06 × 0.06
Crystal system	Hexagonal	Hexagonal	Hexagonal
Space group	$P6_3/mmc$	$P6_3/mmc$	$P6_3/mmc$
a (Å)	19.852(3)	19.900(3)	19.861(8)
b (Å)	19.852(3)	19.900(3)	19.861(8)
c (Å)	6.5659(13)	6.5529(13)	6.571(4)
α(°)	90	90	90
β (°)	90	90	90
γ(°)	120	120	120
V ($Å^3$)	2241.0(7)	2247.3(6)	2244.7(18)
Z	2	2	2
ρ_{calc} (g cm^{-1})	2.093	2.391	2.174
μ (mm^{-1})	10.407	12.550	10.395
F(000) (e)	654	1490	1369
Data Collection			
T/K	110(2)	110(2)	110(2)
Scan mode	ω	ω	ω
hkl range	-22→22, -22→22, -7→7	-22→22, -22→22, -7→7	-25→25, -25→25, -8→8
Measured refl.	13470	12929	18924
Unique refl., [R_{int}]	656 [0.0942]	659 [0.0492]	1021 [0.0885]
Refl. used for refinement	656	659	1021
Absorption Correction	SADABS	SADABS	SADABS
T_{min}/T_{max}	0.357004	0.550232	0.554661
Refinement			
Refined parameters	70	77	80
R_1,[a] wR_2[b] [I>2σ(I)]	0.0319, 0.1016	0.0489, 0.1219	0.0377, 0.0907
ρ_{fin} (max/min) ($eÅ^{-3}$)	1.8630, -1.167	5.544, -1.208	2.115, -2.706

[a] $R_1 = \Sigma (||F_o| - |F_c||)/|F_o|$; [b] $wR_2 = \{\Sigma [w(F_o^2 - F_c^2)^2]/\Sigma [w(F_o^2)^2]\}^{1/2}$; $w = 1/[\sigma^2(F_o^2) + (aP)^2 + bP]$; $P = (F_o^2 + 2F_c^2)/3$. For **21**, $a = 0.1125$, $b = 0$; for **21⊃0.82-$CHBr_3$**, $a = 0.1240$, $b = 15.000$, for **21⊃0.73-C_6H_6**, $a = 0.1000$, $b = 0.000$.

IV.4. Experimental

General. *Warning! Due to the toxicity of the mercury compounds discussed, extra care was taken at all times to avoid contact with solid, solution, and air-borne particulate mercury compounds.* The studies herein were carried out in a well aerated fume hood. Atlantic Microlab, Inc., Norcross, GA, performed the elemental analyses. All commercially available starting materials and solvents were purchased from Aldrich Chemical and VWR, Inc. and used as provided. DSC/TGA experiments were performed with a TA Instruments Q600 SDT under an air purge at heating rates of 20 ºC/min. All solvents were purchased commercially and used as provided for crystallizations. IR spectra were recorded with a ATI-Mattson Genesis series FTIR spectrometer with the samples prepared as compressed KBr pellets. 1,3,5-tris(trimethylsililylethynyl)benzene was prepared as described by Leininger *et al.* [173] Trimeric perfluoro-*ortho*-phenylene mercury (**7**) was prepared as described by Sartori *et al.* [52]

Synthesis of [7•1,3,5-(TMSC≡C)$_3$C$_6$H$_3$] (21). Compound **7** (30 mg, 0.029 mmol) and 1,3,5-(TMSC≡C)$_3$C$_6$H$_3$ (10.6 mg, 0.029 mmol) were dissolved in 10 mL of THF. Slow evaporation of the solvent led to the formation of colorless feathery crystals which were washed twice with CH_2Cl_2 to afford **21** in 80% yield. mp ~196 °C (decomp.). Anal. Calcd for $C_{39}H_{30}F_{12}Hg_3Si_3$: C, 33.16; H, 2.14. Found: C, 33.65; H, 2.09. IR (KBr disc, cm^{-1}): 2959, 2164, 1252, 1162, 1046, 981, 880, 844, 760, 702, 692, 679, 653. ^{13}C MAS NMR (7 kHz spinning): for **1** component: δ = 156.0 (t, Hg-*C*-C, $J_{Hg,C}$ = 743 Hz), 144.1, 136.5 (broad, F-*C*); for 1,3,5-(TMSC≡C)$_3$C$_6$H$_3$ component [174]: δ = ~135 (obscured by peak from **1**), 122.2, ($C_{aromatic}$) 100.2, 97.4 (C_{sp}), -1.9 (C_{silyl}).

Gas adsorption measurments. Sorption isotherm measurements were performed by monitoring the weight change as a function of pressure using a Cahn RG Electrobalance connected to a manifold. A known weight of **21** (10-20 mg) was placed in the weighing pan. After evacuation of the system, the adsorbate was added incrementally via the manifold. Data points were recoded at equilibrium when no further weight change was observed. Guest release was studied by monitoring the weight of the sample every 5-10 seconds under vacuum.

Solid state NMR measurements. The room-temperature solid-state ^{1}H NMR experiments were performed on an Avance-400 Solids NMR spectrometer with a 4 mm probe at a spinning rate of 7 kHz. Saturated samples were packed in the rotor under ambient atmosphere. For ethane and propane, the rotor was packed with **21,** exposed to an atmosphere of the gas, sealed and transferred to the NMR spectrometer.

Crystal structure determinations: X-ray data for **21**, **21⊃0.82-$CHBr_3$**, and **21⊃0.73-C_6H_6** were collected on a Bruker SMART-CCD diffractometer using graphite-monochromated Mo Kα radiation (λ = 0.71073 Å). Specimens of suitable size and quality were selected and glued onto a glass fiber with freshly prepared epoxy resin. The structure was solved by direct methods, which successfully located most of the non-hydrogen atoms. Subsequent refinement on F^2 using the SHELXTL/PC package (version 6.1) allowed location of the remaining non-hydrogen atoms. The bromoform molecules in **21⊃0.82-$CHBr_3$** were found to be disordered about two symmetry equivalent positions. In order to obtain a satisfactory model of the bromoform molecules, the z coordinate of the carbon (C(10)) was fixed so that the resulting C-Br distance is close to 1.86 Å as reported for pure bromoform. [175] The bromoform molecule refined with a partial occupancy of 82%.

XRD experiments. Powder X-ray diffraction patterns were recorded on a Bruker D8 Advanced powder X-ray diffractometer (CuKα radiation; operating at 40 kV and 40 mA; exit slit 1.0 mm, antiscattering slit 1.0 mm, detector slit 0.2 mm), fitted with a diffracted beam monochromator and a scintillation counter. Data were collected by the θ/2θ mode in Bragg-Brentano geometry over the 2θ range 1 to 60 °, with a step size of 0.04 ° and a counting time of 5 sec/step.

Molecular modeling. The conformation and arrangement of the butane and pentane molecules in the channels of **21** as shown in Figure IV.6 were calculated by molecular mechanic calculations using the MM2 force field as implemented by Chem 3D. In these calculations, the walls of the channels were approximated by the hydrogen atoms of the trimethylsilyl groups that are oriented toward the center of the channel. As a starting point, the alkane molecules were placed in the channels and confined to a

portion of the channel in order to reproduce the loading derived from the gravimetric measurements. The channels were then stoppered with dummy atoms so that the alkane molecules remained within the original space corresponding to that derived from gravimetric measurements. The hydrogen atoms of the walls as well as the stoppers were kept in fixed positions while the conformation and arrangement of the alkane molecules were annealed by molecular dynamic simulation at the temperature setting of 300 K for 1000 iterations. The energy of the alkanes were subsequently minimized using an Root Mean Step (RMS) of 0.01. The stoppers were then removed and the energy of the alkanes were again minimized using a Root Mean Square Force (RMS) of 0.01 kcal/mol·Å. These simulations converged to a loading of 0.67 for butane and 0.44 for pentane which can be compared to the values of 0.71 and 0.45 determined gravimetrically.

CHAPTER V

MOLECULAR CRYSTALS INVOLVING TRIMERIC PERFLUORO-*ORTHO*-PHENYLENE MERCURY AND 1,3,5-TRIETHYNYL BENZENES: NOVEL PROPERTIES AND CRYSTAL ENGINEERING

V.1. Introduction

Molecules containing the 1,3,5-triethynyl benzene core are attracting a great deal of attention and have become common motifs in light-harvesting and light-emitting derivatives. [174, 176, 177] Our group has studied the changes that occur in the photophysical properties of unsaturated hydrocarbons upon their complexation to organomercurials such as trimeric perfluoro-*ortho*-phenylene mercury ($[o\text{-}C_6F_4Hg]_3$, **7**). Such changes include fluorescence-quenching and induced phosphorescence that result from heavy-atom effects. [88, 89, 97]

In this chapter, we present results that we have obtained with the complexation of 1,3,5-triethynyl benzenes by **7**. As described in the previous chapter, we have discovered the ready formation of porous crystals composed of the 1:1 adduct of **7** and 1,3,5-tris-(trimethylsilylethynyl) benzene (**21**). [178] We wondered whether modifying the end groups of the 1,3,5-triethynyl benzene building block would change the supramolecular structures of the adducts formed with **7**.

V.2. The interaction of $[o\text{-}C_6F_4Hg]_3$ and 1,3,5-triethynyl benzene

Scheme V.1.

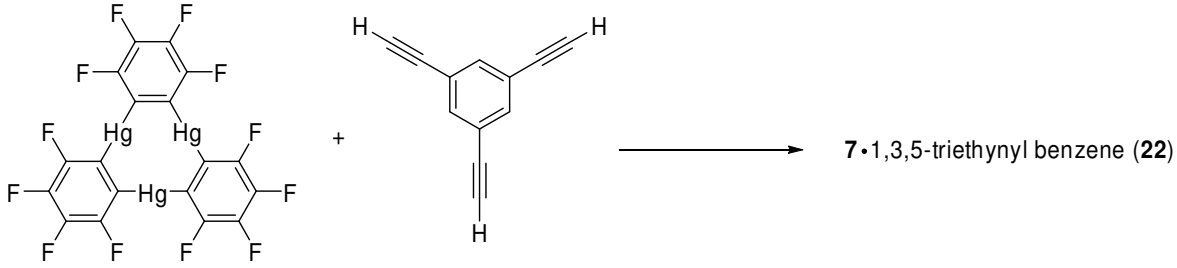

The first adduct synthesized was [**7**•1,3,5-triethynyl benzene] (**22**). This compound was formed by mixing stoichiometric amounts of **7** with 1,3,5-triethynyl benzene in THF and was isolated as a crystalline compound after slow evaporation of the solvent (Scheme V.1). The crystals, formed in moderate yield, belong to the monoclinic space group *C*2/c. The asymmetric unit of **22** contains half a molecule of 1,3,5-triethynyl benzene and half a molecule of **7** (Figure V.1). The two components are co-planar, and form offset 1:1 stacks (Figure V.2). Each 1,3,5-triethynyl benzene molecule has two crystallographically distinct ethynyl groups. Two of the ethynyl arms are directly located over the center of molecules of **7**, one on each side of the plane of the 1,3,5-triethynyl benzene, with short distances to the centroid of **7** (C(16), 3.18 Å and C(17), 3.29 Å). Additionally, the adjacent phenyl carbon atoms, C(11) and C(12), have short contacts with Hg(2) at a distance of 3.30 and 3.50 Å, respectively. The other ethynyl group is oriented away from the mercury centers of the neighboring molecules of **7**, although the hydrogen atom nears a coplanar molecule of **7** at an estimated H-F distance of 2.52 Å.

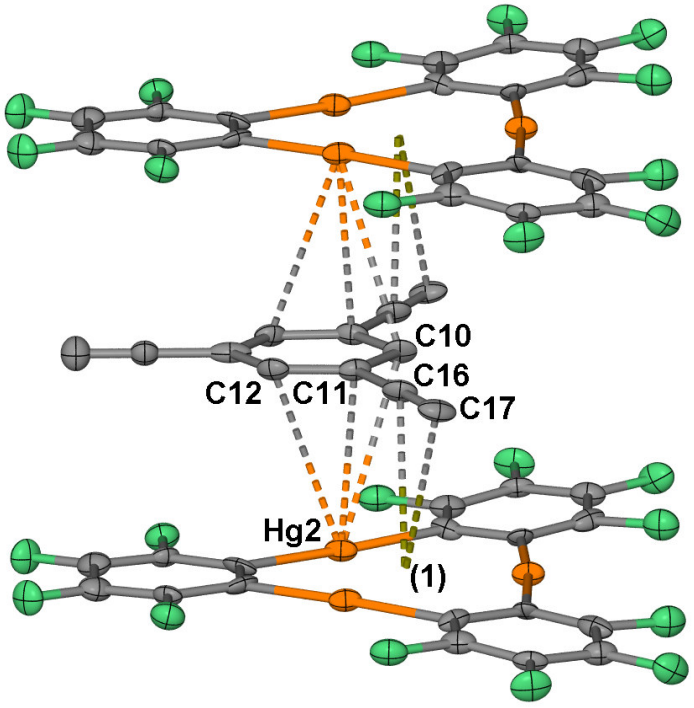

Figure V.1. ORTEP view (50% ellipsoid) of the intermolecular interactions in **22** featuring two C_{alkyne} distances (Å) to the centroid of molecule **7**, (1), C(16)-(1) 3.18, C(17)-(1) 3.29. Representative intermolecular distances (Å): Hg(2)-C(10) 3.49, Hg(2)-C(11) 3.29, Hg(2)-C(12) 3.50.

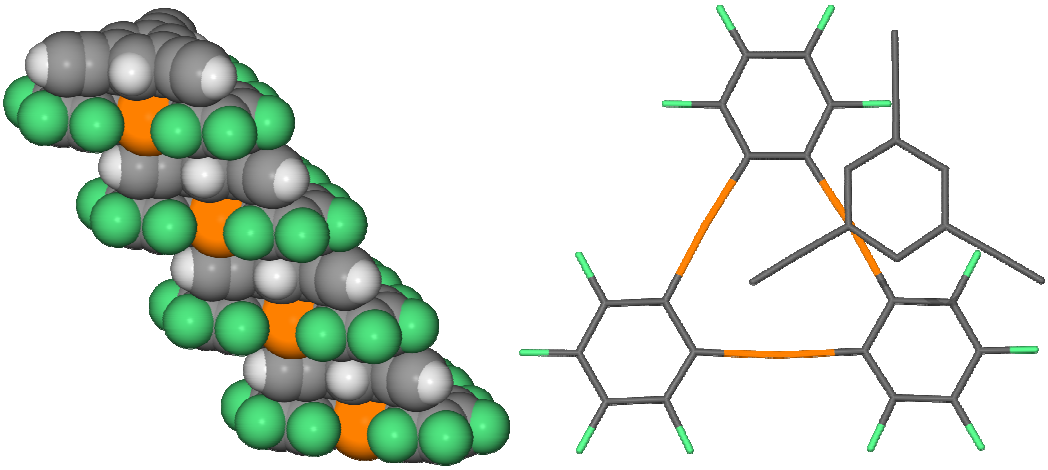

Figure V.2. (Left) Space-filling view of a stack of **22** with four repeating units and (right) a stick representation of the two components along the *c*-axis.

V.3. The interaction of $[o\text{-}C_6F_4Hg]_3$ and 1,3,5-tris(phenylethynyl) benzene

Scheme V.2.

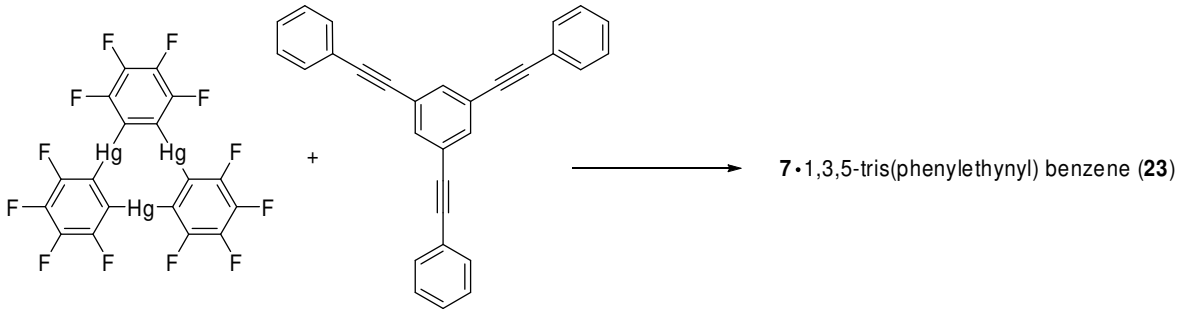

Next, we investigated the interaction of 1,3,5-tris(phenylethynyl) benzene with **7** (Scheme V.2). This compound was studied in the solid state [179] and has also been used for the construction of various supramolecules. Siegel *et al.* used 1,3,5-tris(phenylethynyl) benzene as a co-crystal with its perfluorinated analogue, 1,3,5-tris(perfluorophenylethynyl) benzene. [180] The resulting adduct displayed a higher melting point than either of the individual components as the two molecules alternate and display numerous close fluoroarene-arene interactions with each other in infinite 1:1 binary stacks.

[**7**•1,3,5-tris(phenylethynyl) benzene] (**23**) was synthesized in the same manner as **22**. Crystals of **23** belong to the hexagonal space group $P6_3/mmc$ (Figure V.3) and the asymmetric unit contains one-sixth of each of the two molecules. Examination of the structure reveals the formation of extended ABABA binary columns that propogate along the *c*-axis of the unit cell, perpendicular to the planes formed by the two components (Figure V.4). In fact, the stacks mirror the D_{3h} symmetry of both of the components. The molecules interact via secondary Hg-π contacts (Hg(1)-C(5) = 3.341(7) Å, Hg(1)-C(6) = 3.362(6) Å) with distances within the sum of the van der Waals radii of mercury (1.7-2.0 Å) [110, 111] and carbon (1.7 Å). [129] These stacks are rather

compact as indicated by the distance of 3.27 Å separating the centroids of the two components. This centroid distance can be compared to the 3.24 Å distance found in [**7**•benzene], [86] which adopts a comparable stacked structure in a hexagonal space group (*R*-3c). It is even more similar to [**7**•1,3,5-tris(trimethysilylethynyl) benzene], which crystallizes in the same space group and has a slightly larger centroid-centroid distance of 3.28 Å. [178] The structure was solved twice with data collected at 77 K and room temperature (labeled as **23** and $\mathbf{23}_{RT}$, respectively) and no significant differences in the structures were noted.

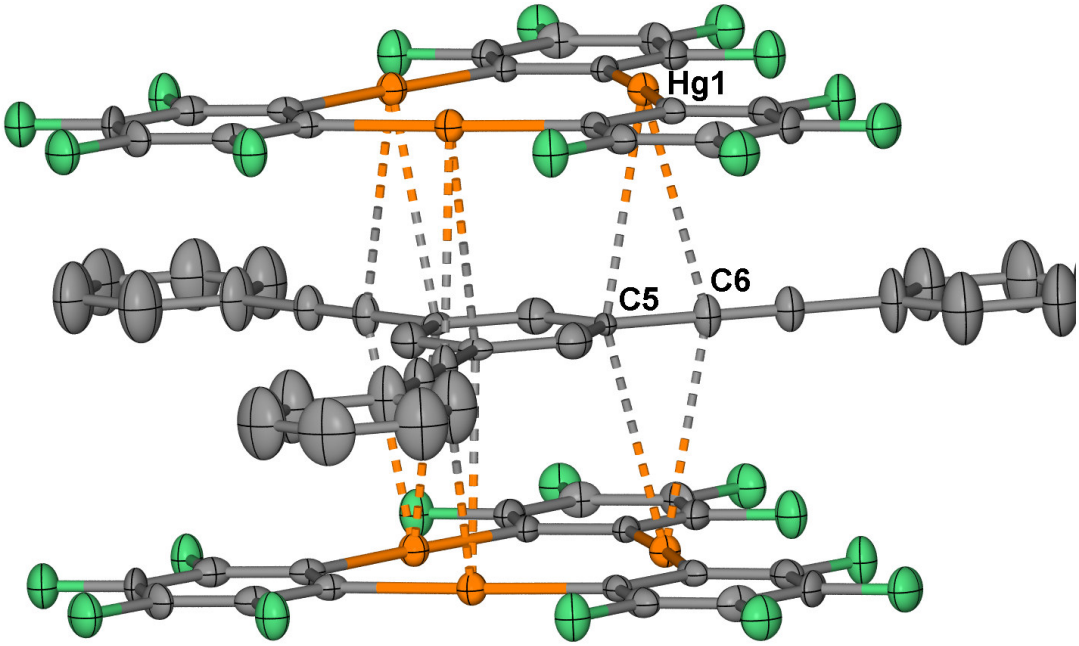

Figure V.3. ORTEP view (30% ellipsoid) of the intermolecular interactions in **23**. Representative intermolecular distances (Å): Hg(1)-C(5) 3.34, Hg(1)-C(6) 3.36.

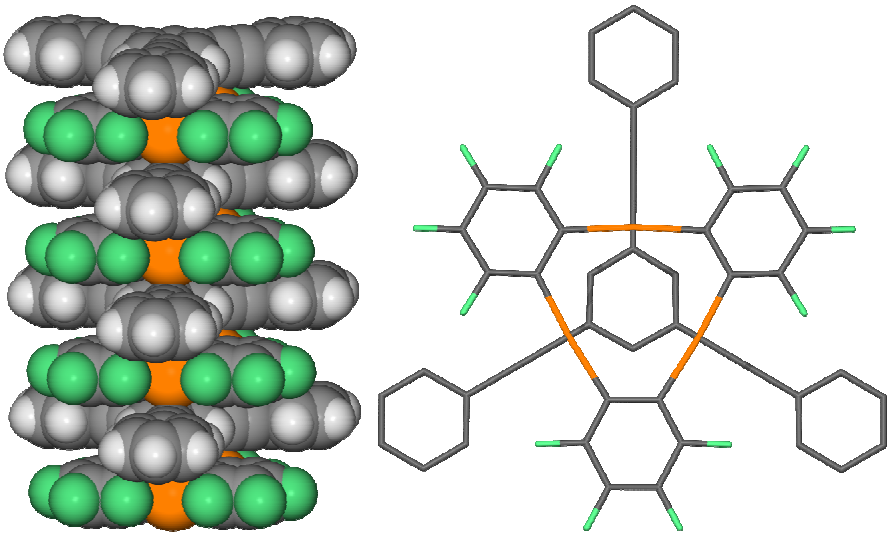

Figure V.4. (Left) Space-filling view of a stack in **23** with four repeating units and (right) a stick representation of the two components viewed along the *c*-axis.

Compound **23** exhibits a strong red emission upon exposure to a handheld UV-lamp. This is in contrast to uncoordinated 1,3,5-tris(phenylethynyl) benzene that displays a blue emission in identical conditions. Fluorescence spectroscopy was used to analyze the sample at room temperature and 77 K, and a series of emission peaks ranging from 545 to 650 nm were recorded, accounting for the red color. No reference to emissions in this region could be found. At 77 K all of the three prominent emission peaks shown in Figure V.5 were found to have lifetimes ranging from 4.3 to 4.6 milliseconds, indicating that these are forbidden transitions even in the presence of heavy-atoms within the adduct. Based on this data it appears reasonable to propose that the emissions correspond to the phosphorescence of 1,3,5-tris(phenylethynyl) benzene. In order to confirm this assumption, we decided to measure the phosphorescence spectrum of 1,3,5-tris(phenylethynyl) benzene, which has not been reported in the literature.

A sample of pure 1,3,5-tris(phenylethynyl) benzene was measured in an EPA matrix (Figure V.6). The emission bands observed between 350-440 nm correspond to the fluorescence of 1,3,5-tris(phenylethynyl) benzene which has been previously

reported. However, new emission peaks in the region of 470-550 nm were also detected with lifetimes of 2.8 seconds. Presumably, these peaks correspond to the phosphorescence of the chromophore. The energy range in which the phosphorescence of 1,3,5-tris(phenylethynyl) benzene appears overlaps with that observed for the emission of **23.** On this basis it is reasonable to assume that the emission of **23** is indeed the phosphorescence of 1,3,5-tris(phenylethynyl) benzene. The vibronic progressions in the spectra of 1,3,5-tris(phenylethynyl) benzene and **23** do not match thus complicating a definitive assignment.

Similar results were obtained with **22**: an unreported red-shifted emission was observed at 496 nm with a room temperature lifetime of 0.47 ms, and again there was a paucity of literature dealing with any triplet emissions in the pure compound.

In an effort to determine the origin of the long-lived emissions that were detailed above, a series of DFT calculations were performed. The purpose was to determine the electronic structures of the singlet and triplet states of 1,3,5-tris(phenylethynyl) benzene and 1,3,5-triethynyl benzene and then assess the calculated energy difference between these states to estimate where a $T_1 \rightarrow S_0$ emission would be expected.

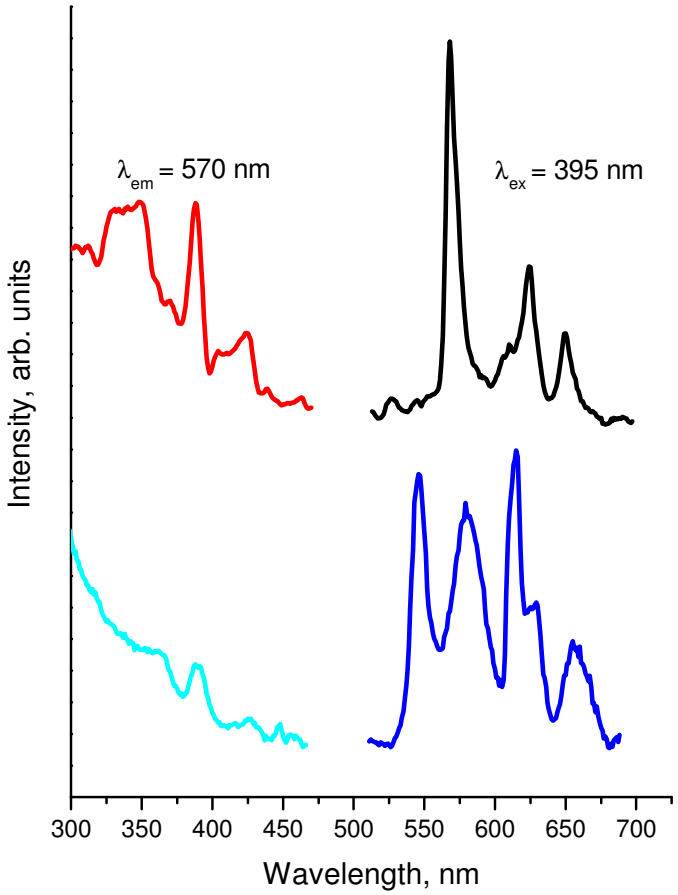

Figure V.5. Excitation and emission of the solid adduct **23** at 77 K (top) and room temperature (bottom).

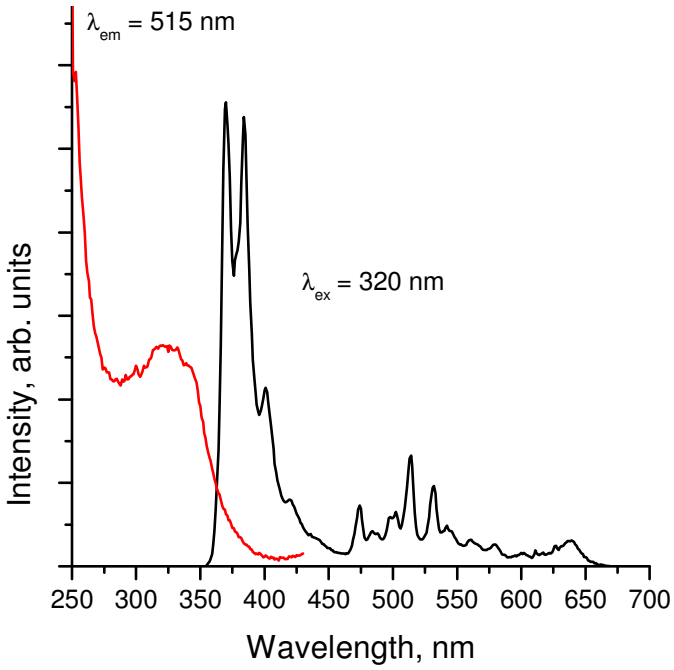

Figure V.6. Excitation and emission of pure 1,3,5- tris(phenylethynyl) benzene in EPA matrix with fluorescence (350-440 nm) and phosphorescence (470-650 nm).

The methodology we devised was to optimize the geometries of each state and then use the sum of electronic and zero-point energies reported in the frequency calculations as the lowest energies of both states. [181] This method was tested with naphthalene at the same level of theory (see experimental section). In this case, the difference in energies was 20670 cm^{-1}, which corresponds very well with the experimentally deteremined $T_1 \rightarrow S_0$ phosphorescence of pure naphthalene. [182]

The difference in the singlet and triplet ground state energies for 1,3,5-triphenylethynyl benzene was nearly 19960 cm^{-1}. This value is 1137 cm^{-1} *less* than the onset of phosphorescence in the aforementioned EPA matrix experiment, and 1600 cm^{-1} *greater* than the 18350 cm^{-1} value of the first emission peak of **23**.

V.4. The interaction of $[o\text{-}C_6F_4Hg]_3$ and 1,3,5-tris(4-*n*-butyl phenylethynyl) benzene

Scheme V.3.

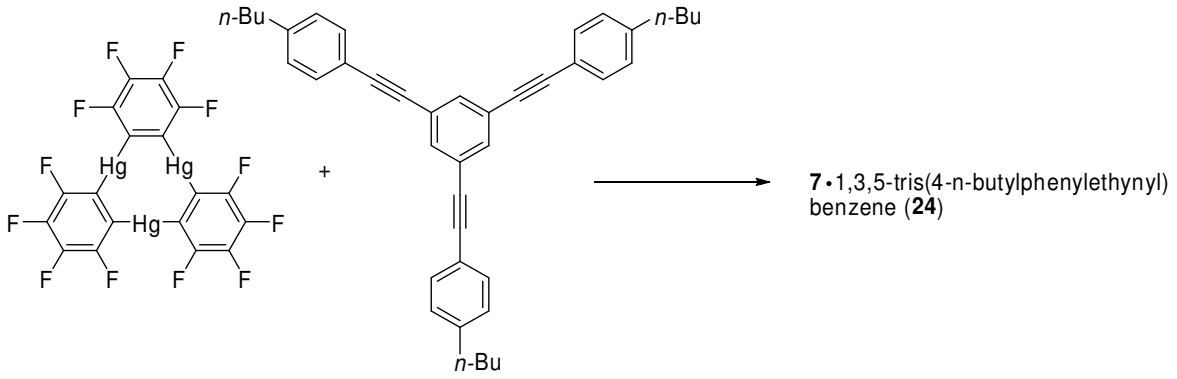

Crystals of [**7**•1,3,5-tri(4-*n*-butyl-phenylethynyl) benzene] (**24**) were formed (Scheme V.3) serendipitously following the concentration of the titration solution detailed below. The crystals belong to the triclinic space group *P*-1. The asymmetric unit contains one molecule of both 1,3,5-tris(4-*n*-butyl-phenylethynyl) benzene (**25**) and **7** (Figure V.7). The three *n*-butyl arms of **25** extend above, below, and within the plane defined by the central benzene ring. The *para*-substituted phenyl groups at the end of the ethynyl moieties are slightly twisted out of the plane defined by the central benzene ring. The molecule of **7** displays a slight curvature that is not noted in the higher symmetry structures hitherto mentioned. The extended structure displays offset stacks of alternating molecules of **7** and **25** (Figure V.8). There are numerous close contacts between the mercury atoms and the carbon atoms of the arene and alkyne moieties, including the very close interaction between Hg(3) and C(50) (3.23 Å).

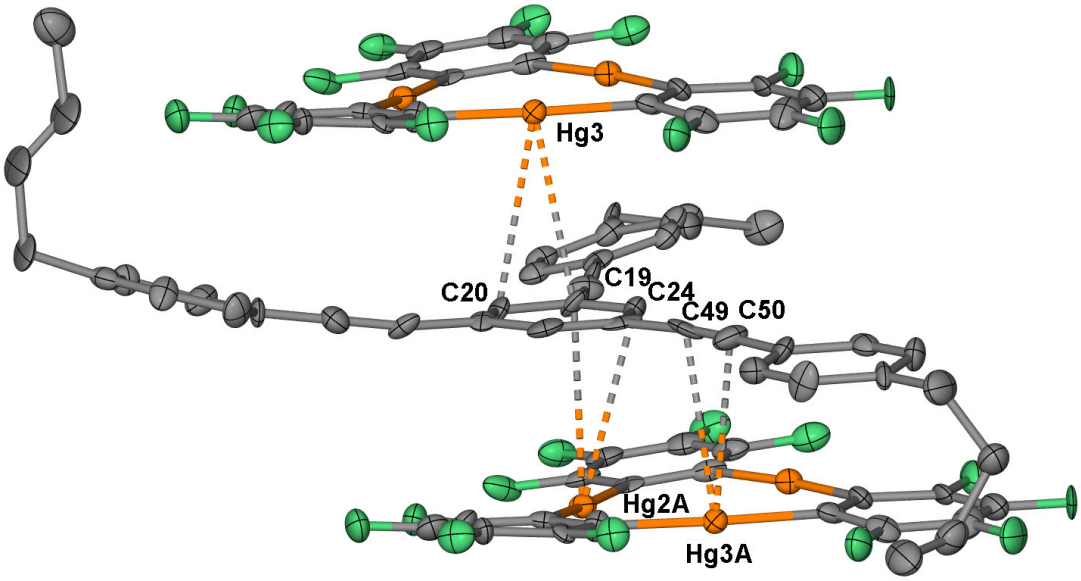

Figure V.7. ORTEP view (50% ellipsoid) of the intermolecular interactions in **24**. Representative intermolecular distances (Å): Hg(3)-C(19) 3.36, Hg(3)-C(20) 3.49, Hg(2A)-C(19) 3.55, Hg(2A)-C(24) 3.51, Hg(3A)-C(49) 3.34, Hg(3A)-C(50) 3.23.

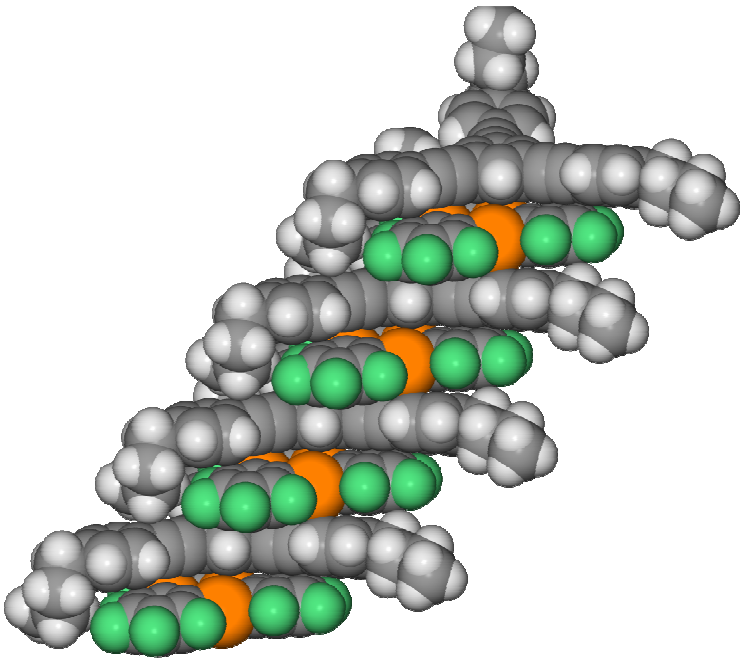

Figure V.8. Space-filling view of a stack of **24** with four repeating units.

We decided to investigate whether the interaction of **7** with 1,3,5-triethynyl benzenes could be detected using ^{199}Hg NMR spectroscopy. It is known that the ^{199}Hg nucleus is very sensitive to changes in the environment and studies utilizing ^{199}Hg NMR spectroscopy on complexes of **7** have been reported. [53-55, 64, 66] However, the solution studies of **7** with 1,3,5- tris(phenylethynyl) benzene and 1,3,5-triethynyl benzene were not feasible in CH_2Cl_2 due to the poor solubility of **22** and **23**. Studies in THF were not viable since this solvent coordinates strongly to **7**. No precipitate was observed when **25** was mixed with **7** in CH_2Cl_2. We attempted to measure the strength of the interaction between **7** and **25** by titrating a solution of **7** with the hydrocarbon in CH_2Cl_2. Assuming that the complex of **7** and **25** has a 1:1 stoichiometry, a K_{eq} of 21 M^{-1} can be calculated for the equilibrium **7** + **25** ⇔ [**7•25**] by fitting the aforementioned NMR data. In this calculation it was assumed that $\delta\ ^{199}Hg_{\text{ free trimer}}$ = -1046.2 ppm (known and standardized *in situ*) and $\delta\ ^{199}Hg_{complex}$ = -1069.3 ppm was extrapolated from the actual fitting of the data (Figure V.9). This K_{eq} value attests to the weakness of the interaction between these two compounds. This may be rationalized at first sight by considering the diffuse structure of the **25** which has three *n*-butyl groups capable of extensive solvation.

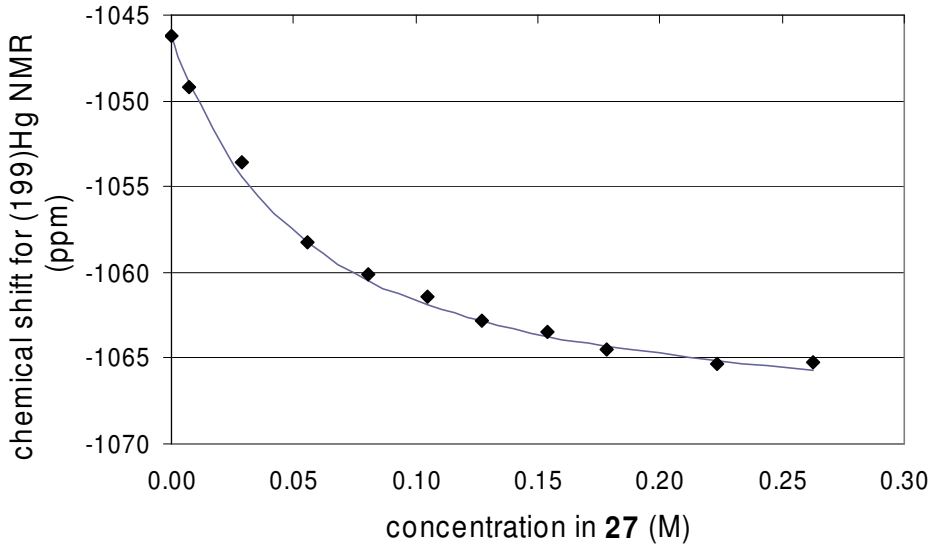

Figure V.9. Graph of the ^{199}Hg NMR signal as a function of concentration of **25**.

Table V.1. Crystal data, data collection, and structure refinement for **22**, **23, 23$_{RT}$,** and **24.**

Crystal data	**22**	**23**	**23$_{RT}$**	**24**
Formula	$C_{30}H_6F_{12}Hg_3$	$C_{48}H_{18}F_{12}Hg_3$	$C_{48}H_{18}F_{12}Hg_3$	$C_{57}H_{45}F_{12}Hg_3$
M_r	1196.12	1424.39	1424.39	1559.70
Crystal size (mm^3)	0.11 × 0.09 × 0.05	0.10 x 0.08 x 0.08	0.12 x 0.10 x 0.10	0.14 × 0.08 × 0.02
Crystal system	Monoclinic	Hexagonal	Hexagonal	Triclinic
Space group	*C*2/c	*P*6$_3$/mmc	*P*6$_3$/mmc	*P*-1
a (Å)	15.073(8)	18.946(3)	19.100(3)	8.386(4)
b (Å)	22.879(13)	18.946(3)	19.100(3)	16.438(8)
c (Å)	8.171(4)	6.4473(13)	6.5488(13)	18.949(9)
α(°)	90	90	90	95.157(9)
β(°)	106.709(8)	90	90	90.667(8)
γ(°)	90	120	120	97.362(8)
V ($Å^3$)	2699(3)	2004.3(6)	2069.0(6)	2579(2)
Z	4	2	2	2
ρcalc (gcm^{-3})	2.944	2.360	2.286	2.008
μ (mm^{-1})	17.128	11.553	11.192	8.987
F(000) (e)	2136	1308	1308	1470
Data Collection				
T/K	110(2)	110(2)	293(2)	110(2)
Scan mode	ω	ω	ω	ω
hkl range	-19→18, -26→29, -10→10	-24→24, -24→24, -8→7	-24→24, -24→22, -8→8	-9→9, -18→18, -21→21
Measured refl.	10541	14922	15868	14131
Unique refl., [R_{int}]	2994[0.0958]	810 [0.1042]	857 [0.0847]	7926[0.0663]
Refl. used for refinement	2994	810	857	7926
Absorption correction	SADABS	SADABS	SADABS	SADABS
T_{min}/T_{max}	0.228524	0.376107	0.657262	0.1577/0.7455
Refinement				
Refined parameters	200	71	71	679
R_1,[a] wR_2[b] [I>2σ(I)]	0.0806, 0.1465	0.0445, 0.0966	0.0745, 0.1800	0.0701, 0.1521
ρfin (max/min) ($eÅ^{-3}$)	3.514, -1.948	2.704, -1.012	1.962, -2.163	3.720, -1.413

R1 = $(F_o - F_c)/ F_o$.[b] wR2 = $\{[w(F_o^2 - F_c^2)^2]/ [w(F_o^2)^2]\}^{1/2}$; $w = 1/[\sigma^2(F_o^2) + (ap)^2 + bp]$; $p = (F_o^2 + 2F_c^2)/3$; *a* = 0.0880 (**22**), 0.0687 (**23**), 0.1200 (**23$_{RT}$**), 0.0876 (**24**); *b* = 0.0 (**22**), 2.1859 (**23**), 9.5000 (**23$_{RT}$**), 0.0 (**24**).

V.5. Experimental

General. Due to the toxicity of the mercury compounds discussed in these studies extra care was taken at all times to avoid contact with solid, solution, and air-borne particulate mercury compounds. The studies herein were carried out in well-aerated fume hoods. Infrared spectroscopy was performed with a ATI Mattson Genesis Series FTIR Spectrometer. Liquid samples were measured neat, solid samples were ground with KBr and compressed into translucent discs. Atlantic Microlab, Inc., Norcross, GA, performed the elemental analyses.

All coupling reactions were performed with freshly degassed solvents (nitrogen flow, 3 minutes) with light excluded. THF was distilled from Na/K alloy for coupling reactions, ACS grade THF was used as is for crystallizations, triethylamine was distilled from calcium hydride, and ACS grade CH_2Cl_2 and 1,2-dichloroethane were used without further purification. 4-*n*-butyliodobenzene, 1,3,5-tris(phenylethynyl) benzene, and copper iodide were purchased from Alfa Aesar and were used without further purification. 1,3,5-tris(trimethylsilylethynyl) benzene and 1,3,5-triethynyl benzene, as well as **7**, were prepared according to literature procedure. [52, 173]

Theoretical calculations. DFT calculations (full geometry optimization) were carried out by the by using the gradient-corrected Becke exchange functional (B3LYP) [183] and the Lee-Yang-Parr correlation functional [184] with the basis set 6-31G(d') [185, 186] for all the carbon and hydrogen atoms. The DFT calculations used the default SCF convergence for geometry optimizations (10^{-8}). Following full optimization of the geometry of both the singlet and triplet states of 1,3,5-tris(phenylethynyl) benzene and 1,3,5-triethynyl benzene, a frequency calculation was carried out and indicated that the optimized structures were true minimums. The triplet geometries were created by breaking the D_{3h} symmetry of the singlet ground state before running the calculations.

NMR measurements and titrations. ^{1}H and ^{13}C NMR spectra were recorded with a Mercury 300 MHz NMR spectrometer and referenced against residual solvent peaks. ^{199}Hg spectra were carried out on an Inova 400 MHz NMR spectrometer at 71.56 MHz. For the titration, dichloromethane solutions of **7** (7 mg/mL, 6.7 mM) and **25** (100

mg/ 0.5 mL, 0.35 M) were prepared. No lock was used during the acquisition: a standard of 1 M dichloromercury in DMSO (-1506.1 ppm) was run after every 3 collections to assure that there was no significant drift with the instrumentation.

Synthesis of [7•1,3,5-triethynyl benzene] (22). Compound **7** (30 mg, 0.029 mmol) and 1,3,5- triethynyl benzene (5.0 mg, 0.029 mmol) were dissolved in 10 mL of THF. Upon concentration by partial evaporation of the solvent, an opaque residue was left intermixed with clear twinned crystals of **22**. 24% yield. mp 325 °C (decomp). Anal. Calcd for $C_{30}H_6F_{12}Hg_3$: C, 30.12; H, 0.51. Found: C, 30.72; H, 0.45.

Synthesis of [7•1,3,5-tris(phenylethynyl) benzene] (23). Compound **7** (40 mgs, 0.038 mmol) and 1,3,5-tris(phenylethynyl) benzene (14.6 mg, 0.038 mmol) were dissolved in 10 mL of THF. Upon concentration by partial evaporation of the solvent, clear hexagonal crystals of **23** formed in 75% yield. mp 370°C. Anal. Calcd for $C_{48}H_{18}F_{12}Hg_3$: C, 40.47; H, 1.27. Found: C, 40.21; H, 1.16.

Synthesis of 1,3,5-tris(4-*n*-butylphenylethynyl) benzene (25). In a 500 mL round-bottom flask, 300 mg of 1,3,5-triethynyl benzene was dissolved in 50 mL triethylamine and 150 mL THF. After degassing, 10 mg copper (I) iodide and 50 mg tetrakis(triphenylphosphine) palladium were added. To the stirred suspension, 2.2 g 4-*n*-butyliodobenzene was added dropwise over 45 minutes. The solution was stirred in the dark for 36 hours. The solvents were removed in a rotary evaporator and the residue was taken up in diethyl ether (50 mL) and washed once with water (50 mL). The organic layer was dried over magnesium sulfate and the solvent was removed. The compound was isolated via silica column; first hexanes were run to remove non-polar impurities, then a hexanes/dichloromethane eluent (4:1) was used. The progress of the product on the column was followed by long-wave UV, and **25** was afforded as a light yellow oil (yield 642 mg, 65%). ^{1}H NMR ($CDCl_3$) [acquisition time= 5 secs. for correct integration] 7.62 (1H, s), 7.44-7.18 (4H, 2 doublets, ABB'A'), 2.63 (2H, triplet), 1.61 (2H, quartet), 1.36 (2H, sextet), 0.93 (3H, triplet). ^{13}C NMR ($CDCl_3$) 143.99, 134.00, 131.84, 128.77, 124.39, 120.21, 90.88, 87.64, 35.87, 33.63, 22.55, 14.18. Anal. Calcd for $C_{42}H_{42}$: C, 92.26; H, 7.74. Found: C, 92.49; H, 7.71.

Synthesis of [7•1,3,5-tris(4-*n*-butylphenylethynyl) benzene] (24). The crystals of **24** were found serendipitously in an NMR tube used for the aforementioned titration experiments after a very slow evaporation of CH_2Cl_2 with a large excess (~50:1) of 1,3,5-tri(4-*n*-butyl)phenylethynyl benzene to **7**. Thin flexible crystals of **24** were found in the dark orange residue and the bulk residue was removed from the crystals by hand before mounting for single crystal X-ray diffraction. Elemental analysis was not successful due to the inability to prepare bulk samples of the product.

Crystal structure determinations. X-ray data for all the structures were collected on a Bruker Smart-CCD diffractometer using graphite-monochromated Mo Kα radiation (=0.71073 Å). Specimens of suitable size and quality were selected and mounted onto a glass fiber with superglue and collected at either 110 K or room temperature. The structures were solved by direct methods, which successfully located most of the non-hydrogen atoms. Subsequent refinement on F2 using the SHELXTL/PC package (version6.1) allowed location of the remaining non-hydrogen atoms.

CHAPTER VI

STRUCTURAL AND PHOTOPHYSICAL STUDIES OF POLYAROMATIC ADDUCTS INVOLVING PENTAFLUOROPHENYL MERCURY CHLORIDE*

VI.1. Introduction

Fluorinated organomercurials display unusual Lewis acidic properties. [187, 188] For example, trimeric perfluoro-*ortho*-phenylene mercury (**7**, [*o*-$C_6F_4Hg]_3$) [189] complexes a number of electron rich molecules including anions and Lewis bases. [12, 43] Remarkably, it also interacts with aromatic substrates such as pyrene, naphthalene, and biphenyl to form extended binary supramolecular stacks in which **7** and the aromatic compound alternate. [88-90, 97, 99, 163] In all cases, the mercury centers of the trinuclear complex approach the π-face of the aromatic substrate and engage in polyhapto secondary Hg–C interactions in the 3.3–3.6 Å range. In order to determine if cooperative effects are essential for the formation of such adducts, we investigated the ability of fluorinated mononuclear mercury compounds to complex aromatic substrates.

Pentafluorophenylmercury chloride (C_6F_5HgCl, **2**) constitutes one of simplest fluorinated mononuclear mercury compounds. [52] Despite its ease of synthesis, its coordination chemistry has not been carefully investigated and appears to be limited to the complexation of DMF and DMSO. [24] As mentioned in a previous chapters, we noted that pentafluorophenylmercury bromide (C_6F_5HgBr, **18**) forms an adduct with 1,4-diphenylbutadiyne. In this chapter, we report the results of a comparative study dealing with the complexation of phenanthrene by **2** and **18**, as well as reporting adducts of other polyaromatic species with **2** and **18**.

---

* Reprinted in part with permission from *Dalton Trans.*, Taylor, T. J.; Burress, C. N.; Pandey, L.; Gabbaï, F. P., "Structural and photophysical studies of phenanthrene adducts involving C_6F_5HgCl and [*o*-$C_6F_4Hg]_3$" 4654, Copyright 2006 by Royal Society of Chemistry.

VI.2. Synthesis and characterization of the adducts

Combining **2** with phenanthrene in $CHCl_3$ followed by slow evaporation of the solvent leads to the crystallization of [**2**•phenanthrene], (**26**). The composition of this adduct has been confirmed by elemental analysis. **26** is air stable and melts at 230 ºC. Interrogation of **26** by single crystal X-ray analysis reveals the formation of extended binary stacks where molecules **2** alternate with molecules of phenanthrene (Fig. VI.1). The presence of short Hg-$C_{phenanthrene}$ distances in the adduct indicates the presence of secondary mercury–π interactions. These interactions, which fall within the sum of the van der Waals radii of the two elements, [111, 129] are comparable to those observed in arene adducts of **7** and might be responsible for the formation of the adduct. [88, 90] As opposed to the reported structure of [**7**•phenanthrene], [91] where each phenanthrene molecule is surrounded by six mercury centers, the phenanthrene only has two close contacts in **26**. The short centroid-centroid distance (3.5 Å) observed between the fluoroarene ring of the molecule of C_6F_5HgCl and the central six-membered ring of the phenanthrene suggests the presence of arene–fluoroarene interactions which probably adds to the stability of the stack. [190] The stacks of **26** are cross-linked by secondary Hg-Cl interactions which range from 3.38 to 3.95 Å. These secondary interactions, which are ubiquitous in the chemistry of chloromercurio compounds, [137] lead to the formation of polymeric arrays of molecules of C_6F_5HgCl that run approximately perpendicular to the direction of the stacks.

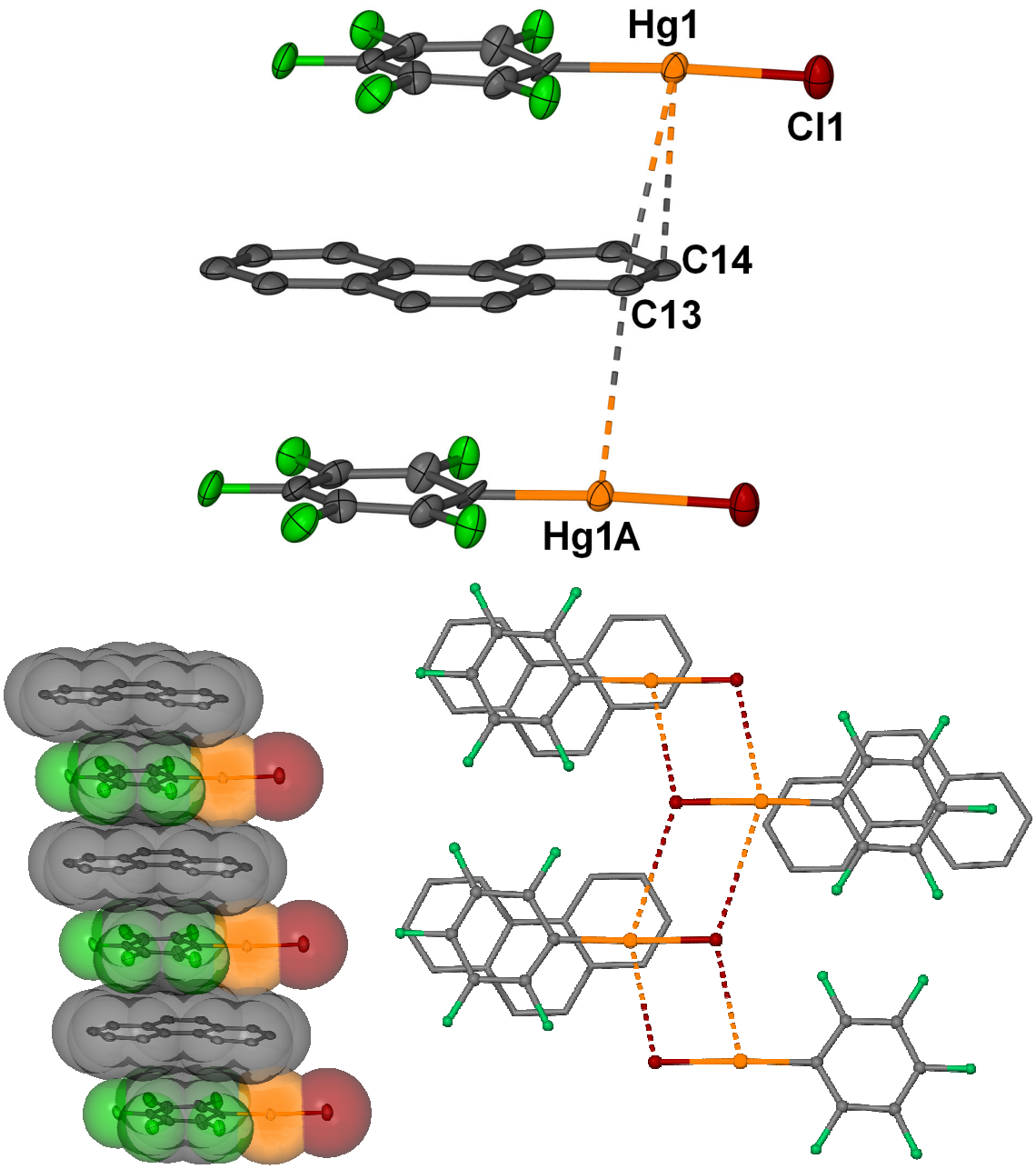

Fig. VI.1 Structure of **26**. (a) ORTEP view (ellipsoids at 50%, H atoms excluded for clarity) with close intermolecular Hg-C contacts (dashed lines). Representative intermolecular distances (Å): Hg(1)-C(13) 3.53, Hg(1)-C(14) 3.29, Hg(1A)-C(13) 3.45 .

Additionally, the structure of the bromo- analogue, [**18**•phenanthrene], (**27**) has been determined and is isomorphous with **26** as indicated by the virtually identical unit cells (Figure VI.2,

Table VI.1).

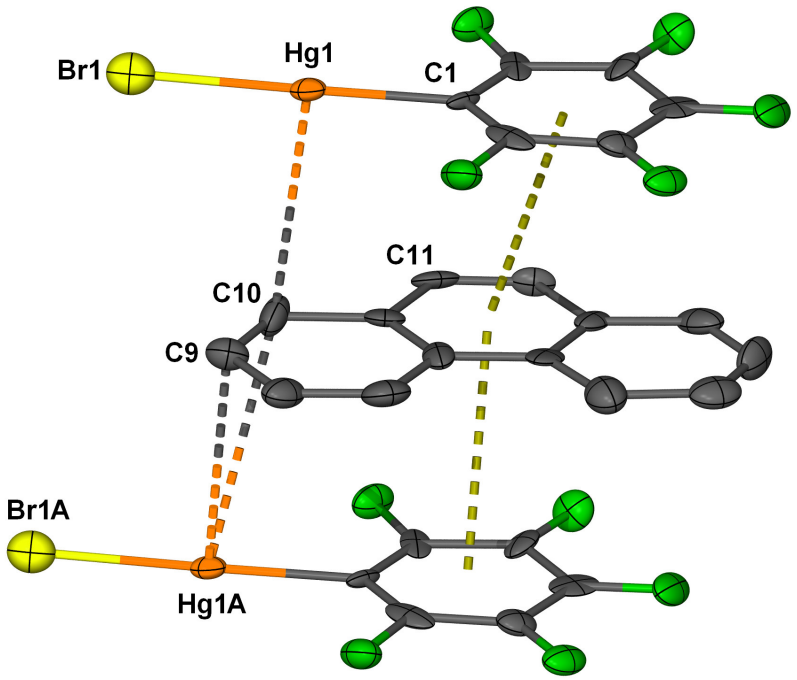

Figure VI.2. ORTEP view of **27** (ellipsoids at 50%, H atoms excluded for clarity) with close intermolecular Hg-C contacts (dashed lines). Representative intermolecular distances (Å): Hg(1A)-C(10) 3.51, Hg(1A)-C(9) 3.25, Hg(1)-C(10) 3.46 .

Adduct **26** gives rise to intense photoluminescence in the visible region. The energy and vibrational progressions observed for the emission of [**7**•phenanthrene] [91] correspond almost exactly to that observed for the phosphorescence of free phenanthrene in an EPA matrix. [191] In contrast, adduct **26** displays only the fluorescence of pure phenanthrene at room temperature. However, at 77 K, both the $S_1 \rightarrow S_0$ emission (386–460 nm) and $T_1 \rightarrow S_0$ emission (480–584 nm) of the arene are observed (Figure. VI.3).

The observed phosphorescence results from an external mercury heavy-atom effect which affects the photophysical properties of the arene. Such behavior is reminiscent of that observed for the naphthalene, biphenyl or pyrene adducts of **7**, which also display room temperature phosphorescence. [88] The temperature dependence of the emission spectrum of **26** suggests that the magnitude of the spin-orbit coupling induced by **2** is not as intense as that induced by **7**. With a weaker spin orbit perturbation, the phosphorescence of **26** might be sufficiently slow to be quenched by competing non-radiative processes at room temperature. The difference observed in the phosphorescence may be correlated to the lower number of mercury atoms surrounding the chromophore in **26**.

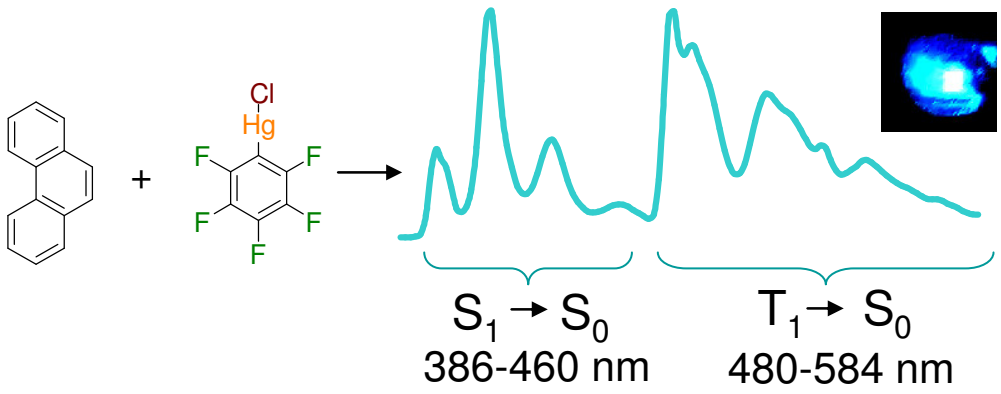

Figure. VI.3 Solid-state luminescence spectra for **26** (λ_{ex}= 282 nm @ RT, 313 nm @ 77 K). The insets show the light emitted by the samples at 77 K under a UV lamp.

We have also been able to confirm that **2** forms binary adducts with fluorene and pyrene. While the pyrene adduct has only been determined by elemental analysis, the 1:1 fluorene adduct of **2**, (**28**), crystallizes in the monoclinic space group *C*2/c with one half of a molecule of **2** and half of a molecule of fluorene (Figure VI.4). The fluorene is disordered over two positions related by a mirror plane. Thus any extended discussion

about particular intermolecular Hg-$C_{aromatic}$ interactions is somewhat misleading, though close interactions ranging from 3.35 to 3.62 Å are certainly present in the extended structure. Again, as in the case of **26** and **27**, there are cross-linking secondary Hg-Cl interactions with a repeating Hg-Cl distance of 3.63 Å.

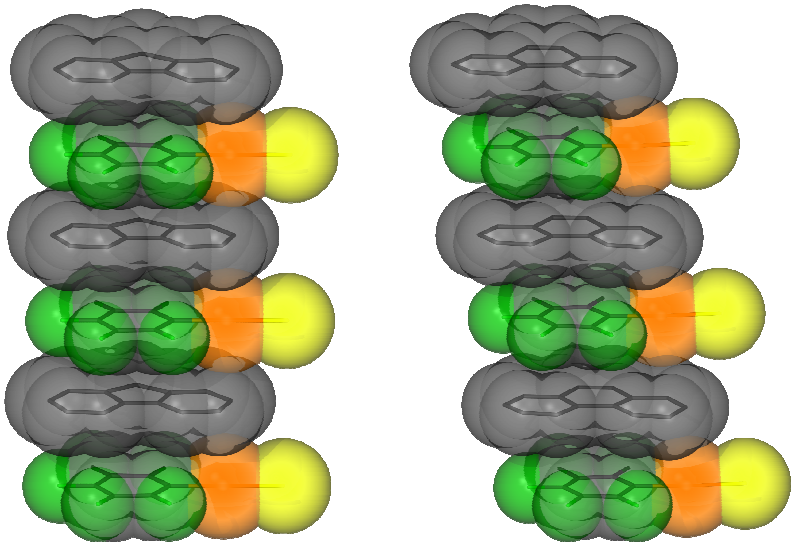

Figure VI.4. Side by side comparison of stacks of **26** (with one orientation of the fluorene molecule) and **28**.

While it may have been implied from earlier work that the complexation of aromatic substrates by fluorinated organomercurials is limited to the case of **7**, the results presented here demonstrate that the use of a trincluear organomercurial is not a requirement. Instead, simple fluorinated organomercurials such as **18** and **2** are capable complexing agents which readily assemble with arenes to form stacked assemblies.

Further results, with the mononuclear species bis(pentafluorophenyl)mercury, have been recently reported. [85]

Table VI.1. Crystal data, data collection, and structure refinement for **26, 27,** and **28.**

Crystal data	**26**	**27**	**28**
Formula	$C_{20}H_{10}ClF_5Hg$	$C_{20}H_{10}BrF_5Hg$	$C_{19}H_{10}ClF_5Hg$
M_r	581.32	625.78	569.31
Crystal size (mm^3)	0.15 × 0.11 × 0.08	0.05 × 0.05 × 0.04	0.20 × 0.11 × 0.04
Crystal system	Triclinic	Triclinic	Monoclinic
Space group	*P*-1	*P*-1	*C*2/c
A (Å)	6.8616(13)	6.8477(14)	6.770(3)
B (Å)	7.0831(15)	7.1015(14)	35.555(16)
c (Å)	17.709(4)	17.737(4)	7.066(3)
α(°)	86.437(3)	86.90(3)	90
β(°)	85.845(4)	86.28(3)	102.402(8)
γ(°)	80.699(5)	80.67(3)	90
V ($Å^3$)	846.0(3)	848.5(3)	1661.3(13)
Z	2	2	4
ρ_{calc} (gcm^{-3})	2.282	2.449	2.276
μ (mm^{-1})	9.308	11.477	9.477
F(000) (e)	544	580	1064
Data Collection			
T/K	110(2)	110(2)	110(2)
Scan mode	ω	ω	ω
hkl range	-8→8, -9→5, -20→22	-8→8, -9→8, -22→22	-9→6, -45→46, -8→9
Measured refl.	4319	8604	4377
Unique refl., [R_{int}]	3463 [0.0650]	3748 [0.0571]	1873 [0.0946]
Refl. used for refinement	3463	3748	1873
Absorption Correction	SADABS	SADABS	SADABS
T_{min}/T_{max}	0.176868	0.0685235	0.192399
Refinement			
Refined parameters	244	244	144
R_1,[a] wR_2[b] [I>2σ(I)]	0.0721, 0.1505	0.0976, 0.2494	0.0684, 0.1496
ρ_{fin} (max/min) ($eÅ^{-3}$)	4.093, -3.379	5.580, -9.519	2.549, -3.376

[a] $R1 = (F_o - F_c)/ F_o$.[b] $wR2 = \{[w(F_o^2 - F_c^2)^2]/ [w(F_o^2)^2]\}^{1/2}$; $w = 1/[\sigma^2(F_o^2) + (ap)^2 + bp]$; $p = (F_o^2 + 2F_c^2)/3$; *a* = 0.0610 (**26**), 0.2000 (**27**), 0.0550 (**28**); *b* = 0.0 (**26**), 0.0 (**27**), 0.0 (**28**)

VI.3. Experimental

General. Due to the toxicity of the mercury compounds discussed, extra care was taken at all times to avoid contact with solid, solution, and air-borne particulate mercury compounds. The studies herein were carried out in a well aerated fume hood. Atlantic Microlab, Inc., Norcross, GA, performed the elemental analyses. All commercially available starting materials and solvents were purchased from Aldrich Chemical and VWR, Inc. and used as provided. Compound **18** [139] and **2** [138] were prepared according to published procedures.

Synthesis of adducts. All compounds were prepared by mixing compound **18** or **2** with the corresponding arene in $CHCl_3$ (5–10 mL). Crystals formed upon slow evaporation of the solvent. Reagent quantities, yields, elemental analysis results (where available), and melting points (where available), are provided for each adduct hereafter.

Synthesis of [2•phenanthrene] (26). **2** (0.014 g, 0.035 mmol), phenanthrene (0.0061 g, 0. 035 mmol) in $CHCl_3$. Yield: 0.0187 g, 92%. Anal. Calcd for $C_{20}H_{10}F_5HgCl$: C, 41.32; H, 1.73. Found: C, 41.37; H, 1.74. mp 230 °C.

Synthesis of [18•phenanthrene] (27). **18** (0.015 g, 0.034 mmol), phenanthrene (0.0061 g, 0. 035 mmol) in $CHCl_3$. Yield: 0.0158 g, 75%.

Synthesis of [2•fluorene] (28). **2** (0.015 g, 0.037 mmol), fluorene (0.0061 g, 0.037 mmol) in $CHCl_3$. Yield: 0.0183 g, 87%. Anal. Calcd for $C_{19}H_{10}F_5HgCl$: C, 40.08; H, 1.77. Found: C, 40.21; H, 1.85. mp 219 °C.

Synthesis of [2•pyrene]. **2** (0.015 g, 0.037 mmol), pyrene (0.0075 g, 0.037 mmol) in $CHCl_3$. Yield: 0.0183 g, 87%. Anal. Calcd for $C_{19}H_{10}F_5HgCl$: C, 40.08; H, 1.77. Found: C, 40.21; H, 1.85. mp 219 °C.

Crystal structure determinations. X-ray data for **26** and **28** were collected on a Bruker SMART-CCD diffractometer using graphite-monochromated Mo Kα radiation (λ = 0.71073 Å). Specimens of suitable size and quality were selected and glued onto a glass fiber with freshly prepared epoxy resin. The structure was solved by direct methods, which successfully located most of the non-hydrogen atoms. Subsequent refinement on F^2 using the SHELXTL/PC package (version 6.1) allowed location of the

remaining non-hydrogen atoms. Details of the crystal structures can be found in the CIF files.

Luminescence measurements. The solid luminescence spectra were recorded on a SLM/AMINCO, Model 8100 spectrofluorometer equipped with a xenon lamp. Low-temperature measurements were made in a cryogenic device of local design. Collodion was used to attach the powder samples to the holder. The collodion was scanned for baseline substraction. Liquid nitrogen was used to obtain the 77 K measurements.

CHAPTER VII

OTHER ADDUCTS OF TRIMERIC PERFLUORO-*ORTHO*-PHENYLENE MERCURY WITH MOLECULES CONTAINING THE DIPHENYLACETYLENE MOTIF

VII.1. Introduction

The results that we have obtained in investigating the chemistry of **7** with substrates such as diphenylacetylene have led us to question whether larger unsaturated hydrocarbons featuring the same phenyl-alkyne-phenyl motif would also form adducts with **7** (Scheme VII.1).

Scheme VII.1

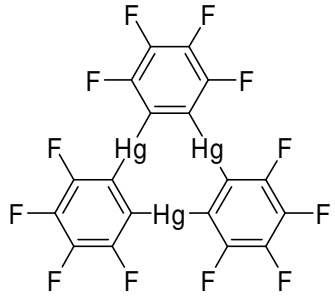

7

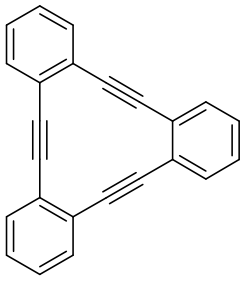

Tribenzocyclotriyne

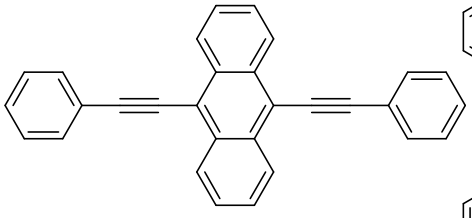

9,10-bisphenylethynyl anthracene

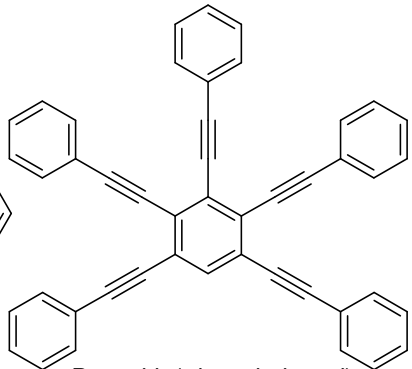

Pentakis(phenylethynyl) benzene

VII.2. The interaction of [*o*-$C_6F_4Hg]_3$ and tribenzocyclotriyne

The symmetry and size of tribenzocyclotriyne (TBC) appears to complement that of **7**, and we were curious to see if offset binary stacks would result from their co-crystallization. This is in part inspired by the extended binary structure of the adduct of bis-pentafluoro mercury and diphenylacetylene, which have similar molecular shapes. [192] Additionally, there is has been a great deal of academic interest in TBC. [193, 194]

When TBC and **7** are co-crystallized from THF, binary stacks of [**7**•TBC] (**29**) form without attendant solvent in the extended structure. **29** crystallizes in the triclinic space group *P*-1 with two inequivalent molecules of both **7** and TBC in the asymmetric unit. In fact, these inequivalent sets of molecules engender two crystallographically distinct binary stacks. Both stacks are tilted from the normal of the plane defined by the trinuclear core of **7** by 21.36 ° and 21.55 °, respectively (Figure VII.1). Both of the molecules of **7** in **29** exhibit deviations from planarity. While the two stacks are crystallographically inequivalent, the intermolecular forces responsible for holding them together must be very similar. All of the aryl moieties of the molecules of TBC interact with the fluorinated aryl moieties of **7** above and below the plane, with distances between the centroids of the rings ranging from 3.56 to 3.68 Å. Consequently, each column is held by three infinite arene-fluoroarene stacks. There are also numerous Hg-$C_{aromatic}$ distances that range from 3.44 to 3.58 Å.

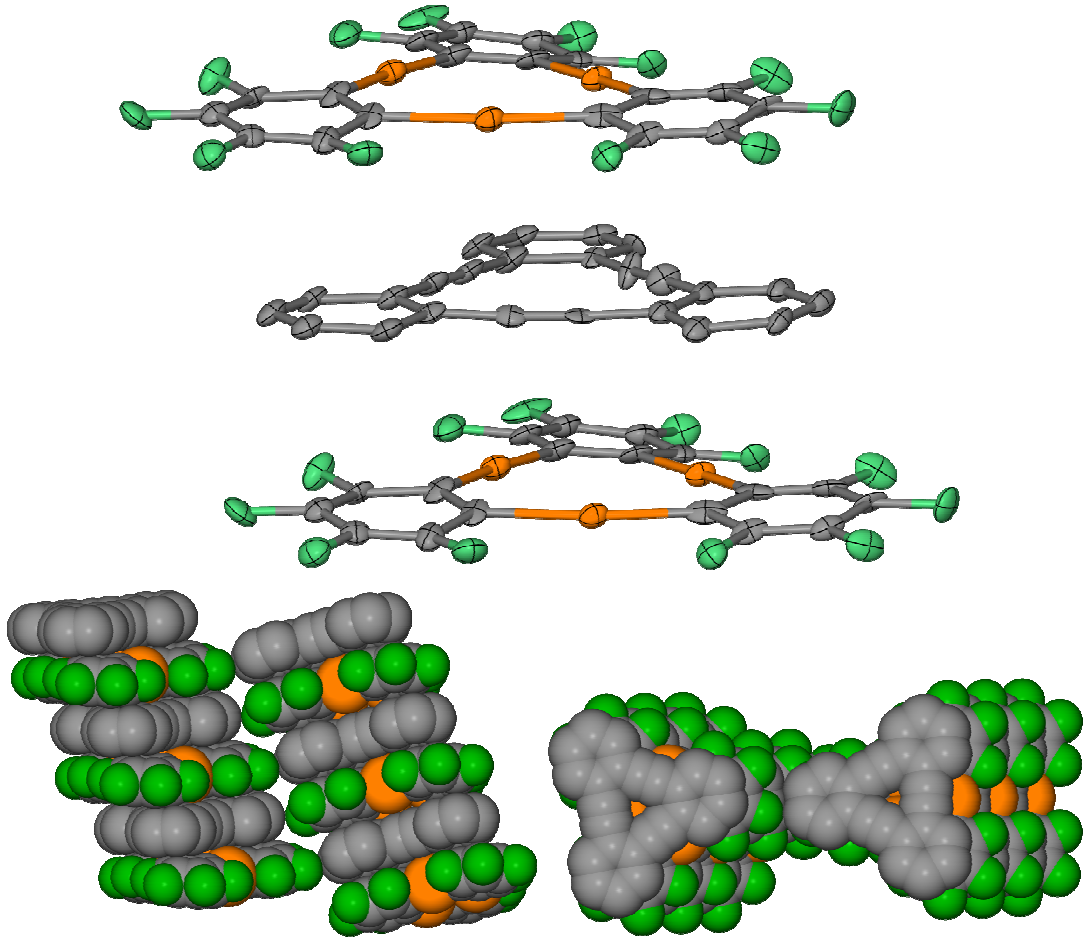

Figure VII.1. (above) ORTEP view (50% ellipsoids) of one of the inequivalent binary stacks of **29**. (bottom left) Space-filling view of the two inequivalent stacks side by side and (bottom right) looking perpendicular to the molecular plane of the **7** molecules.

VII.3. The interaction of $[o\text{-}C_6F_4Hg]_3$ and 9,10-bisphenylethynyl anthracene

The molecule 9,10-bis(phenylethynyl) anthracene (BPEA) has been studied extensively since it is has a high emission efficiency in the visible region. [195] We studied the complexation of BPEA by **7** to determine if significant changes in the photochemistry of BPEA occurred upon complexation.

The 1:1 adduct (**30**) was synthesized in very poor yield by the slow evaporation of a dichloroethane solution containing stoichiometric equivalents of BPEA and **7**.

Elemental analysis of the adduct indicated that decomposition by solvent loss occurs. Compound **30** crystallizes in the triclinic space group *P*-1 with one molecule of BPEA, one molecule of **7**, and half a molecule of dichloroethane that straddles an inversion center in the asymmetric unit. While the molecule of **7** has no significant intramolecular distortions, the pendant phenyl groups of the molecule of BPEA have a different orientation from the solid state structure of pure BPEA (Figure VII.2). [196] The pendant phenyl rings form dihedral angles of 25.7 º with the anthracene moiety and 51.4 º from each other in pure BPEA. In adduct **30**, however, they form dihedral angles of 4.8 and 88.2 º to the anthracene and 83.4 º to one another. There are eight close Hg-$C_{aromatic}$ interactions involving all three mercury atoms and the central anthracene moiety with distances ranging from 3.21 to 3.59 Å. There are also three close Hg-C_{alkyne} interactions ranging from 3.36 to 3.48 Å. Additionally, the phenyl group containing C(19) appears to engage in a secondary arene-fluoroarene interaction with the ring of **7** containing C(7) (centroid-centroid distance of 3.60 Å).

The photochemistry of **30** was studied by the Omary group at the University of North Texas. Under hand-held UV lamp crystals of **30** only emitted a pale orange-red emission which appeared much less marked than pure BPEA. However, room temperature and 77 K measurements showed that no novel emissions were present and the peaks were almost identical to those observed for the free hydrocarbon (Figure VII.3). [195] This result suggests the possible involvement of heavy atom effects which may depopulate the excited singlet state and lead to a weakened emission intensity.

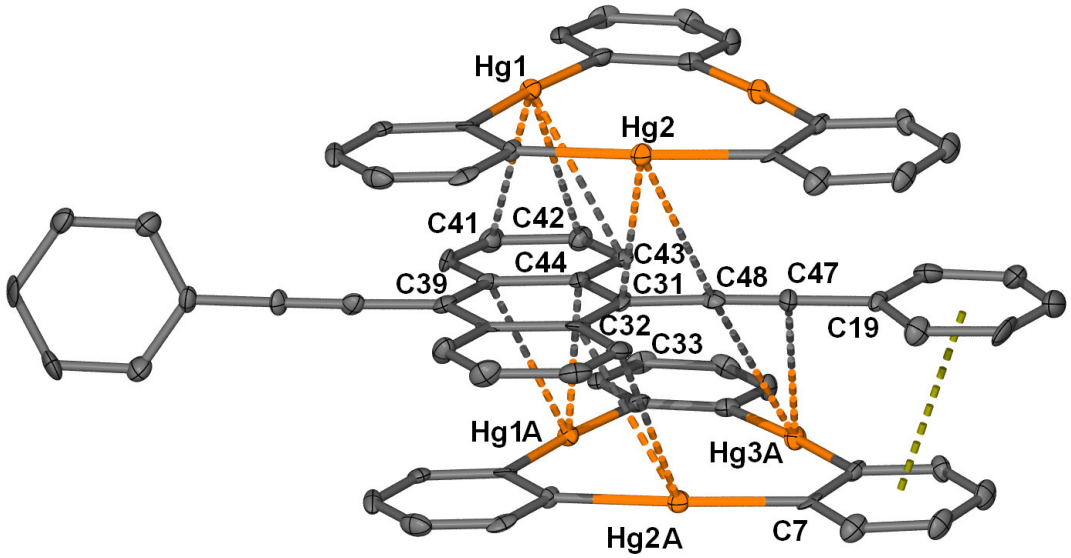

Figure VII.2. ORTEP view (50% ellipsoids) of **30** (adventitious 1,2-dichlorethane and H atoms omitted). Representative intermolecular distances (Å): Hg(1)-C(41) 3.40, Hg(1)-C(42) 3.31, Hg(2)-C(31) 3.51, Hg(2)-C(48) 3.48, Hg(1A)-C(39) 3.48, Hg(1A)-C(44) 3.47, Hg(2A)-C(32) 3.59, Hg(2A)-C(33) 3.26, Hg(3A)-C(47) 3.36, Hg(3A)-C(48) 3.40.

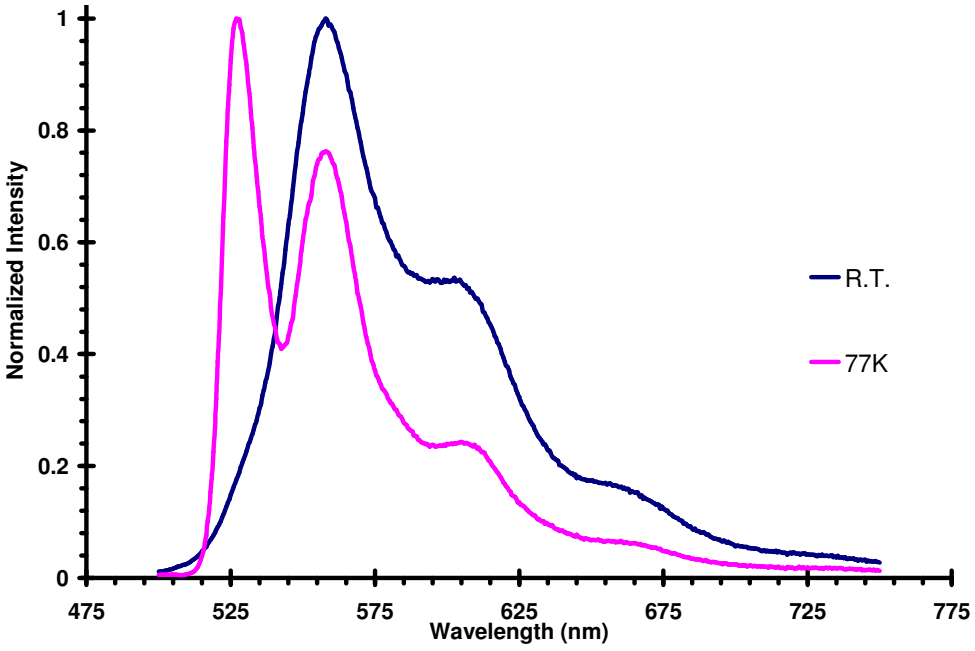

Figure VII.3. Emission spectra of **30** at room temperature and 77 K (λ_{ex} = 450 nm).

VII.4. The interaction of [*o*-$C_6F_4Hg]_3$ and pentakis(phenylethynyl) benzene

Another hydrocarbon adduct was formed with pentakis(phenylethynyl) benzene.[176, 197] This was combined with **7** in THF which led to the formation of co-crystals by slow evaporation of the solution. The structure was solved by X-ray diffraction confirming the formation of the 1:1 adduct [**7**•pentakis(phenylethynyl) benzene] (**31**).

Compound **31** forms as small light orange crystals which belong to the monoclinic space group *C*c with one molecule of pentakis(phenylethynyl) benzene and one molecule of **7** in the asymmetric unit.(Table VII.1) There are no unusual bond distances in the individual molecules in the structure. The pendant phenylethynyl groups of the pentakis(phenylethynyl) benzene all twist from the plane of the core benzene ring with dihedral angles ranging from 18.5 to 32.1 °. The two components alternate with one another to form 1:1 binary stacks even though they are of quite disparate size and shape. Examination of the cell-packing diagram along the *b*-axis indicates that one of the phenylethynyl groups sticks out from the perpendicular stacks (Figure VII.4). There are numerous secondary interactions holding the infinite stacks together (Figure VII.5). The central benzene ring (containing C(19)) engages in three short contacts (3.56-3.58 Å) with Hg(3) atoms above and below the molecular plane, while the alkyne groups C(41)-C(42) and C(49)-C(50) have close contacts (3.26-3.51 Å) with multiple mercury centers of neighboring molecules of **7**.

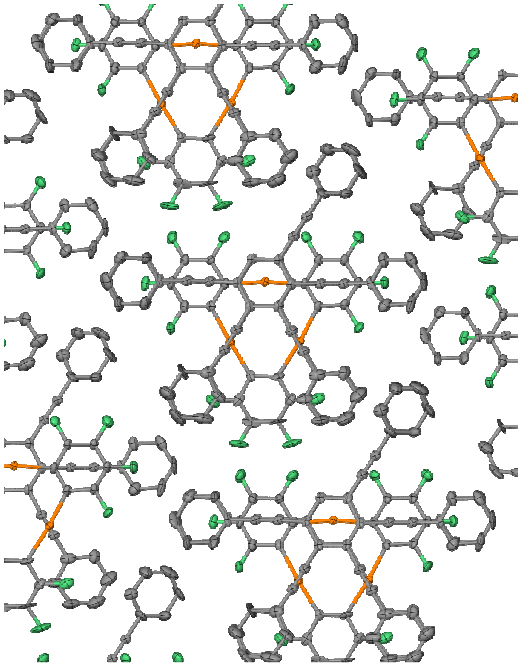

Figure VII.4. View of **31** along the *b*-axis.

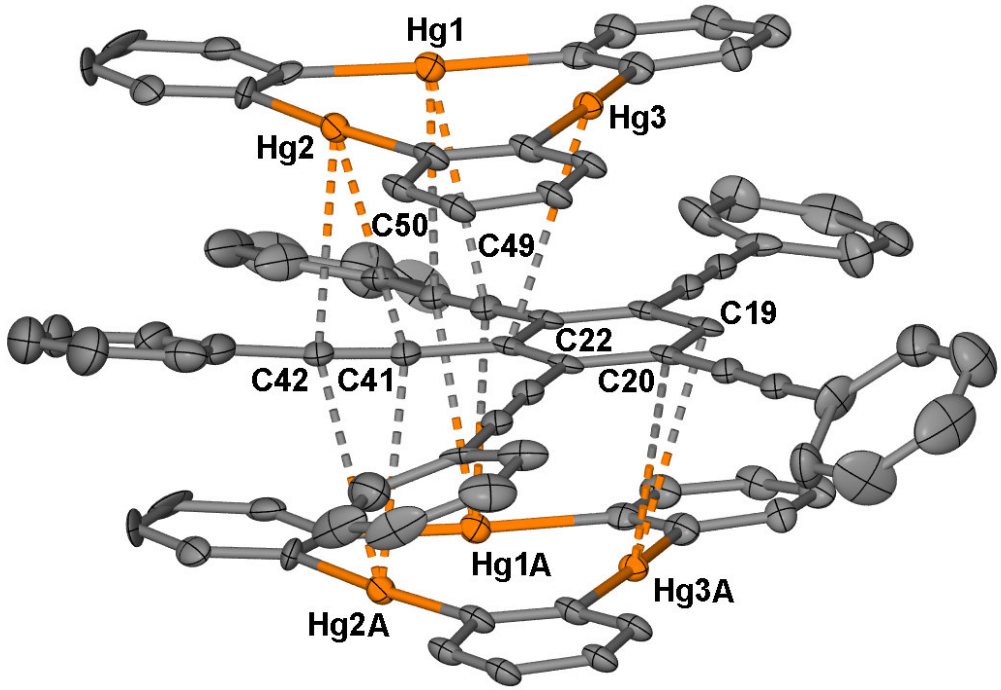

Figure VII.5. ORTEP view (50% ellipsoids) of **31**, H and F atoms are omitted for clarity. Representative intermolecular distances (Å): Hg(1)-C(49) 3.46, Hg(1)-C(50) 3.44, Hg(2)-C(41) 3.44, Hg(2)-C(42) 3.26, Hg(3)-C(22) 3.59, Hg(1A)-C(49) 3.37, Hg(1A)-C(50) 3.32, Hg(2A)-C(41) 3.38, Hg(2A)-C(42) 3.51, Hg(3A)-C(19) 3.58, Hg(3A)-C(20) 3.56.

Table VII.1. Crystal data, data collection, and structure refinement for **29**, **30**, and **31**.

Crystal data	**29**	**30**	**31**
Formula	$C_{84}H_{24}F_{24}Hg_6$	$C_{49}H_{20}Cl_1F_{12}Hg_3$	$C_{64}H_{26}F_{12}Hg_3$
M_r	2692.57	1335.42	1624.64
Crystal size (mm3)	0.03× 0.01 × 0.01	0.60 × 0. 18 × 0.04	0.20 × 0. 03 × 0.03
Crystal system	Tricilinic	Tricilinic	Monoclinic
Space group	*P*-1	*P*-1	*C*c
a (Å)	7.2337(15)	7.0990(14)	32.184(6)
b (Å)	18.257(3)	13.161(3)	6.6821(13)
c (Å)	26.143(6)	21.838(4)	25.652(5)
α(°)	99.368(14)	91.88(3)	90
β(°)	91.323(14)	95.05(3)	110.05(3)
γ(°)	92.938(12)	94.05(3)	90
V (Å^3)	3400.3(12)	2025.8(7)	5182.3(18)
Z	2	2	4
ρcalc (gcm^{-3})	2.630	2.301	2.082
μ (mm^{-1})	24.723	11.494	8.951
F(000) (e)	2448	1286	3032
Data Collection			
T/K	110(2)	110(2)	110(2)
Scan mode	ω	ω	ω
hkl range	-8→8, -20→20, -28→29	-8→9, -16→17, -28→26	-35→35, -7→7, -28→28
Measured refl.	20044	17352	14518
Unique refl., [R_{int}]	9133 [0.1222]	9110 [0.1143]	7070 [0.0472]
Refl. used for Refinement	9133	9110	7070
Absorption correction	SADABS	SADABS	SADABS
T_{min}/T_{max}	0.0519/0.4062	0.129805	0.115346
Refinement			
Refined parameters	1027	586	658
R_1,[a] wR_2[b] [I>2σ(I)]	0.0792, 0.1705	0.0538, 0.0819	0.0414, 0.0987
ρfin (max/min) (eÅ^{-3})	4.150, -2.617	1.451, -1.883	0.927, -1.932

[a] R1 = $(F_o - F_c)/ F_o$.[b] wR2 = $\{[w(F_o^2 - F_c^2)^2]/ [w(F_o^2)^2]\}^{1/2}$; $w = 1/[\sigma^2(F_o^2) + (ap)^2 + bp]$; $p = (F_o^2 + 2F_c^2)/3$; a = 0.0950 (**29**), 0.0306 (**30**), 0.0688 (**31**); b = 0.0 (**29**), 0.0 (**30**), 0.33 (**31**).

VII.5. Experimental

General. Due to the toxicity of the mercury compounds discussed, extra care was taken at all times to avoid contact with solid, solution, and air-borne particulate mercury compounds. The studies herein were carried out in a well aerated fume hood. Atlantic Microlab, Inc., Norcross, GA, performed the elemental analyses. All commercially available starting materials and solvents were purchased from Aldrich Chemical and VWR, Inc. and used as provided. Compound **7** was prepared according to the published procedure. [52]

Synthesis of [7•TBC] (29). Compound **7** (0.020 g, 0.019 mmol) and tribenzocyclotriene [198] (0.0063 g, 0.021 mmol) were dissolved in THF (15 mL). Upon concentration by slow evaporation of the solvent, pale yellow blocks of **29** were formed in 85% yield (0.022 g, 0.016 mmol). mp 490 ° C (decomp). Anal. Calcd for $C_{42}H_{12}F_{24}Hg_3$: C, 37.47; H, 0.90. Found: C, 36.83; H, 0.76.

Synthesis of [7•BPEA•(1,2-DCE)$_{0.5}$] (30). Compound **7** (0.026 g, 0.025 mmol) and 9,10-bis(phenylethynyl)anthracene (0.020 g, 0.053 mmol) were dissolved in 1,2-dichloroethane (15 mL). Upon concentration by slow evaporation of the solvent, thin bright orange crystals (slightly paler than the starting material 9,10-bis(phenylethynyl)anthracene) of **30** were formed in <20% yield (~0.005 g, 0.003 mmol) due to the manual extraction of the product from the starting material. Anal. Calcd for $C_{48}H_{18}F_{12}Hg_3$ (Weight of adduct after losing the 1,2-dichloroethane): C, 40.47; H, 1.27. Found: C, 40.61; H, 1.09.

Synthesis of [7•pentakis(phenylethynyl) benzene] (31). Compound **7** (0.020 g, 0.019 mmol) and pentakis(phenylethynyl) benzene [176, 197] (0.012 g, 0.021 mmol) were dissolved in THF (5 mL). Upon concentration by slow evaporation of the solvent, small orange crystals of **31** were formed in 55% yield (0.022 g, 0.016 mmol) and washed with *n*-pentane. Anal. Calcd for $C_{64}H_{26}F_{12}Hg_3$: C, 47.31; H, 1.61. Found: C, 47.50; H, 1.43.

Crystal structure determinations. X-ray data for structures **30** and **31** were collected on a Bruker SMART-CCD diffractometer using graphite-monochromated Mo Kα radiation (λ = 0.71073 Å). X-ray data for **29** was collected on a Bruker D8 Adv

GADDS diffractometer, using a graphite monochromator with Cu (K_α = 1.54178 Å). Specimens of suitable size and quality were selected and glued onto a glass fiber with freshly prepared epoxy resin or mounted on nylon loops with Apeizon grease. The structure was solved by direct methods, which successfully located most of the non-hydrogen atoms. Subsequent refinement on *F2* using the SHELXTL/PC package (version 5.1) allowed location of the remaining nonhydrogen atoms.

CHAPTER VIII

GENERAL CONCLUSIONS*

The primary emphasis and more original side of this body of work has been the study of adducts containing $[o\text{-}C_6F_4Hg]_3$ (Scheme VIII.1) and a variety of conjugated hydrocarbons, including alkynes. Novel properties arising from these adducts have also been investigated.

Scheme VIII.1.

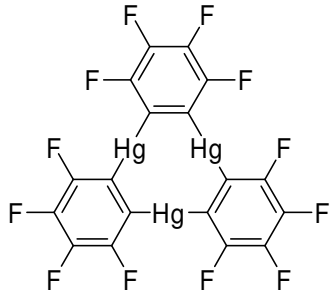

The interaction of $[o\text{-}C_6F_4Hg]_3$ with α,ω-diphenylpolyynes containing 4, 6, 8, and 12 sp-carbon atoms in CH_2Cl_2 leads to formation of $[([o\text{-}C_6F_4Hg]_3)_2\bullet Ph(C{\equiv}C)_2Ph]$, $[[o\text{-}C_6F_4Hg]_3\bullet Ph(C{\equiv}C)_3Ph]$, $[([o\text{-}C_6F_4Hg]_3)_2\bullet Ph(C{\equiv}C)_4Ph]$, $[([o\text{-}C_6F_4Hg]_3)_2\bullet Ph(C{\equiv}C)_6Ph\bullet CH_2Cl_2]$ and $[[o\text{-}C_6F_4Hg]_3\bullet(Ph(C{\equiv}C)_6Ph)_2]$. In the solid state, the α,ω-diphenylpolyynes, which are approximately planar, are associated to molecules of **7** on either side of the molecular plane via secondary Hg···π interactions (Figure VIII.1 above). The acetylenic stretches of these adducts as measured by IR spectroscopy

---

* Reprinted in part with permission from, Taylor, T. J.; Burress, C. N., Gabbaï, F. P. "Lewis Acidic Behavior of Fluorinated Organomercurials" *Organometallics*, submitted, Copyright 2007 by the American Chemical Society.

are essentially identical to those of the free polyyne. DSC/TGA studies indicate that adducts $[([o\text{-}C_6F_4Hg]_3)_2 \bullet Ph(C\equiv C)_2Ph]$, $[[o\text{-}C_6F_4Hg]_3 \bullet Ph(C\equiv C)_3Ph]$, and $[([o\text{-}C_6F_4Hg]_3)_2 \bullet Ph(C\equiv C)_4Ph]$ are more thermally stable than the respective free α,ω-diphenylpolyynes (Figure VIII.1 below). For $Ph(C\equiv C)_4Ph$, the stability range is increased by almost 120 ºC in an oxidizing atmosphere. Similar conclusions are derived by monitoring the acetylenic stretch of $Ph(C\equiv C)_4Ph$ and $[([o\text{-}C_6F_4Hg]_3)_2 \bullet Ph(C\equiv C)_4Ph]$ as a function of temperature in KBr. The increase in stability of the α,ω-diphenylpolyynes in these adducts results from their entrapment and physical separation in a supramolecular lattice. Paradoxically, the supramolecular forces responsible for the formation of these adducts are weak and do not affect the structure of the polyynes.

Compound $[o\text{-}C_6F_4Hg]_3$ also reacts with 1,3,5-tris(trimethylsilylethynyl)benzene to afford binary columns (Figure VIII.2).[178] These columns are rather compact as indicated by the distance of 3.28 Å separating the centroids of the two components. Remarkably, these columns display peripheral trimethylsilyl groups and self-aggregate to generate a hexagonal microporous solid featuring 6 Å wide channels. With non-polar methyl groups decorating their walls, the channels of this solid exhibit a high affinity for alkanes which are reversibly trapped as indicated by gravimetric measurements and NMR spectroscopy (Figure VIII.3). Surprisingly, the uptake observed for *n*-butane (2.9 weight %) is greater than that for *n*-pentane (2.4 weight %) and *n*-hexane (2.5 weight %) (Table VIII.1). Molecular mechanics simulations suggest that this difference results from a more efficient packing of the *n*-butane molecules in the channels. This microporous solid is rather robust as indicated by gas exchange experiments which occur with retention of the original structure.

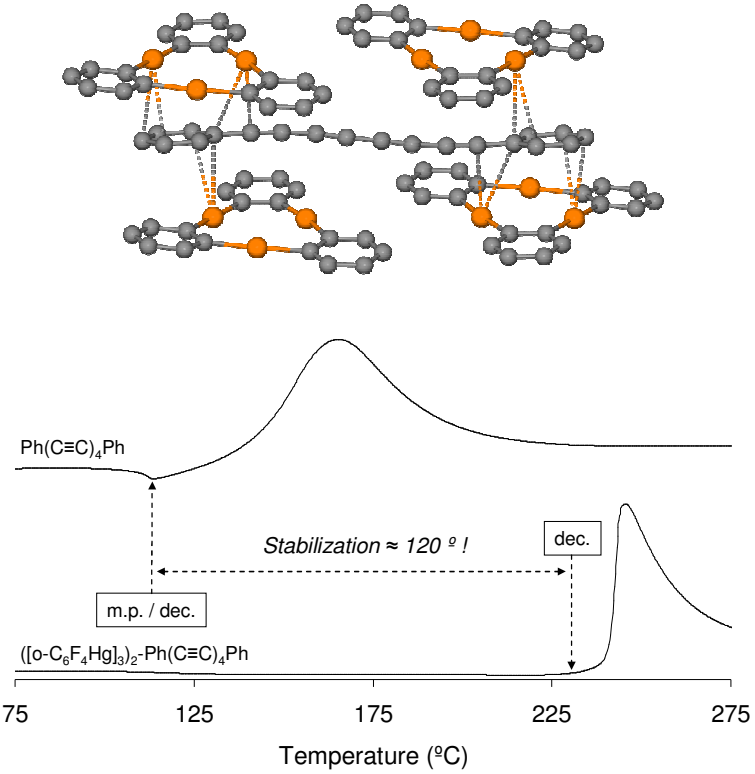

Figure VIII.1. (above) Molecular structure of [[*o*-$C_6F_4Hg]_3$•$Ph(C{\equiv}C)_4Ph$] and (below) DSC traces of $Ph(C{\equiv}C)_4Ph$ and [($[o\text{-}C_6F_4Hg]_3)_2$•$Ph(C{\equiv}C)_4Ph$] showing the stabilization of the polyyne induced by complexation to [*o*-$C_6F_4Hg]_3$.

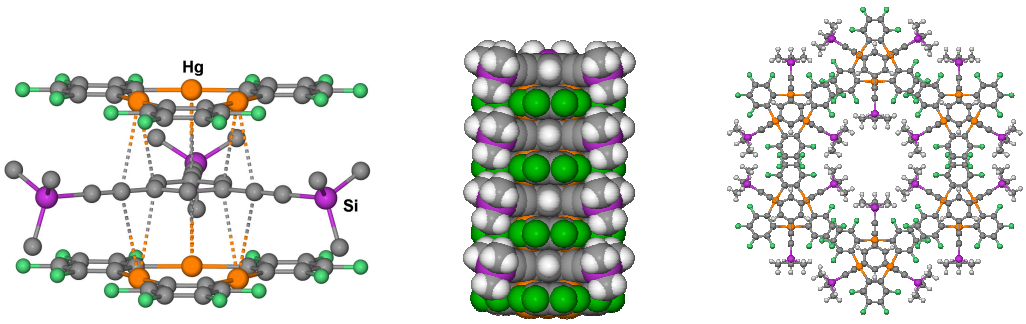

Figure VIII.2. Structure of [[*o*-$C_6F_4Hg]_3$•1,3,5-tris(trimethylsilylethynyl) benzene]. Left: stick and ball view of a portion of the stacks; middle: space filling view of a stack showing 4 repeating units; right: top-view of the honeycomb structure of [[*o*-$C_6F_4Hg]_3$•1,3,5-tris(trimethylsilylethynyl) benzene] along the *c*-axis showing a micropore.

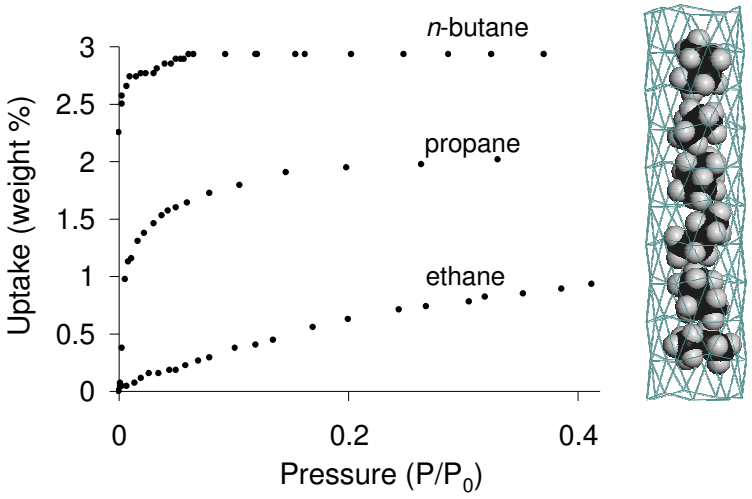

Figure VIII.3. Left: alkane sorption isotherms for [[*o*-$C_6F_4Hg]_3$•1,3,5-tris(trimethylsilylethynyl) benzene] at room temperature. Right: arrangements and conformations of the *n*-butane molecules in the channels of [[*o*-$C_6F_4Hg]_3$•1,3,5-tris(trimethylsilylethynyl) benzene] derived from MM2 calculations.

Table VIII.1. Gravimetric data for hydrocarbon uptake in **[[***o*-$C_6F_4Hg]_3$•1,3,5-tris(trimethylsilylethynyl) benzene].

Gas/Vapor	Weight % uptake	Molar uptake
Methane	0.4	0.45
Ethane	1.2	0.57
Propane	2.1	0.67
n-Butane	2.9	0.71
n-Pentane	2.4	0.45
n-Hexane	2.5	0.41
n-Heptane	2.5	0.35
3,3-dimethylebut-1-ene	1.5	0.26
Benzene	3.8	0.69
Toluene	3.5	0.53
m-Xylene	3.5	0.47
1,3,5-tris(*i*-Pr)benzene	0.0	-

7 crystallizes with 1,3,5-tris(phenylethynyl) benzene (Figure VIII.4a) to form stacks similar to those observed for **[[***o*-$C_6F_4Hg]_3$•1,3,5-tris(trimethylsilylethynyl) benzene**]** (Figure VIII.4b). Solid-state luminescence studies on this compound revealed a novel emission hitherto unreported in the literature. This emission has been tentatively assigned to a $T_1 \rightarrow S_0$ phosphorescence induced by the "heavy" mercury atoms of [*o*-$C_6F_4Hg]_3$. Computer calculations confirmed that such an emission would be at a similar wavelength, and the lifetime of the emission was found to be in the millisecond regime. Titration of solution of [*o*-$C_6F_4Hg]_3$ in CH_2Cl_2 with incremental amounts of 1,3,5-tri(4-*n*-butyl phenylethynyl) benzene suggest the formation of a 1:1 adduct with a stability constant of 21 M^{-1}. This experiment shows that [*o*-$C_6F_4Hg]_3$ interacts with 1,3,5-triethynyl benzenes in solution.

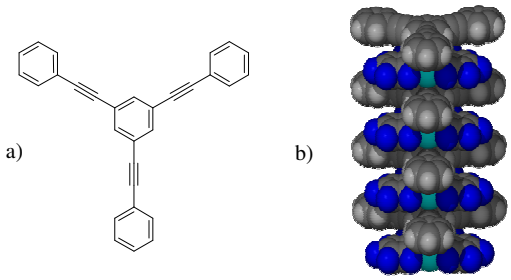

Figure VIII.4. a) 1,3,5-tris(phenylethynyl)benzene, b) 1:1 stack of [o-$C_6F_4Hg]_3$ and 1,3,5-tris(phenylethynyl)benzene.

Other fluorinated organomercurials have been investigated for the complexation of phenylalkynyl substrates and arenes. For example, pentafluorophenyl mercury bromide (C_6F_5HgBr) was found to complex $Ph(C{\equiv}C)_2Ph$. Pentafluorophenyl mercury chloride, (C_6F_5HgCl), complexes phenanthrene, fluorene and pyrene in $CHCl_3$ to form 1:1 adducts. The structure of the phenanthrene adduct has been determined and shows extended binary stacks where molecules of C_6F_5HgCl alternate with molecules of phenanthrene (Figure VIII.5). The short Hg···C contacts of 3.29–3.53 Å indicate the presence of secondary Hg–π interactions. These interactions are complemented by perfluoroarene–arene interactions which presumably add to the stability of the stacks. However, while [*o*-$C_6F_4Hg]_3$ is found to completely quench the fluorescence and emit only the phosphorescence of phenathrene in the solid state, the adduct with C_6F_5HgCl shows both fluorescence *and* phosphorescence (Figure VIII.6). This suggests that the magnitude of the spin-orbit coupling induced by the monofunctional C_6F_5HgCl is not as intense as that induced by the trifunctional [*o*-$C_6F_4Hg]_3$.

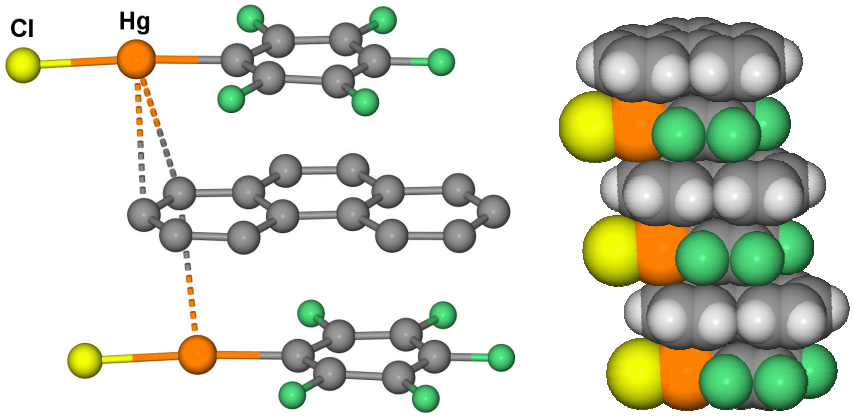

Figure VIII.5. Stick and ball (left) and space filling represenation (right) of a portion of the structure of [C_6F_5HgCl•phenanthrene].

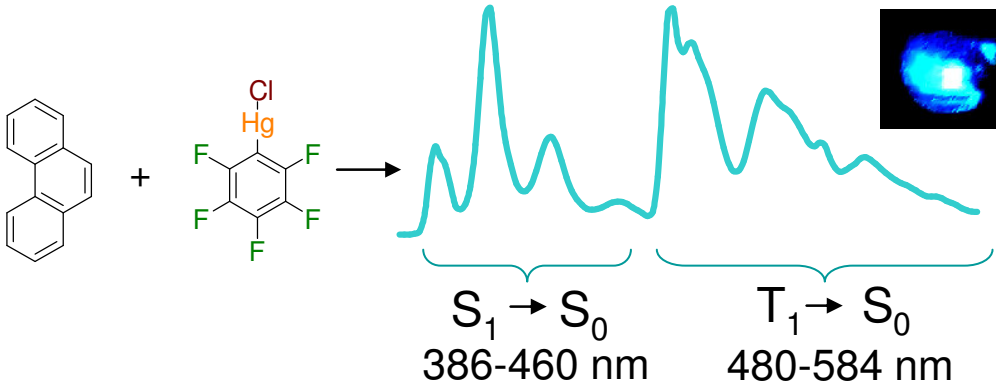

Figure VIII.6. Fluorescence and phosphorescence emissions from the adduct [C_6F_5HgCl•phenanthrene].

REFERENCES

1. Seyferth, D., *Organometallics* **2001,** *20*, 2940-2955.
2. Frankland, E., *Philos. Trans.* **1852,** *142*, 417-444.
3. Frankland, E., *Ann.* **1853,** *85*, 329-373.
4. Frankland, E., *J. Chem. Soc.* **1863,** *16*, 415-425.
5. Frankland, E., *Ann.* **1864,** *130*, 104-124.
6. Gabbaï, F. P.; Melaimi, M.; Burress, C. N.; Taylor, T. J. in *Comprehensive Organometallic Chemistry III*; Crabtree, R. H., Mingos, D. M. P., Eds.; Elsevier: Oxford, 2006; Vol. 2, pp 419-474.
7. Korpar-Colig, B.; Popovic, Z.; Bruvo, M.; Vickovic, I., *Inorg. Chim. Acta* **1988,** *150*, 113-18.
8. Canty, A. J.; Gatehouse, B. M., *Acta Crystallogr., Sect. B: Struct. Sci.* **1972,** *B 28*, 1872-1888.
9. Goggin, P. L.; Goodfellow, R. J.; Hurst, N. W., *J. Chem. Soc., Dalton Trans.* **1978,** 561-566.
10. Emeleus, H. J.; Lagowski, J. J., *Proc. Chem. Soc.* **1958,** 231-231.
11. Emeleus, H. J.; Lagowski, J. J., *J. Chem. Soc.* **1959,** 1497-1501.
12. Shur, V. B.; Tikhonova, I. A., *Russ. Chem. Bull.* **2003,** *52*, 2539-2554.
13. Shur, V. B.; Tikhonova, I. A.; Dolgushin, F. M.; Yanovsky, A. I.; Struchkov, Y. T.; Volkonsky, A. Y.; Solodova, E. V.; Panov, S. Y.; Petrovskii, P. V.; et al., *J. Organomet. Chem.* **1993,** *443*, C19-C21.
14. Naumann, D.; Schulz, F.; Pantenburg, I.; Tyrra, W., *Z. Anorg. Allg. Chem.* **2004,** *630*, 529-534.
15. Viets, D.; Lork, E.; Watson, P. G.; Mews, R., *Angew. Chem., Int. Ed. Engl.* **1997,** *36*, 623-624.
16. Schulz, F.; Pantenburg, I.; Naumann, D., *Z. Anorg. Allg. Chem.* **2003,** *629*, 2312-2316.
17. Powell, H. B.; Maung, M. T.; Lagowski, J. J., *J. Chem. Soc.* **1963,** 2484-2487.

18. Powell, H. B.; Lagowski, J. J., *J. Chem. Soc. A* **1966,** 1282-1285.
19. Nolte, M.; Pantenburg, I.; Meyer, G., *Z. Anorg. Allg. Chem.* **2005,** *631*, 2923-2927.
20. Nockemann, P.; Schulz, F.; Naumann, D.; Meyer, G., *Z. Anorg. Allg. Chem.* **2005,** *631*, 649-653.
21. Kamenar, B.; Korpar-Colig, B.; Hergold-Brundic, A.; Popovic, Z., *Acta Crystallogr., Sect. B: Struct. Sci.* **1982,** *B38*, 1593-1595.
22. Rebek, J., Jr.; Costello, T.; Marshall, L.; Wattley, R.; Gadwood, R. C.; Onan, K., *J. Am. Chem. Soc.* **1985,** *107*, 7481-7487.
23. Onan, K.; Rebek, J., Jr.; Costello, T.; Marshall, L., *J. Am. Chem. Soc.* **1983,** *105*, 6759-6760.
24. Tschinkl, M.; Schier, A.; Riede, J.; Gabbaï, F. P., *Organometallics* **1999,** *18*, 2040-2042.
25. Canty, A. J.; Gatehouse, B. M., *J. Chem. Soc., Dalton Trans.* **1972,** 511-531.
26. Kienitz, C. O.; Thone, C.; Jones, P. G., *Inorg. Chem.* **1996,** *35*, 3990-3997.
27. Deacon, G. B.; Felder, P. W.; Junk, P. C.; Muller-Buschbaum, K.; Ness, T. J.; Quitmann, C. C., *Inorg. Chim. Acta* **2005,** *358*, 4389-4393.
28. Maruoka, K., *Catal. Today* **2001,** *66*, 33-45.
29. Ooi, T.; Takahashi, M.; Yamada, M.; Tayama, E.; Omoto, K.; Maruoka, K., *J. Am. Chem. Soc.* **2004,** *126*, 1150-1160.
30. Oh, T.; Lopez, P.; Reilly, M., *Eur. J. Org. Chem.* **2000,** 2901-2903.
31. Lopez, P.; Oh, T., *Tetrahedron Lett.* **2000,** *41*, 2313-2317.
32. Lee, H.; Diaz, M.; Hawthorne, M. F., *Tetrahedron Lett.* **1999,** *40*, 7651-7655.
33. Reilly, M.; Oh, T., *Tetrahedron Lett.* **1994,** *35*, 7209-7212.
34. Wuest, J. D., *Acc. Chem. Res.* **1999,** *32*, 81-89.
35. Vaugeois, J.; Wuest, J. D., *J. Am. Chem. Soc.* **1998,** *120*, 13016-13022.
36. Vaugeois, J.; Simard, M.; Wuest, J. D., *Organometallics* **1998,** *17*, 1215-1219.
37. Vaugeois, J.; Simard, M.; Wuest, J. D., *Coord. Chem. Rev.* **1995,** *145*, 55-73.
38. Simard, M.; Vaugeois, J.; Wuest, J. D., *J. Am. Chem. Soc.* **1993,** *115*, 370-372.

39. Nadeau, F.; Simard, M.; Wuest, J. D., *Organometallics* **1990,** *9*, 1311-1314.

40. Wuest, J. D.; Zacharie, B., *J. Am. Chem. Soc.* **1987,** *109*, 4714-4715.

41. Beauchamp, A. L.; Olivier, M. J.; Wuest, J. D.; Zacharie, B., *Organometallics* **1987,** *6*, 153-156.

42. Schmidbaur, H.; Oeller, H. J.; Wilkinson, D. L.; Huber, B.; Mueller, G., *Chem. Ber.* **1989,** *122*, 31-36.

43. Haneline, M. R.; Taylor, R. E.; Gabbaï, F. P., *Chem. Eur. J.* **2003,** *9*, 5189-5193.

44. Beckwith, J. D.; Tschinkl, M.; Picot, A.; Tsunoda, M.; Bachman, R.; Gabbaï, F. P., *Organometallics* **2001,** *20*, 3169-3174.

45. Tschinkl, M.; Schier, A.; Riede, J.; Gabbaï, F. P., *Organometallics* **1999,** *18*, 1747-1753.

46. Tschinkl, M.; Gabbaï, F. P., *J. Chem. Crystallogr.* **2003,** *33*, 595-598.

47. Gardinier, J. R.; Gabbaï, F. P., *Dalton* **2000,** 2861-2865.

48. Tschinkl, M.; Bachman, R. E.; Gabbaï, F. P., *Organometallics* **2000,** *19*, 2633-2636.

49. Tschinkl, M.; Schier, A.; Riede, J.; Gabbaï, F. P., *Angew. Chem. Int. Ed.* **1999,** *38*, 3547-3549.

50. King, J. B.; Gabbaï, F. P., *Organometallics* **2003,** *22*, 1275-1280.

51. Density functional theory (DFT) calculations (full geometry optimization) were carried out with Gaussian03. Frequency calculations carried out on the optimized structure of this compound confirmed the absence of any imaginary frequencies. The frontier orbitals and the electrostatic potential surface were obtained from the optimized geometry.

52. Sartori, P.; Golloch, A., *Chem. Berichte* **1968,** *101*, 2004-2009.

53. Tikhonova, I. A.; Dolgushin, F. M.; Tugashov, K. I.; Ellert, O. G.; Novotortsev, V. M.; Furin, G. G.; Antipin, M. Y.; Shur, V. B., *J. Organomet. Chem.* **2004,** *689*, 82-87.

54. Shubina, E. S.; Tikhonova, I. A.; Bakhmutova, E. V.; Dolgushin, F. M.; Antipin, M. Y.; Bakhmutov, V. I.; Sivaev, I. B.; Teplitskaya, L. N.; Chizhevsky, I. T.;

Pisareva, I. V.; Bregadze, V. I.; Epstein, L. M.; Shur, V. B., *Chem. Eur. J.* **2001,** *7*, 3783-3790.

55. Saitkulova, L. N.; Bakhmutova, E. V.; Shubina, E. S.; Tikhonova, I. A.; Furin, G. G.; Bakhmutov, V. I.; Gambaryan, N. P.; Chistyakov, A. L.; Stankevich, I. V.; Shur, V. B.; Epstein, L. M., *J. Organomet. Chem.* **1999,** *585*, 201-210.
56. Chistyakov, A. L.; Stankevich, I. V.; Gambaryan, N. P.; Struchkov, Y. T.; Yanovsky, A. I.; Tikhonova, I. A.; Shur, V. B., *J. Organomet. Chem.* **1997,** *536/537*, 413-424.
57. Tikhonova, I. A.; Dolgushin, F. M.; Yanovsky, A. I.; Struchkov, Y. T.; Gavrilova, A. N.; Saitkulova, L. N.; Shubina, E. S.; Epstein, L. K.; Furin, G. G.; Shur, V. B., *J. Organomet. Chem.* **1996,** *508*, 271-273.
58. Shur, V. B.; Tikhonova, I. A.; Yanovskii, A. I.; Struchkov, Y. T.; Petrovskii, P. V.; Panov, S. Y.; Furin, G. G.; Vol'pin, M. E., *J. Organomet. Chem.* **1991,** *418*, C29-C32.
59. Shur, V. B.; Tikhonova, I. A.; Yanovskii, A. I.; Struchkov, Y. T.; Petrovskii, P. V.; Panov, S. Y.; Furin, G. G.; Vol'pin, M. E., *Dokl. Akad. Nauk SSSR* **1991,** *321*, 1002-1004.
60. Haneline, M. R.; Gabbaï, F. P., *Z. Naturforsch., B: Chem. Sci.* **2004,** *59*, 1483-1487.
61. Ball, M. C.; Brown, D. S.; Massey, A. G.; Wickens, D. A., *J. Organomet. Chem.* **1981,** *206*, 265-277.
62. King, J. B.; Tsunoda, M.; Gabbaï, F. P., *Organometallics* **2002,** *21*, 4201-4205.
63. King, J. B.; Haneline, M. R.; Tsunoda, M.; Gabbaï, F. P., *J. Am. Chem. Soc.* **2002,** *124*, 9350-9351.
64. Tikhonova, I. A.; Dolgushin, F. M.; Tugashov, K. I.; Petrovskii, P. V.; Furin, G. G.; Shur, V. B., *J. Organomet. Chem.* **2002,** *654*, 123-131.
65. Baldamus, J.; Deacon, G. B.; Hey-Hawkins, E.; Junk, P. C.; Martin, C., *Aust. J. Chem.* **2002,** *55*, 195-198.

66. Tikhonova, I. A.; Dolgushin, F. M.; Tugashov, K. I.; Furin, G. G.; Petrovskii, P. V.; Shur, V. B., *Russ. Chem. Bull.* **2001,** *50*, 1673-1678.

67. Tikhonova, I. A.; Dolgushin, F. M.; Yanovsky, A. I.; Starikova, Z. A.; Petrovskii, P. V.; Furin, G. G.; Shur, V. B., *J. Organomet. Chem.* **2000,** *613*, 60-67.

68. Purcell, K. F.; Drago, R. S., *J. Am. Chem. Soc.* **1966,** *88*, 919-924.

69. Tsunoda, M.; Gabbaï, F. P., *J. Am. Chem. Soc.* **2003,** *125*, 10492-10493.

70. Tsunoda, M.; Gabbaï, F. P., *Heteroatom Chemistry* **2005,** *16*, 292-297.

71. Haneline, M. R.; Gabbai, F. P., *Comptes Rendus Chimie* **2004,** *7*, 871-876.

72. Haneline, M. R.; Gabbaï, F. P., *Inorg. Chem.* **2005,** *44*, 6248-6255.

73. Tikhonova, I. A.; Dolgushin, F. M.; Yakovenko, A. A.; Tugashov, K. I.; Petrovskii, P. V.; Furin, G. G.; Shur, V. B., *Organometallics* **2005,** *24*, 3395-3400.

74. Tikhonova, I. A.; Yakovenko, A. A.; Tugashov, K. I.; Dolgushin, F. M.; Novikov, V. V.; Antipin, M. Y.; Shur, V. B., *Organometallics* **2006,** *25*, 6155-6158.

75. Burini, A.; Fackler, J. P., Jr.; Galassi, R.; Grant, T. A.; Omary, M. A.; Rawashdeh-Omary, M. A.; Pietroni, B. R.; Staples, R. J., *J. Am. Chem. Soc.* **2000,** *122*, 11264-11265.

76. Olah, G. A.; Yu, S. H.; Parker, D. G., *J. Org. Chem.* **1976,** *41*, 1983-1986.

77. Lau, W.; Huffman, J. C.; Kochi, J. K., *J. Am. Chem. Soc.* **1982,** *104*, 5515-5517.

78. Damude, L. C.; Dean, P. A. W.; Sefcik, M. D.; Schaefer, J., *J. Organomet. Chem.* **1982,** *226*, 105-114.

79. Damude, L. C.; Dean, P. A. W., *J. Organomet. Chem.* **1979,** *181*, 1-15.

80. Branch, C. S.; Barron, A. R., *J. Am. Chem. Soc.* **2002,** *124*, 14156-14161.

81. Borovik, A. S.; Barron, A. R., *J. Am. Chem. Soc.* **2002,** *124*, 3743-3748.

82. Borovik, A. S.; Bott, S. G.; Barron, A. R., *J. Am. Chem. Soc.* **2001,** *123*, 11219-11228.

83. Borovik, A. S.; Bott, S. G.; Barron, A. R., *Angew. Chem. Int. Ed.* **2000,** *39*, 4117-4118.

84. Kuzmina, L. G.; Struchkov, Y. T., *Croat. Chem. Acta* **1984,** *57*, 701-724.

85. Burress, C. N.; Bodine, M. I.; Elbjeirami, O.; Reibenspies, J. H.; Omary, M. A.; Gabbaï, F. P., *Inorg. Chem.* **2007,** *46*, 1388-1395.

86. Tsunoda, M.; Gabbaï, F. P., *J. Am. Chem. Soc.* **2000,** *122*, 8335-8336.

87. Haneline, M. R.; King, J. B.; Gabbaï, F. P., *Dalton Trans.* **2003,** 2686-2690.

88. Haneline, M. R.; Tsunoda, M.; Gabbaï, F. P., *J. Am. Chem. Soc.* **2002,** *124*, 3737-3742.

89. Omary, M. A.; Kassab, R. M.; Haneline, M. R.; Elbjeirami, O.; Gabbaï, F. P., *Inorg. Chem.* **2003,** *42*, 2176-2178.

90. Tikhonova, I. A.; Tugashov, K. I.; Dolgushin, F. M.; Yakovenko, A. A.; Strunin, B. N.; Petrovskii, P. V.; Furin, G. G.; Shur, V. B., *Inorg. Chim. Acta* **2006,** *359*, 2728-2735.

91. Taylor, T. J.; Burress, C. N.; Pandey, L.; Gabbaï, F. P., *Dalton Trans.* **2006,** 4654-4656.

92. Griffith, J. S., *Theory of Transition Metal Ions*. Cambridge University Press: Cambridge, United Kingdom, **1964**.

93. Baldo, M. A.; Thompson, M. E.; Forrest, S. R., *Pure Appl. Chem.* **1999,** *71*, 2095-2106.

94. Stoffers, C.; Yang, S.; Zhang, F.; Jacobsen, S. M.; Wagner, B. K.; Summers, C. J., *Appl. Phys. Lett.* **1997,** *71*, 1759-1761.

95. McGlynn, S. P., *Chem. Rev.* **1958,** *58*, 1113-1156.

96. Nijegorodov, N.; Mabbs, R., *Spectrochim. Acta, Part A* **2001,** *57*, 1449-1462.

97. Burress, C.; Elbjeirami, O.; Omary, M. A.; Gabbaï, F. P., *J. Am. Chem. Soc.* **2005,** *127*, 12166-12167.

98. Burress, C. N.; Gabbaï, F. P., *Heteroatom Chemistry* **2007,** *in press*.

99. Haneline, M. R.; Gabbaï, F. P., *Angew. Chem. Int. Ed.* **2004,** *43*, 5471-5474.

100. Burini, A.; Fackler, J. P., Jr.; Galassi, R.; Macchioni, A.; Omary, M. A.; Rawashdeh-Omary, M. A.; Pietroni, B. R.; Sabatini, S.; Zuccaccia, C., *J. Am. Chem. Soc.* **2002,** *124*, 4570-4571.

101. Wedge, T. J.; Hawthorne, M. F., *Coord. Chem. Rev.* **2003,** *240*, 111-128.

102. Hawthorne, M. F.; Zheng, Z., *Acc. Chem. Res.* **1997,** *30*, 267-276.

103. Vecchiotti, L., *Chem. Berichte* **1930,** *63*, 2275-2276.

104. Wittig, G.; Bickelhaupt, F., *Chem. Ber.* **1958,** *91*, 883-894.

105. Aljabar, N. A. A.; Massey, A. G., *J. Organomet. Chem.* **1984,** *275*, 9-18.

106. Brown, D. S.; Massey, A. G.; Wickens, D. A., *Acta Crystallogr., Sect. B: Struct. Sci.* **1978,** *34*, 1695-1697.

107. Brown, D. S.; Massey, A. G.; Wickens, D. A., *Inorg. Chim. Acta* **1980,** *44*, L193-L194.

108. Tsunoda, M., Gabbai, F. P., unpublished results, please inquire with the Gabbaï research group at Texas A&M University.

109. Nyburg, S. C.; Faerman, C. H., *Acta Crystallogr., Sect. B: Struct. Sci.* **1985,** *41*, 274-279.

110. Canty, A. J.; Deacon, G. B., *Inorg. Chim. Acta* **1980,** *45*, L225-L227.

111. Pyykko, P.; Straka, M., *Phys. Chem. Chem. Phys.* **2000,** *2*, 2489-2493.

112. Nightingale, D. V.; Brooker, R. M., *J. Am. Chem. Soc.* **1950,** *72*, 5539-5543.

113. Flack, H. D., *Acta Crystallogr., Sect. A* **1983,** *39*, 876-881.

114. Batsanov, S. S., *Zh. Neorg. Khim.* **1991,** *36*, 3015-3037.

115. Goedheijt, M. S.; Nijbacker, T.; Akkerman, O. S.; Bickelhaupt, F.; Veldman, N.; Spek, A. L., *Angew. Chem., Int. Ed. Engl.* **1996,** *35*, 1550-1552.

116. Tschinkl, M.; Schier, A.; Riede, J.; Gabbaï, F. P., *Inorg. Chem.* **1998,** *37*, 5097-5101.

117. Casari, C. S.; Bassi, A. L.; Ravagnan, L.; Siviero, F.; Lenardi, C.; Piseri, P.; Bongiorno, G.; Bottani, C. E.; Milani, P., *Phys. Rev. B: Condens. Matter* **2004,** *69*, 075422.1-075422.7.

118. Heimann, R. B. E., S. E.; Kavan, L., Eds, *Carbyne and Carbynoid Structures*. Kluwer Academic Publishers: Dordrecht, The Netherlands, **1999**.

119. Lagow, R. J.; Kampa, J. J.; Wei, H. C.; Battle, S. L.; Genge, J. W.; Laude, D. A.; Harper, C. J.; Bau, R.; Stevens, R. C.; Haw, J. F.; Munson, E., *Science* **1995,** *267*, 362-367.

120. Eastmond, R.; Walton, D. R. M.; Johnson, T. R., *Tetrahedron* **1972,** *28*, 4601-4616.

121. Eisler, S.; Slepkov, A. D.; Elliott, E.; Luu, T.; McDonald, R.; Hegmann, F. A.; Tykwinski, R. R., *J. Am. Chem. Soc.* **2005,** *127*, 2666-2676.

122. Dembinski, R.; Bartik, T.; Bartik, B.; Jaeger, M.; Gladysz, J. A., *J. Am. Chem. Soc.* **2000,** *122*, 810-822.

123. Mohr, W.; Stahl, J.; Hampel, F.; Gladysz, J. A., *Chem. Eur. J.* **2003,** *9*, 3324-3340.

124. Zheng, Q. L.; Gladysz, J. A., *J. Am. Chem. Soc.* **2005,** *127*, 10508-10509.

125. Diederich, F. S., P. J.; Tykwinski, R. R., Eds.; , *Acetylene Chemistry: Chemistry, Biology, and Material Science*. Wiley-VCH: Weinheim, **2004**.

126. Stahl, J.; Bohling, J. C.; Bauer, E. B.; Peters, T. B.; Mohr, W.; Martin-Alvarez, J. M.; Hampel, F.; Gladysz, J. A., *Angew. Chem. Int. Ed.* **2002,** *41*, 1872-1876.

127. Gibtner, T.; Hampel, F.; Gisselbrecht, J. P.; Hirsch, A., *Chem. Eur. J.* **2002,** *8*, 408-432.

128. Davies, A. G., Wardell, J. L., *Comprehensive Organometallic Chemistry II*. Pergamon Press: Oxford, **1995**.

129. Caillet, J.; Claverie, P., *Acta Crystallogr., Sect. A* **1975,** *31*, 448-461.

130. Wong, W.-Y.; Lu, G.-L.; Liu, L.; Shi, J.-X.; Lin, Z., *Eur. J. Inorg. Chem.* **2004,** 2066-2077.

131. Faville, S. J.; Henderson, W.; Mathieson, T. J.; Nicholson, B. K., *J. Organomet. Chem.* **1999,** *580*, 363-369.

132. Szafert, S.; Gladysz, J. A., *Chem. Rev.* **2003,** *103*, 4175-4205.

133. Nagano, Y.; Ikoma, T.; Akiyama, K.; Tero-Kubota, S., *J. Am. Chem. Soc.* **2003,** *125*, 14103-14112.

134. Armitage, J. B.; Entwistle, N.; Jones, E. R. H.; Whiting, M. C., *J. Chem. Soc.* **1954,** 147-154.

135. Coates, G. W.; Dunn, A. R.; Henling, L. M.; Dougherty, D. A.; Grubbs, R. H., *Angew. Chem., Int. Ed. Engl.* **1997,** *36*, 248-251.

136. Xiao, J.; Yang, M.; Lauher, J. W.; Fowler, F. W., *Angew. Chem. Int. Ed.* **2000,** *39*, 2132-2135.

137. Venkatasubbaiah, K.; Bats, J. W.; Rheingold, A. L.; Jakle, F., *Organometallics* **2005,** *24*, 6043-6050.

138. Jukes, A. E.; Gilman, H., *J. Organomet. Chem.* **1969,** *17*, 145-148.

139. Chambers, R. D.; Musgrave, W. K.; Coates, G. E.; Livingstone, J. G., *J. Chem. Soc.* **1962,** 4367-4371.

140. Brandsma, L., *Preparative Acetylenic Chemistry*. Elsevier Publishing Company: Amsterdam, The Netherlands, **1971**.

141. Jiang, M. X. W.; Rawat, M.; Wulff, W. D., *J. Am. Chem. Soc.* **2004,** *126*, 5970-5971.

142. Dabdoub, M. J.; Baroni, A. C. M.; Lenardao, E. J.; Gianeti, T. R.; Hurtado, G. R., *Tetrahedron* **2001,** *57*, 4271-4276.

143. Ziegler, C. B.; Harris, S. M.; Baldwin, J. E., *J. Org. Chem.* **1987,** *52*, 443-446.

144. Baranovic, G.; Colombo, L.; Furic, K.; Durig, J. R.; Sullivan, J. F.; Mink, J., *J. Mol. Struct.* **1986,** *144*, 53-69.

145. Rubin, Y.; Lin, S. S.; Knobler, C. B.; Anthony, J.; Boldi, A. M.; Diederich, F., *J. Am. Chem. Soc.* **1991,** *113*, 6943-6949.

146. Kostrovskii, V. G. S., M. S.; Andrievskii, V. N.; Kotlyarevskii, I. L *Bull. Acad. Sci. USSR Div. Chem. Sci. (EN)* **1968**, 2324-2330.

147. Rowsell, J. L. C.; Yaghi, O. M., *Angew. Chem. Int. Ed.* **2005,** *44*, 4670-4679.

148. Ferey, G.; Latroche, M.; Serre, C.; Millange, F.; Loiseau, T.; Percheron-Guegan, A., *Chem. Comm.* **2003**, 2976-2977.

149. Dybtsev, D. N.; Nuzhdin, A. L.; Chun, H.; Bryliakov, K. P.; Talsi, E. P.; Fedin, V. P.; Kim, K., *Angew. Chem. Int. Ed.* **2006,** *45*, 916-920.

150. Forster, P. M.; Eckert, J.; Chang, J. S.; Park, S. E.; Ferey, G.; Cheetham, A. K., *J. Am. Chem. Soc.* **2003,** *125*, 1309-1312.

151. Pan, L.; Sander, M. B.; Huang, X. Y.; Li, J.; Smith, M.; Bittner, E.; Bockrath, B.; Johnson, J. K., *J. Am. Chem. Soc.* **2004,** *126*, 1308-1309.

152. Zhao, X. B.; Xiao, B.; Fletcher, A. J.; Thomas, K. M.; Bradshaw, D.; Rosseinsky, M. J., *Science* **2004,** *306*, 1012-1015.

153. Kubota, Y.; Takata, M.; Matsuda, R.; Kitaura, R.; Kitagawa, S.; Kato, K.; Sakata, M.; Kobayashi, T. C., *Angew. Chem. Int. Ed.* **2005,** *44*, 920-923.

154. Kesanli, B.; Cui, Y.; Smith, M. R.; Bittner, E. W.; Bockrath, B. C.; Lin, W. B., *Angew. Chem. Int. Ed.* **2005,** *44*, 72-75.

155. Kaye, S. S.; Long, J. R., *J. Am. Chem. Soc.* **2005,** *127*, 6506-6507.

156. Sozzani, P.; Bracco, S.; Comotti, A.; Ferretti, L.; Simonutti, R., *Angew. Chem. Int. Ed.* **2005,** *44*, 1816-1820.

157. Pan, L.; Olson, D. H.; Ciemnolonski, L. R.; Heddy, R.; Li, J., *Angew. Chem. Int. Ed.* **2006,** *45*, 616-619.

158. Chen, B. L.; Liang, C. D.; Yang, J.; Contreras, D. S.; Clancy, Y. L.; Lobkovsky, E. B.; Yaghi, O. M.; Dai, S., *Angew. Chem. Int. Ed.* **2006,** *45*, 1390-1393.

159. Sozzani, P.; Comotti, A.; Bracco, S.; Simonutti, R., *Chem. Comm.* **2004,** 768-769.

160. Desiraju, G. R., *Acc. Chem. Res.* **2002,** *35*, 565-573.

161. Meyer, E. A.; Castellano, R. K.; Diederich, F., *Angew. Chem. Int. Ed.* **2003,** *42*, 1210-1250.

162. Blin, J. L.; Su, B. L., *Langmuir* **2002,** *18*, 5303-5308.

163. Taylor, T. J.; Gabbaï, F. P., *Organometallics* **2006,** *25*, 2143-2147.

164. Spek, A. L. *PLATON, A Multipurpose Crystallographic Tool*, University of Utrecht: Utrecht, 2005.

165. Eddaoudi, M.; Li, H.; Yaghi, O. M., *J. Am. Chem. Soc.* **2000,** *122*, 1391-1397.

166. Fang, Q.; Zhu, G.; Xue, M.; Sun, J.; Sun, F.; Qiu, S., *Inorg. Chem.* **2006,** *45*, 3582-3587.

167. Galvez, J., *J. Chem. Inf. Comput. Sci.* **2003,** *43*, 1231-1239.

168. Stallmach, F.; Groger, S.; Kunzel, V.; Karger, J.; Yaghi, O. M.; Hesse, M.; Muller, U., *Angew. Chem. Int. Ed.* **2006,** *45*, 2123-2126.

169. Datema, K. P.; Denouden, C. J. J.; Ylstra, W. D.; Kuipers, H.; Post, M. F. M.; Karger, J., *J. Chem. Soc., Faraday Trans.* **1991,** *87*, 1935-1943.

170. Arzumanov, S. S.; Reshetnikov, S. I.; Stepanov, A. G.; Parmon, V. N.; Freude, D., *J. Phys. Chem. B* **2005,** *109*, 19748-19757.

171. Zorine, V. E.; Magusin, P. C. M.; van Santen, R. A., *J. Phys. Chem. B* **2004,** *108*, 5600-5608.

172. Roland, J.; Michel, D., *Magn. Reson. Chem.* **2000,** *38*, 587-595.

173. Leininger, S.; Stang, P. J.; Huang, S., *Organometallics* **1998,** *17*, 3981-3987.

174. Gaab, K. M.; Thompson, A. L.; Xu, J.; Martinez, T. J.; Bardeen, C. J., *J. Am. Chem. Soc.* **2003,** *125*, 9288-9289.

175. Kawaguchi, T.; Takashina, K.; Tanaka, T.; Watanabé, T., *Acta Crystallogr., Sect. B: Struct. Sci.* **1972,** *B 28*, 967-972.

176. Kondo, K.; Yasuda, S.; Sakaguchi, T.; Miya, M., *J. Chem. Soc., Chem. Comm.* **1995,** 55-56.

177. Thompson, A. L.; Gaab, K. M.; Xu, J.; Bardeen, C. J.; Martinez, T. J., *J. Phys. Chem. A* **2004,** *108*, 671-682.

178. Taylor, T. J.; Bakhmutov, V. I.; Gabbaï, F. P., *Angew. Chem., Int. Ed. Engl.* **2006,** *45*, 7030-7033.

179. Bochkarev, M. N.; Katkova, M. A.; Fedorova, E. A.; Makarenko, N. P.; Schumann, H.; Girgsdies, F., *Z. Naturforsch., B: Chem. Sci.* **1998,** *53*, 833-835.

180. Ponzini, F.; Zagha, R.; Hardcastle, K.; Siegel, J. S., *Angew. Chem. Int. Ed.* **2000,** *39*, 2323-2325.

181. Bauernschmitt, R.; Ahlrichs, R., *Chem. Phys. Lett.* **1996,** *256*, 454-464.

182. Ramamurthy, V.; Eaton, D. F.; Caspar, J. V., *Acc. Chem. Res.* **1992,** *25*, 299-307.

183. Becke, A. D., *J. Chem. Phys.* **1993,** *98*, 5648-5652.

184. Lee, C. T.; Yang, W. T.; Parr, R. G., *Phys. Rev. B: Condens. Matter* **1988,** *37*, 785-789.

185. Miehlich, B.; Savin, A.; Stoll, H.; Preuss, H., *Chem. Phys. Lett.* **1989,** *157*, 200-206.

186. Hehre, W. J.; Ditchfie, R.; Pople, J. A., *J. Chem. Phys.* **1972,** *56*, 2257-2261.

187. Viets, D.; Lork, E.; Watson, P. G.; Mews, R., *Angew. Chem., Int. Ed. Engl.* **1997,** *36*, 623-624.

188. Schulz, F.; Pantenburg, I.; Naumann, D., *Zeit. Anorg. Allg. Chem.* **2003,** *629*, 2312-2316.

189. Deacon, G. B.; Tunaley, D., *J. Organomet. Chem.* **1978,** *156*, 403-426.

190. Lorenzo, S.; Lewis, G. R.; Dance, I., *New J. Chem.* **2000,** *24*, 295-304.

191. Langelaar, J.; Jansen, G.; Rettschn, R.; Hoytink, G. H., *Chem. Phys. Lett.* **1971,** *12*, 86-91.

192. Burress, C. N.; Bodine, M. I.; Gabbaï, F. P., *Unpublished results,* please inquire with the Gabbaï research group at Texas A&M University.

193. Gu, J.-S.; Ren, Z.-G.; Jiang, R.; Ziang, S.-L., *Guangpu Shiyanshi* **1999,** *16*, 485-487.

194. Koning, R. E.; Zandstra, P. J., *Chem. Phys.* **1977,** *20*, 53-59.

195. Levitus, M.; Garcia-Garibay, M. A., *J. Phys. Chem. A* **2000,** *104*, 8632-8637.

196. Nguyen, P.; Todd, S.; Vandenbiggelaar, D.; Taylor, N. J.; Marder, T. B.; Wittmann, F.; Friend, R. H., *Synlett* **1994,** 299-301.

197. Nierle, J.; Barth, D.; Kuck, D., *Eur. J. Org. Chem.* **2004,** 867-872.

198. Huynh, C.; Linstrumelle, G., *Tetrahedron* **1988,** *44*, 6337-6344.

VITA

Thomas Jackson Taylor

c/o Prof. François Gabbaï
Department of Chemistry
Texas A&M University
College Station, TX 77843-3255

Education:

Ph.D. in Chemistry from Texas A&M University
Graduated: May 2007

B.S. in Chemistry from University of Chicago
Graduated: June 1999

Publications:

Taylor, T. J.; Burress, C. N.; Pandey, L.; Gabbaï, F. P. "Structural and photophysical studies of phenanthrene adducts involving C_6F_5HgCl and [*o*-$C_6F_4Hg]_3$." *Dalton Trans.* **2006,** 4654-4656.

Taylor, T. J.; Bakhmutov, V. I.; Gabbaï, F. P. "Hydrocarbon Uptake in the Alkylated Micropores of a Columnar Supramolecular Solid." *Angew. Chem. Intl. Ed.* **2006**, *45*, 7030-7033, *featured on the cover for issue 42.*

Taylor, T. J.; Gabbaï, F. P. "Supramolecular Stabilization of α,ω–Diphenylpolyynes by Complexation to the Tridentate Lewis Acid [*o*-$C_6F_4Hg]_3$." *Organometallics* **2006**, *25*, 2143-2147.

Burress, C. N.; Melaimi, M.; Taylor, T. J.; Gabbaï, F. P. "Mercury and Cadmium" *Comprehensive Organometallic Chemistry - 3rd Edition* **2006**, 419-474.

Awards:

AFS Distinguished Graduate Assistant Research Award, March 2007.
Outstanding Oral Presentation at the Graduate Research in General Chemistry Symposium, October 2006.
Research/Presentation Grant, (Office of Graduate Studies, TAMU), Summer 2006.
Martin Corera Travel Award (Department of Chemistry, TAMU), Spring 2005.
Richter Research Grant (University of Chicago), Summer 1997.